

---

**Title 40 CFR Part 191  
Compliance Certification  
Application  
for the  
Waste Isolation Pilot Plant  
  
MASS Attachment 15-1**



**THIS PAGE INTENTIONALLY LEFT BLANK**



WFO 38801

## Sandia National Laboratories

Albuquerque, New Mexico 87185-1341

date: June 10, 1996

to: M. S. Tierney, MS-1328 (Org. 6741)

L. H. Brush

from: L. H. Brush, MS-1341 (Org. 6748)

INFORMATION ONLY

subject: Ranges and Probability Distributions of  $K_d$ s for Dissolved Pu, Am, U, Th, and Np in the Culebra for the PA Calculations to Support the WIPP CCA



### INTRODUCTION

This memorandum contains ranges and probability distributions of matrix distribution coefficients ( $K_d$ s) for dissolved Pu, Am, U, Th, and Np under conditions expected during transport in the Culebra Dolomite member of the Rustler Formation. In this memo, a matrix  $K_d$  is the equilibrium ratio of the mass of Pu, Am, U, Th, or Np adsorbed on the solid phase(s) per unit mass of solid(s) divided by the concentration of that element in the aqueous phase (see, for example, Freeze and Cherry, 1979). Performance-assessment (PA) personnel require  $K_d$ s for Pu, Am, U, Th, and Np for their calculations to support the Waste Isolation Pilot Plant (WIPP) Compliance Certification Application (CCA) (Ramsey, 1996). (We will include this memorandum and all of the other memoranda cited herein in the parameter and analysis records packages for these  $K_d$ s.) Actually, PA requires  $K_d$ s for various isotopes of these elements, but Ramsey (1996) did not specify them. However, Garner (1996) stated that PA needs  $K_d$ s for  $^{239}\text{Pu}$ ,  $^{241}\text{Am}$ ,  $^{234}\text{U}$ , and  $^{230}\text{Th}$ . It is reasonable to assume that, in view of the small differences among the masses of different isotopes of these elements, one can apply a  $K_d$  determined for one isotope to any other isotope of the same element. We are submitting  $K_d$ s for Np in case PA requires them for sensitivity calculations to show that omitting this element does not affect the long-term performance of the repository significantly.

We, the Sandia-National-Laboratories (SNL), and SNL-subcontractor personnel working on or familiar with the dissolved-actinide Retardation Research Program (RRP) or related aspects of PA, have established these ranges and distributions from results obtained by the RRP through May 31, 1996 (see Table 1 below). These ranges and distributions pertain to dolomite-rich rock in the matrix (intact rock between the fractures) of the Culebra. (We use the terms

“matrix” and “fractures” in a general sense, corresponding to transport pathways with relatively low and high transmissivities, respectively. Our use of these terms is consistent with the double-porosity conceptual model of the Culebra proposed by L. Meigs and her colleagues at SNL and its subcontractors.) The ranges and distributions in Table 1 *do not* include  $K_{ds}$  for the clay-rich rock associated with fracture surfaces and dispersed in the matrix of the Culebra. We believe that, based on Sowards (1991) and Sowards et al. (1991, 1992) and recent, yet-to-be published studies of Culebra mineralogy, clay minerals such as corrensite (an ordered mixture of chlorite and saponite) *are* present on fracture surfaces *and* in the matrix of the Culebra at concentrations high enough to increase the retardation of Pu, Am, U, Th, and Np relative to that observed in laboratory studies with dolomite-rich rock (see Description of Laboratory Studies Used to Determine Matrix  $K_{ds}$  below). However, we *have not* included  $K_{ds}$  for clay minerals in these ranges and distributions because we do not have sufficient laboratory data for clay-rich rock under expected Culebra conditions at this time. Furthermore, we *have not* taken any credit for sorption by clay minerals on fractures. We believe that omitting  $K_{ds}$  for clays is conservative.

#### FRACTURE-SURFACE $K_{ds}$



We recommend that PA personnel set the fracture-surface  $K_{ds}$  (actually,  $K_{as}$ ) for Pu, Am, U, Th, and Np in the Culebra to zero. A distribution coefficient expressed on a per-unit-surface-area basis, or  $K_a$ , is the equilibrium ratio of the mass of Pu, Am, U, Th, or Np adsorbed on the solid phase(s) per unit area of solid(s) divided by the concentration of that element in the aqueous phase (Freeze and Cherry, 1979). We also recommend that PA not include sorption by a discrete layer of material associated with fracture surfaces. Setting these  $K_a$ s to zero will not affect the predicted retardation of actinide elements by the Culebra because: (1) we *have not* taken credit for sorption by clay minerals on fracture surfaces; (2) the surface area of the dolomite-rich rock lining the fractures is very small relative to that of the dolomite-rich rock in the matrix. WIPP Performance Assessment Department (1992) discussed sorption on fractures in detail.

#### MATRIX $K_{ds}$

This section briefly describes the laboratory studies used to determine matrix  $K_{ds}$  for dissolved Pu, Am, U, Th, and Np, and the modeling study used to predict the oxidation-state distributions of these elements under conditions expected in the Culebra. It then discusses the methodologies used to establish ranges and probability distributions of these  $K_{ds}$ .

Description of Laboratory Studies  
Used to Determine Matrix  $K_d$ s

The RRP carried out several laboratory studies of the sorption of Pu, Am, U, Th, and Np by dolomite-rich rock from the Culebra. Papenguth and Behl (1996) described these studies in detail. These studies used different experimental methods and considered the effects of several factors on actinide sorption in the Culebra. The results used to establish ranges and probability distributions of matrix  $K_d$ s for Pu, Am, U, Th, and Np in the Culebra appear in Appendices B through F, respectively, of this memorandum. (These lengthy appendices are available on request to anyone who did not receive them with this memo.) Detailed descriptions of these laboratory studies and the complete results will appear as SNL and/or SNL subcontractor reports by the time of submission of the CCA.

I. Triay and her group at Los Alamos National Laboratory (LANL) carried out an empirical study of the sorption of Pu(V), Am(III), U(VI), Th(IV), and Np(V) by samples of dolomite-rich rock from the Culebra. Triay used four synthetic fluids, Brine A, ERDA-6, AISinR, and H-17, for her experiments with dolomite-rich rock. Brine A, developed by Molecke (1983) to simulate fluids equilibrated with K- and Mg-bearing minerals in overlying potash-rich zones in the Salado Formation prior to entering WIPP disposal rooms, is also similar to intergranular Salado brines at or near the stratigraphic horizon of the repository. These brines could accumulate in WIPP disposal rooms after filling and sealing, and flow from the repository into the Culebra in the event of human intrusion into the repository. ERDA-6 simulates brines that occur in isolated but occasionally large reservoirs in the underlying Castile Formation (Popielak et al., 1983). These brines could flow through the repository and into the Culebra in the event of human intrusion. AISinR simulates brine sampled from the Culebra in the WIPP Air Intake Shaft (AIS). H-17 simulates Culebra brine from the H-17 Hydropad. Triay also studied the effects of the partial pressure of CO<sub>2</sub> (and, hence, dissolved CO<sub>2</sub> concentration and, to some extent, pH) on sorption. She carried out experiments on the bench top (in contact with atmospheric CO<sub>2</sub>, which contains about 0.035% CO<sub>2</sub>) and in glove boxes with atmospheres containing 0.24, 1.4, and 4.1% CO<sub>2</sub>. The CO<sub>2</sub> partial pressures in these runs were 10<sup>-3.5</sup>, 10<sup>-2.73</sup>, 10<sup>-1.98</sup>, and 10<sup>-1.50</sup> atm, respectively, the range of P<sub>CO2</sub> calculated for Culebra ground waters by Siegel et al. (1991). Furthermore, Triay studied the effects of dissolved actinide concentration on sorption. These experiments yielded sorption isotherms, plots of the quantity of radionuclide sorbed by the solid phase or phases versus the final dissolved radionuclide concentration, or plots of  $K_d$ s versus the final dissolved radionuclide concentration. (We will include these isotherms in the parameter and analysis records packages for these  $K_d$ s.) These plots in turn provided information on the nature of the reaction(s) responsible for removal of radionuclides from solution. Finally, Triay studied the effects of equilibration time (3-days and 1-, 3-, 6-, or 8-weeks) and direction of reaction (sorption or desorption) on sorption. Triay crushed the samples, selected the 75-to-500- $\mu$ m

size fraction (significantly larger than the mean dolomite grain diameter of about 2  $\mu\text{m}$ ), washed these subsamples with dilute HCl to remove crystallographically strained surfaces, fine particles of dolomite, and Fe- and Mn-oxyhydroxides, and pretreated them with the same type of brine to be used for the actual experiment for periods of time for the most part identical to those of the sorption and desorption runs. Triay carried out each of the pretreatments and the actual experiments with 20 ml of brine and 1 g of rock. During the runs that yielded the  $K_d$ s to be used by PA, she used one actinide element at a time. At the end of her runs, Triay separated the aqueous and solid phases by sequential filtration to 0.2  $\mu\text{m}$ , analyzed the solutions by liquid scintillation counting (LSC), and determined  $K_d$ s from the differences between the initial and the final radionuclide concentrations in the solutions. She carried out most of her experiments, and all of the runs that yielded the  $K_d$ s to be used by PA, with samples of dolomite-rich rock taken from AIS core segments adjacent to those used for the column-transport study (see below). X-ray-diffraction analysis of this rock failed to detect clay minerals in most cases. Because the detection limit of this technique is about 1%, the rock that yielded the  $K_d$ s for PA contains a lower concentration of clay minerals than the Culebra as a whole (estimated, based on previously published and ongoing studies of Culebra mineralogy, to be about 1 to 5%). Triay also carried out a few experiments with dolomite from the H-19 Hydropad and clay-rich rock from the lower, unnamed member of the Rustler. (The clay minerals in the lower member are identical to those lining fracture surfaces and dispersed in the matrix of the Culebra.) This study yielded a large number of  $K_d$ s for actual samples of nearly pure Culebra dolomite and actinide-bearing synthetic fluids closely resembling those that could actually flow through the Culebra after human intrusion.

P. V. Brady and his colleagues at SNL and LANL carried out a mechanistic study of the sorption of Pu(V), Am(III), Nd(III) (a nonradioactive analog of Am(III) and Pu(III)), U(VI), Th(IV), and Np(V) from synthetic 0.05, 0.5, and 5 M NaCl solutions by samples of well characterized, pure dolomite from Norway. Brady used a limited-residence-time (1 min.) reaction vessel to minimize the extent of dolomite dissolution, actinide precipitation, and other reactions unrelated to sorption during his experiments. This allowed him to study the effects of pH (from about 3 or 4 to 9 or 10 in most cases), the  $\text{CO}_2$  concentration of the headspace (atmospheric, 0.5, and 5%), and the concentrations of potentially significant cations and anions on sorption in the absence of complexities caused by other reactions. Brady crushed the samples, selected the <106- $\mu\text{m}$  size fraction, washed them with dilute HCl, and pretreated them overnight in an NaCl solution with the same concentration to be used for the actual experiments, and a solution-to-solid ratio of 100 ml per g of dolomite. He carried out the actual experiments with several actinide elements at a time, and a solution-to-solid ratio of 200 ml/g. After his runs, Brady separated the aqueous and solid phases with a 0.22- $\mu\text{m}$  filter, analyzed the solutions by inductively coupled plasma emission/mass spectrometry, and determined  $K_d$ s from the differences between the initial and the final radionuclide concentrations in the solutions. Although

this study did not yield  $K_{ds}$  for actual samples of Culebra rock nor for synthetic Culebra fluids, it did yield results that have proven highly useful for interpreting the results of the empirical sorption study at LANL, and for extending the empirical data to the basic conditions (pH values of about 9 to 10) expected to result from use of an MgO backfill in WIPP disposal rooms (see below).

D. A. Lucero and his colleagues at SNL have studied actinide transport through intact, 5.7-inch-diameter cores obtained from the Culebra in the WIPP AIS. Lucero obtained the cores used for this study from 16-to-18-ft.-long horizontal boreholes aligned in the current direction of ground-water flow in the vicinity of the AIS (see Predictions of Actinide Oxidation States in the Culebra below) and stored them under conditions that minimized evaporation of pore water. Prior to his experiments, Lucero cut 4-to-20-inch sections from the original cores and potted them in Neoprene. He then placed the potted core sections in Al core holders, mounted them vertically in a glove box, and pressurized them to about 50 atm, the *in situ* pressure at the depths (716 and 721 ft.) from which these cores were obtained. Lucero carried out spike injections or, in a few experiments, continuous injections of Pu(V), Am(III), U(VI), Th(IV), and/or Np(V) by introducing synthetic AISinR or, in a few runs, synthetic ERDA-6 with low concentrations of the radionuclide(s) into a cavity cut in the top of each core. He then pumped additional brine through these cores at low flow rates (0.1 ml/min and, in a few runs, 0.05 ml/min) for periods of up to 237 days (equivalent to pumping up to 34.2 pore volumes of brine through these cores). These flow rates are at or close to the upper limit of the range of *in situ* fluid velocities. He collected the effluent continuously and analyzed it every 5 ml by  $\gamma$  spectrometry or LSC. He also used scanning  $\gamma$  emission tomography to image the cores. By injecting different radionuclides at different times and, in some cases, by using different brines, Lucero carried out multiple, sequential experiments with the same core. Because this study quantified actinide sorption from fluids flowing through intact samples of Culebra rock, it complements the static empirical and mechanistic sorption studies with crushed Culebra rock or pure dolomite. However, this study did not yield  $K_{ds}$  directly. For U and Np, which were moderately retarded by sorption, the observed delays between the elution peaks of nonsorbed radionuclides (such as  $^3\text{H}$  or  $^{22}\text{Na}$ ) and those of U and Np yielded discrete values for the retardation factors R, which were then used, along with porosities determined with the nonsorbing tracers, to calculate  $K_{ds}$ . For Pu, Am, and Th, which were strongly retarded by sorption, Lucero did not observe breakthrough, even after pumping brine through these cores for 61, 118, and 211 days (Pu and Am) and 133, 146, and 237 days (Th) (equivalent to 8.83, 17.0, and 30.4 pore volumes for Pu and Am, and 19.1, 21.0, and 34.2 pore volumes for Th). Therefore, he was only able to calculate minimum values of R and  $K_d$ . These minimum values depend on factors such as the initial concentration of each radionuclide, the volume of brine pumped through the core, and the analytical detection limit for the radionuclide.

## Predictions of Actinide Oxidation States in the Culebra

Because oxidation state significantly affects the chemical behavior, including sorption, of the actinide elements, predictions of the oxidation-state distributions of Pu, U, and Np in the Culebra are necessary to establish ranges and probability distributions of matrix  $K_d$ s for use in the PA calculations. For Pu, U, and Np, the following oxidation states are possible in low-temperature, geochemical systems: Pu(III), Pu(IV), Pu(V), and Pu(VI); U(IV) and U(VI); and Np(IV), Np(V), and Np(VI). For Am and Th, only one oxidation state, Am(III) or Th(IV), respectively, is possible.

We have used experimentally based predictions of the oxidation-state distributions of Pu, U, and Np in WIPP disposal rooms from the Actinide Source Term Program (ASTP) to specify the oxidation states of these elements in the Culebra. Based on a laboratory study carried out under expected WIPP conditions by D. Clark and his colleagues at LANL and previously published results obtained for applications other than the WIPP Project, ASTP personnel have predicted that Pu will speciate as Pu(III) or Pu(IV), but not as Pu(V) nor Pu(VI), that U will speciate as U(IV) and U(VI), and that Np will speciate as Np(IV) and Np(V), but not as Np(VI), in deep (Castile and Salado) brines in the repository. To evaluate the applicability of these predictions to the Culebra, H. W. Stockman of SNL carried out a modeling study of the oxidation states of Pu, U, and Np in the Culebra (see below). This study showed that Culebra fluids are poorly poised (have limited capacity to either oxidize or reduce actinide elements). Therefore, it is reasonable to use the oxidation-state distributions of Pu, U, and Np predicted for WIPP disposal rooms to specify the oxidation states of these elements in the Culebra. Using the ASTP predictions for the Culebra will ensure consistency between the oxidation-state distributions of these elements in WIPP disposal rooms and at the point of injection of deep (Castile or Salado) brines into the Culebra following human intrusion into the repository. This will in turn obviate the need to specify redox reactions in the Culebra, and the need to incorporate possible, concomitant dissolution and/or precipitation reactions in SECO, the PA model for Culebra flow and transport.

ASTP and PA personnel will calculate solubilities for *either* Pu(III), U(IV), and Np(IV), *or* Pu(IV), U(VI), and Np(V) in any given vector. PA will specify the oxidation states of these elements by sampling "oxstat," a parameter with a uniform probability distribution of 0 to 1. If the sampled value of oxstat is 0.5 or less, PA will use the solubilities predicted for Pu(III), U(IV), and Np(IV). (These solubilities are also sampled parameters.) If oxstat is greater than 0.5, PA will use solubilities for Pu(IV), U(VI), and Np(V). We recommend that PA use the ranges and distributions of  $K_d$ s for the oxidation states of Pu, U, and Np sampled for each vector.

This approach is equivalent to assuming that the oxidation-state distributions of Pu, U, and Np predicted for WIPP disposal rooms will be maintained along the



entire off-site transport pathway in the Culebra. (Previous PA calculations have predicted that, in the absence of climatic change, fluid will flow from the point of injection into the Culebra to the south or the southeast, and that the distance from the point of injection to the boundary of the Land Withdrawal Area will be about 2.5 or 3 km.) This assumption is certainly reasonable at the point of injection of deep brines into the Culebra and for some, perhaps significant, distance along the flow path. Because, in general, redox equilibrium is not observed in low-temperature aqueous solutions (see, for example, Lindberg and Runnells, 1984), the oxidation states of Pu, U, and Np predicted for the repository *could* persist along the entire flow path in the Culebra. At some point, however, the oxidation-state distributions of these elements *might* equilibrate with ambient conditions in the Culebra.

To evaluate the applicability of ASTP predictions to the Culebra, Stockman used the EQ3/6 geochemical software package (Daveler and Wolery, 1992; Wolery, 1992a, 1992b; Wolery and Daveler, 1992) to predict the oxidation-state distributions of Pu, U, and Np after mixing deep (Castile and Salado) brines containing these elements with Culebra brines. Stockman made various assumptions as to: (1) which naturally occurring or waste-derived dissolved species will control redox conditions in the deep brines after injection into the Culebra; (2) which naturally occurring dissolved or solid species control redox conditions in Culebra brines; (3) whether to use the data base in EQ3/6, or to modify it based on recently published studies of actinide chemistry. By calculating oxidation-state distributions of Pu, U, and Np before and after mixing deep brines with Culebra brines *under all possible combinations of these assumptions*, Stockman showed that Culebra fluids are poorly poised (have limited capacity to either oxidize or reduce actinide elements). Therefore, it is reasonable to assume that the oxidation-state distributions of Pu, U, and Np predicted for WIPP disposal rooms will be maintained along the entire off-site transport pathway.



### Predictions of Brine Mixing in the Culebra

Brine composition could also affect the sorptive behavior of actinide elements in the Culebra. Therefore, predictions of the extent to which deep (Castile and Salado) and Culebra brines mix in the Culebra are necessary to specify weighting factors to combine the ranges and probability distributions of matrix  $K_d$ s for dissolved Pu, Am, U, Th, and Np established for deep and Culebra brines and obtain an overall range and distribution for a given element or elemental oxidation state.

Opinions differ significantly on the extent to which deep and Culebra brines will mix in the Culebra. One extreme of a range of possibilities is that, because of the density difference between deep and Culebra brines and/or limited spreading due to heterogeneity, a "slug" of deep brine will flow along the entire off-site transport pathway without significant mixing. The other extreme is that, because

of relatively high heterogeneity, hydrodynamic dispersion will result in rapid mixing, and the composition of the injected fluid will resemble that of Culebra ground water on the order of hundreds of meters from the point of injection.

We are submitting these ranges and distributions to PA concurrently with the submission of Culebra hydrologic parameters by personnel from Geohydrology Department 6115. Therefore, we could not carry out brine-mixing calculations with the current hydrologic parameters prior to establishing these ranges and distributions. In the absence of mixing calculations, E. J. Nowak, Manager of Chemical & Disposal Room Processes Department 6831, instructed us to take the following, conservative approach: (1) establish *separate* ranges and distributions for deep and the Culebra brines for each actinide element or elemental oxidation state; (2) recommend that PA personnel use the range and distribution that results in less retardation for each element or elemental oxidation state.

#### Methods Used to Establish Ranges of Matrix $K_d$ s

This subsection briefly describes the methods used to establish ranges of matrix  $K_d$ s for dissolved Pu, Am, U, Th, and Np under conditions expected in the Culebra. We carried out most of the work described in this subsection at a meeting held April 1 and 2, 1996, here at the BDM Building. Sixteen SNL and SNL-subcontractor personnel working on or familiar with the RRP or related aspects of PA participated in all or part of this meeting. Two US DOE Carlsbad-Area-Office and Carlsbad-Technical-and-Administrative-Contractor personnel observed all or part of it. Appendix A (see below) contains the invitation to, agenda for, and list of the participants and observers at this meeting. (This and the other six appendices are available on request to anyone who did not receive them with this memorandum.) Detailed descriptions, including all of the empirical-sorption, mechanistic-sorption, and column-transport data considered and included or excluded, appear in Appendices B through F, respectively. Appendix G contains the results of experiments on the effects of four organic ligands on these  $K_d$ s.

At this meeting, we decided to establish *experimentally obtained* ranges for Am(III), U(VI), Th(IV), and Np(V), and to use the experimentally obtained ranges for Am(III) and Th(IV), and the oxidation-state analogy to establish ranges for Pu(III), and Pu(IV), U(IV), and Np(IV). Based on the ASTP predictions of oxidation-state distributions for Pu, U, and Np in WIPP disposal rooms and Stockman's predictions for the Culebra *under most of the possible combinations of assumptions* (see Predictions of Actinide Oxidation States in the Culebra above), we *did not* plan to establish an experimentally obtained range for Pu(V), nor to use the experimentally obtained range for U(VI) and the oxidation-state analogy to establish ranges for Pu(VI) and Np(VI).

We established *separate* ranges for the deep (Castile and Salado) and the Culebra brines for each actinide element or elemental oxidation state (see



Predictions of Brine Mixing in the Culebra above). However, we *did not* establish separate ranges for the two deep brines studied by Triay and her group in the LANL empirical sorption study (Brine A and ERDA-6) because the PA calculations carried out with the multiphase flow code Brine and Gas Flow to support the WIPP CCA have predicted that, in some vectors, the brine in WIPP disposal rooms will comprise mainly Castile brine; in other vectors, it will comprise mainly Salado brine; and in the rest, it will comprise various proportions of these and Culebra brines that will seep into the repository from above. (The latter brines will resemble Castile brines after reacting with Salado minerals.) Therefore, we established one range for Brine A and ERDA-6 to simulate these compositional variations. Similarly, the Culebra off-site transport pathway predicted by previous PA calculations (see Predictions of Actinide Oxidation States in the Culebra) contains ground waters that resemble *both* Culebra fluids used by Triay (AISinR and H-17). Therefore, we established one range and distribution for these fluids to simulate possible compositional variations along the flow path.

For U(VI), Th(IV), and Np(V) (see Appendices , we used the following methods to establish separate, *experimentally obtained* ranges for the deep and the Culebra brines. First, we considered *all* of the 6-week sorption data from the empirical study by Triay, the only experiments in which she has extensively studied the effects of dissolved actinide concentration on sorption. Because these are the only experiments carried out using a range of dissolved radionuclide concentrations, they are the only runs for which sorption isotherms have provided information on the nature of the reaction(s) responsible for removal of radionuclides from solution. (We will include these isotherms in the parameter and analysis records packages for these  $K_d$ s.) At the time of this meeting, Triay had not completed the 6-week desorption experiments. We would not, however, have included the results of the 6-week desorption runs, and did not include any data from the 3-day, nor the 1- nor 3-week desorption runs because these data could be artificially higher than those obtained from the sorption runs. Possible reasons for this include: (1) removal of a weakly sorbed actinide species concentrated in the aqueous phase by discarding the solution at the conclusion of a sorption experiment, thereby concentrating a strongly sorbed species prior to the start of a desorption run; (2) saturation of a sorption site with a high  $K_d$  followed by removal of the dissolved actinide after a sorption experiment, thereby resulting in sorption of a higher proportion of the actinide on the sorption site with a high  $K_d$  during the desorption run.

To establish the *initial* ranges for the deep brines, we first considered *all* the data obtained from the 6-week sorption experiments carried out with Brine A and ERDA-6 on the bench top (in contact with ambient atmospheric  $\text{CO}_2$ ). Atmospheric  $\text{CO}_2$  has a partial pressure of about  $10^{-3.5}$  atm, the lowest  $\text{CO}_2$  partial pressure used in the LANL study. This partial pressure is equivalent to a  $\text{CO}_2$  content of 0.033% in the LANL study. We did not use data from runs equilibrated with higher partial pressures of  $\text{CO}_2$  for the initial ranges for the deep

brines because we anticipate that an MgO backfill will be emplaced in WIPP disposal rooms to remove CO<sub>2</sub>. Next, we discarded the data from runs in which the difference between the activity of the radionuclide in a standard (the radionuclide-bearing brine with which runs were started) and that in a control (a run conducted identically to that of an actual run, but without any rock) exceeded 3σ, where the standard deviation σ equals the square root of the total number of LSC counts. Discarding these data yielded the *initial* ranges for deep brines.

To establish the *initial* ranges for the Culebra brines (AISinR and H-17), we first considered *all* the data obtained from the 6-week sorption experiments carried out on the bench top (0.033% CO<sub>2</sub>) and in glove boxes with atmospheres containing 0.24 and 1.4% CO<sub>2</sub>. These three atmospheres had CO<sub>2</sub> partial pressures of 10<sup>-3.5</sup>, 10<sup>-2.73</sup>, and 10<sup>-1.98</sup> atm, respectively. Siegel now considers this range more likely for groundwaters in the predicted off-site transport pathway than the previous range of 10<sup>-3.5</sup> to 10<sup>-1.50</sup> atm calculated for the Culebra as a whole by Siegel et al. (1991). We also discarded the data from runs in which the difference between the activity of the radionuclide in a standard and that in a control exceeded 3σ to obtain the *initial* ranges for Culebra brines.

We then compared these initial ranges with the data from the mechanistic sorption study by Brady and his colleagues at SNL and LANL. For the most part, we used Brady's data to extend Triay's empirical sorption data for the deep brines to the basic conditions expected to result from the use of an MgO backfill in WIPP disposal rooms. We assumed that, if mixing is sufficient to produce fluids with compositions similar to those of Culebra brines, the pH of these mixtures will also be similar to those of Culebra brines. Therefore, we *did not* use Brady's data to extend Triay's data for the Culebra brines to basic conditions. So far, Brady has reported data obtained with 0.05 and 0.5 M NaCl solutions, but not with 5 M NaCl. Therefore, we used only his data for 0.5 M NaCl and atmospheric CO<sub>2</sub> (the lowest CO<sub>2</sub> partial pressure used in this study) to extend Triay's data for the deep brines to basic conditions. This comparison yielded our *revised* ranges for the deep brines.

Next, we compared the revised ranges with the data from the transport study with intact Culebra cores by Lucero and his colleagues at SNL. Lucero carried out his experiments under ambient atmospheric conditions; therefore, the CO<sub>2</sub> content of these experiments was probably similar to that in the LANL bench-top runs. Because Lucero *did not* observe breakthrough of Th(IV) (nor of Pu(V) nor Am(III)), it was only possible to determine minimum values of K<sub>d</sub> for Th(IV) (and for Pu(V) and Am(III)). This minimum K<sub>d</sub> (and those for Pu(V)) are consistent with the revised ranges based on the empirical and mechanistic sorption studies. Lucero *did* observe breakthrough of U(VI) and Np(V) in his experiments. Therefore, it was possible to determine actual K<sub>d</sub>s for these elements. In most cases, the K<sub>d</sub>s determined for U(VI) and Np(V) from the transport study are less than the lower limits of the ranges obtained for these elements from the sorption studies. Therefore, we extended the revised ranges where necessary to obtain

*final* ranges for U(VI) and Np(V) in the deep brines (Castile and Salado) and Culebra brines (see Table 1).

Finally we used the experimentally obtained ranges for Th(IV) and the oxidation-state analogy to establish ranges for Pu(IV), U(IV), and Np(IV).

We attempted to use the same methods to establish experimentally obtained ranges for Am(III) (see Appendix C). Inspection of the sorption isotherms for the 6-week LANL sorption data, however, revealed that the  $K_d$ s are proportional to the final dissolved Am(III) concentration. (We did not observe significant trends such as this in the isotherms for U(VI), Th(IV), nor Np(V)). These trends suggest that sorption of Am by the container walls, precipitation of an Am-bearing solid phase, coprecipitation of Am by another phase, incomplete separation of the aqueous and the solid phases at the end of an experiment, or some combination of these processes occurred in the runs with Am(III). Triay carried out additional posttest analyses of the brines from some of her 6-week sorption experiments with Am(III) to determine, if possible, what caused these trends, and to redetermine these  $K_d$ s. However, she continued to obtain data that displayed trends similar to those described above, and thus cannot rule out the occurrence of processes other than sorption. Therefore, we recommend using the *experimentally obtained* ranges for Pu(V) (Appendix B) for Am(III) by assuming that the  $K_d$ s for Am(III) are greater than or equal to those for Pu(V). This assumption is reasonable in view of results such as those in Figure 5 of Canepa (1992). In this case, the Am(III)  $K_d$  obtained for the Yucca Mountain Project is about one order of magnitude higher than that obtained for Pu(V) under the same conditions. (We will cite additional examples of differences between the  $K_d$ s for Am(III) and Pu(V) in future reports and presentations.) We *have not* used the oxidation-state analogy to justify the use of Pu(V) data for Am(III); instead, this approach is based on *differences* in the behavior of these oxidation states. Furthermore, we recommend using the range for Am(III) for Pu(III) (Table 1); for this recommendation, we invoke the oxidation-state analogy.

#### Methods Used to Establish Probability Distributions of Matrix $K_d$ s

M. S. Tierney, the PA Parameter Task Leader, provided guidance on establishing probability distributions of parameters for use in the PA calculations to support the CCA (see Tierney, 1996a; 1996b).

The RRP has studied the effects of several factors on sorption (see Description of Laboratory Studies Used to Determine Matrix  $K_d$ s, Predictions of Actinide Oxidation States in the Culebra, and Predictions of Brine Mixing in the Culebra above). Papenguth and Behl (1996) designed these studies to encompass the ranges of these factors expected in the Culebra. Therefore, the ranges of matrix  $K_d$ s established above correspond to the expected ranges of these factors in the Culebra. However, because of uncertainties about the extent to which deep (Castile and Salado) and Culebra brines will mix, there are uncertainties as to the

probability distributions of these factors (especially brine type, the partial pressure of CO<sub>2</sub>, and the resulting pH) in the Culebra. Therefore, we *do not* recommend that PA use a Student t distribution based on the data included in these ranges, despite the fact that we included more than three data points for every range shown in Table 1.

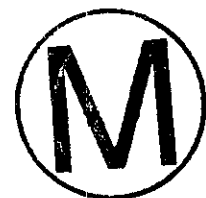
Tierney (1996a) states that use of the uniform or log-uniform [probability] distribution "is appropriate when all that is known about a parameter is its range." Because we cannot specify probability distributions for the factors that affect sorption, we recommend that PA personnel use a uniform or a log-uniform distribution. Tierney (1996a) specifies use of a log-uniform distribution "when the range ... spans many orders of magnitude." Inspection of the ranges for deep and Culebra brines in Table 1 reveals that these ranges span 1.40 and 2.60 orders of magnitude (deep and Culebra brines, respectively) for Pu(III) and Am(III); 1.35 orders of magnitude (deep brines only) for Pu(IV), U(IV), Th(IV), and Np(IV); 3.00 orders of magnitude (deep brines only) for U(VI); and 2.65 and 2.30 orders of magnitude (deep and Culebra brines, respectively) for Np(V). (Each of these values is the common logarithm of the maximum value of each range divided by its minimum value. We could not calculate this parameter for Th(IV) and Culebra brines because we were unable to establish this range; see Appendix E below. We could not calculate this parameter for the range for U(VI) and Culebra brines because its minimum value is 0.) Because these ranges all span three orders of magnitude or less, we recommend that PA use a uniform distribution instead of a log-uniform distribution for all of them.

#### Methods Used for Final Selection of the Range of Matrix K<sub>d</sub>s for Use in PA Calculations

We recommend that PA personnel use the range and probability distribution of matrix K<sub>d</sub>s for deep (Castile and Salado) or Culebra brines that results in less retardation for each element or elemental oxidation state (see Predictions of Brine Mixing in the Culebra above). Because we have recommended that PA use a uniform distribution for *all* the ranges (see Methods Used to Establish Probability Distributions of Matrix K<sub>d</sub>s above), the *average* K<sub>d</sub> that PA will sample for all of its vectors is the mean of the maximum and minimum values of each range. Therefore, we compared the means of the ranges for deep and Culebra brines to determine which range results in less retardation for each element or elemental oxidation state. Inspection of the ranges in Table 1 reveals that the means are 260 and 2005 ml/g (deep and Culebra brines, respectively) for Pu(III) and Am(III); 10,450 ml/g (deep brines only) for Pu(IV), U(IV), Th(IV), and Np(IV); 15.015 and 35 ml/g (deep and Culebra brines, respectively) for U(VI); and 451 and 100.5 ml/g (deep and Culebra brines, respectively) for Np(V). (Each of these values is the sum of the maximum and the minimum values of each range divided by two; to facilitate this comparison, we *did not* round each result to one significant figure. We could not calculate this parameter for Th(IV) and Culebra brines because we could not establish this range; see Appendix E below.)

Therefore, we recommend that PA use a range of 20 to 500 ml/g (the range for deep brines) for Pu(III) and Am(III); a range of 900 to 20,000 ml/g (deep brines) for Pu(IV), U(IV), Th(IV), and Np(IV); a range of 0.03 to 30 ml/g (deep brines) for U(VI); and a range of 1 to 200 ml/g (Culebra brines) for Np(V). In Table 1, these ranges appear in bold font.

Because the ASTP has decided to specify the oxidation states of Pu, U, and Np by sampling the "oxstat" parameter (see Predictions of Actinide Oxidation States in the Culebra), the range and distribution for each specified oxidation state will constitute the range and distribution for each of these elements during a given vector.



#### REFERENCES

- Canepa, J.A. 1992. *Proceedings of the DOE/Yucca Mountain Site Characterization Project Radionuclide Adsorption Workshop at Los Alamos National Laboratory, September 11-12, 1990.* LA-12325-C. Los Alamos, NM: Los Alamos National Laboratory.
- Daveler, S.A., and T.J. Wolery. 1992. *EQPT, A Data File Preprocessor for the EQ3/6 Software Package: User's Guide and Related Documentation (Version 7.0).* UCRL-MA-110662 PT II. Livermore, CA: Lawrence Livermore National Laboratory.
- Freeze, R.A., and J.A. Cherry. 1979. *Groundwater.* Englewood Cliffs, NJ: Prentice-Hall.
- Garner, J. 1996. "Radioisotopes to Be Used in the 1996 CCA Calculations." Unpublished memorandum to C. T. Stockman, March 15, 1996. Albuquerque, NM: Sandia National Laboratories.
- Molecke, M.A. 1983. *A Comparison of Brines Relevant to Nuclear Waste Experimentation.* SAND83-0516. Albuquerque, NM: Sandia National Laboratories.
- Lindberg, R.D., and D.D. Runnells. 1984. "Ground Water Redox Reactions: An Analysis of Equilibrium State Applied to Eh Measurements and Geochemical Modeling," *Science*. Vol. 225, no. 4665, 925-927.
- Molecke, M.A. 1983. *A Comparison of Brines Relevant to Nuclear Waste Experimentation.* SAND83-0516. Albuquerque, NM: Sandia National Laboratories.

- Papenguth, H.W. and Y.K. Behl. 1996. *Test Plan for Evaluation of Dissolved Actinide Retardation at the Waste Isolation Pilot Plant*. TP 96-02. Albuquerque, NM: Sandia National Laboratories.
- Popielak, R.S., R.L. Beauheim, S.R. Black, W.E. Coons, C.T. Ellingson and R.L. Olsen 1983. *Brine Reservoirs in the Castile Formation, Waste Isolation Pilot Plant Project, Southeastern New Mexico*. TME 3153. Carlsbad, NM: U.S. Department of Energy WIPP Project Office.
- Ramsey, J. 1996. "Culebra Dissolved Actinide Parameter Request." Unpublished memorandum to E. J. Nowak, March 18, 1996. Albuquerque, NM: Sandia National Laboratories.
- Sewards, T. 1991. *Characterization of Fracture Surfaces in Dolomite Rock, Culebra Dolomite Member, Rustler Formation*. SAND90-7019. Albuquerque, NM: Sandia National Laboratories.
- Sewards, T., A. Brearly, R. Glenn, I.D.R. MacKinnon, and M.D. Siegel. 1992. *Nature and Genesis of Clay Minerals of the Rustler Formation in the Vicinity of the Waste Isolation Pilot Plant in Southeastern New Mexico*. SAND90-2569. Albuquerque, NM: Sandia National Laboratories.
- Sewards, T., M.L. Williams, and K. Keil. 1991. "Mineralogy of the Culebra Dolomite," *Hydrogeochemical Studies of the Rustler Formation and Related Rocks in the Waste Isolation Pilot Plant Area, Southeastern New Mexico*. SAND88-0196. Eds. M.D. Siegel, S.J. Lambert, and K.L. Robinson. Albuquerque, NM: Sandia National Laboratories, 3-1 to 3-43.
- Siegel, M.D., K.L. Robinson, and J. Myers. 1991. "Solute Relationships in Groundwaters from the Culebra Dolomite and Related Rocks in the Waste Isolation Pilot Plant Area, Southeastern New Mexico," *Hydrogeochemical Studies of the Rustler Formation and Related Rocks in the Waste Isolation Pilot Plant Area, Southeastern New Mexico*. SAND88-0196. Eds. M.D. Siegel, S.J. Lambert, and K.L. Robinson. Albuquerque, NM: Sandia National Laboratories, 6-1 to 6-35.
- Tierney, M.S. 1996a. "Distributions." Unpublished memorandum to distribution, March 21, 1996. Albuquerque, NM: Sandia National Laboratories.
- Tierney, M.S. 1996b "Development of Parameter Values Distribution Functions." Unpublished memorandum to distribution, April 16, 1996. Albuquerque, NM: Sandia National Laboratories.



- WIPP Performance Assessment Department. 1992. *Preliminary Performance Assessment for the Waste Isolation Pilot Plant, December 1992. Volume 2: Technical Basis*. SAND92-0700/2. Albuquerque, NM: Sandia National Laboratories.
- Wolery, T.J. 1992a. *EQ3/6, A Software Package for Geochemical Modeling of Aqueous Systems: Package Overview and Installation Guide (Version 7.0)*. UCRL-MA-110662 PT I. Livermore, CA: Lawrence Livermore National Laboratory.
- Wolery, T.J. 1992b. *EQ3NR, A Computer Program for Geochemical Aqueous Speciation-Solubility Calculations: Theoretical Manual, User's Guide, and Related Documentation (Version 7.0)*. UCRL-MA-110662 PT III. Livermore, CA: Lawrence Livermore National Laboratory.
- Wolery, T.J., and S.A. Daveler. 1992. *EQ6, A Computer Program for Reaction-Path Modeling of Aqueous Geochemical Systems: Theoretical Manual, User's Guide, and Related Documentation (Version 7.0)*. UCRL-MA-110662 PT IV. Livermore, CA: Lawrence Livermore National Laboratory.

Table 1. Ranges of Matrix  $K_{ds}$  (ml/g) for Pu, Am, U, Th, and Np, and Dolomite-Rich Culebra Rook. Ranges in bold font to be used by PA. Oxidation state of Pu, U, and Np to be specified by the value of "oxstat" parameter sampled to calculate dissolved actinide concentrations in WIPP disposal rooms. All probability distributions are uniform (see text). Table compiled by L. H. Brush on April 3, 1996, based on results of meeting held April 1 and 2, 1996. Table checked by Brush and Y. Behl on April 3, 1996. Table revised by Brush on April 6, 1996, based on memo by D. A. Lucero and G. O. Brown dated April 5, 1996. Table checked by Behl on April 8, 1996.

Oxidation State	Element				
	Pu	Am	U	Th	Np
VI	NA	NA	<b>0.03 to 30<sup>A,C</sup></b> 0 to 70 <sup>B,C</sup>	NA	NA
V	NA	NA	NA	NA	2 to 900; <sup>A,C</sup> <b>1 to 200<sup>B,C</sup></b>
IV	<b>900 to 20,000;<sup>A,D</sup></b> NE	NA	<b>900 to 20,000;<sup>A,E</sup></b> NE	<b>900 to 20,000;<sup>A,C</sup></b> NE	<b>900 to 20,000;<sup>A,G</sup></b> NE
III	<b>20 to 500;<sup>A,H</sup></b> 10 to 4,000 <sup>B,H</sup>	<b>20 to 500;<sup>A,I</sup></b> 10 to 4,000 <sup>B,I</sup>	NA	NA	NA

A: range for deep (Castile and Salado) brines only (see text).

B: range for Culebra brines only (see text).

C: experimentally obtained range (see text).

D: experimentally obtained range for Th(IV) applied to Pu(IV) by oxidation-state analogy.

E: experimentally obtained range for Th(IV) applied to U(IV) by oxidation-state analogy.

F: experimentally obtained range for Th(IV) and deep brines applied to Th(IV) and Culebra brines.

G: experimentally obtained range for Th(IV) applied to Np(IV) by oxidation-state analogy.

H: experimentally obtained range for Pu(V) applied to Pu(III) (see text).

I: experimentally obtained range for Pu(V) applied to Am(III) (see text).

NA: not applicable (element will not speciate in this oxidation state).

NE: not established for Culebra brines (see Appendix E).

APPENDIX A: MEETING TO ESTABLISH RANGES AND PROBABILITY  
DISTRIBUTIONS OF ACTINIDE  $K_d$ s FOR THE WIPP PA  
CALCULATIONS AND THE CCA

Invitation



March 25, 1996

Dear Colleague:

Attached is the agenda for the meeting to establish ranges and probability distributions of actinide  $K_d$ s for use in the long-term performance-assessment (PA) calculations to support the WIPP Compliance Certification Application (CCA). We will hold this meeting at the BDM Sandia Vista Building at 2301 Buena Vista SE in Albuquerque, NM, on Monday and Tuesday, April 1 and 2, 1996. Currently, we plan to meet in the Nuclear Waste Management Conference Room, the large conference room, all day Monday and Tuesday morning, and in Room 2105, a small conference room, on Tuesday afternoon. Because a key is required to enter the building in which the large conference room is located, I or someone else will meet you in the reception area of the Sandia Vista Building at 8:45 on Monday morning to take you to the large conference room if you do not have a key.

I view this as our main opportunity to reach consensus on the ranges and probability distributions of  $K_d$ s for Pu, Am U, Th, and Np that we will submit to the US DOE's Carlsbad Area Office for their use in meeting the requirements of the Consultation and Cooperation (C & C) Agreement with the State of New Mexico, and then to PA personnel for their calculations to support the CCA.

Because most of you presented most of your results at the Retardation Research Program Review Meeting in Carlsbad last month, I have scheduled only one presentation for next week's meeting, Predictions of Actinide Oxidation States in the Culebra by Harlan Stockman of Sandia. However, please bring viewgraphs updated to include as many of your new data as possible for use in our discussions. Because you are very busy, please do not feel obligated to spend a lot of time making nice viewgraphs.

Thank you very much in advance for taking time out of your busy schedule to participate in this meeting. I am looking forward to your input next week.

Best regards,

Larry Brush  
WIPP Chemical & Disposal Room  
Processes Department 6748

Distribution:

R. J. Lark, DOE/CAO  
I. Triay, LANL  
MS 0750 P. V. Brady (Org. 6118)  
MS 0750 H. W. Stockman (Org. 6118)  
MS 1320 E. J. Nowak (Org. 6831)  
MS 1320 Y. Behl (Org. 6748)  
MS 1320 G. O. Brown (Org. 6748)  
MS 1320 K. G. Budge (Org. 6748)  
MS 1320 R. V. Bynum (Org. 6831)  
MS 1320 R. Holt (Org. 6748)  
MS 1320 D. A. Lucero (Org. 6748)  
MS 1320 H. W. Papenguth (Org. 6748)  
MS 1320 W. G. Perkins (Org. 6748)  
MS 1320 M. D. Siegel (Org. 6748)  
MS 1328 M. S. Tierney (Org. 6741)  
MS 1328 M. A. Martell (Org. 6749)  
MS 1335 M. S. Y. Chu (Org. 6801)  
MS 1337 W. D. Weart (Org. 6000)  
MS 1341 J. T. Holmes (Org. 6748)  
MS 1341 L. H. Brush (Org. 6748)  
MS 1341 L. J. Storz (Org. 6748)  
MS 1341 R. F. Weiner (Org. 6751)  
MS 1395 L. E. Shephard (Org. 6800)  
MS 1395 M. G. Marietta (Org. 6821)  
MS 1330 SWCF (Org. 6352), WBS 1.1.10.3.1 (2)



## Agenda

Monday and Tuesday, April 1 and 2, 1996  
BDM Sandia Vista Building  
2301 Buena Vista SE  
Albuquerque, NM

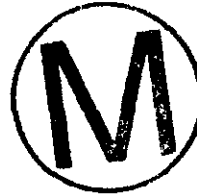
## Monday, April 1

9:00 - 9:30	Introduction	L. H. Brush, SNL
9:30 - 10:30	Predictions of Actinide Oxidation States in the Culebra	H. W. Stockman, SNL
10:30 - 10:45	Break	
10:45 - 11:45	Proposed Use of Ranges and Distributions of $K_d$ s by PA	M. S. Tierney, SNL
11:45 - 13:00	Lunch	BDM Cafeteria
13:00 - 15:00	Discussion of Range and Distribution of $K_d$ s for Pu(V)	All participants
15:00 - 15:15	Break	
15:15 - 17:15	Discussion of Range and Distribution of $K_d$ s for Am(III) and Pu(III)	All participants

## Agenda (continued)

Tuesday, April 2

8:00 - 10:00	Discussion of Range and Distribution of $K_d$ s for Th(IV), Pu(IV), and U(IV)	All participants
10:00 - 10:15	Break	
10:15 - 11:45	Discussion of Range and Distribution of $K_d$ s for U(VI) and, if necessary, Pu(VI)	All participants
11:45 - 13:00	Lunch	BDM Cafeteria
13:00 - 13:30	Discussion of Range and Distribution of $K_d$ s for U(VI) (continued)	All participants
13:30 - 13:45	Break	
13:45 - 15:45	Discussion of Range and Distribution of $K_d$ s for Np(V)	All participants



## Participants

- Y. Behl, SciRes (SNL column transport study)
- P. V. Brady, SNL (Principal Investigator for the SNL/LANL mechanistic sorption study)
- L. H. Brush, SNL (Principal Investigator for the dissolved-actinide Retardation Research Program (RRP))
- R. V. Bynum, SAIC (Actinide Source Term Program management)
- C. Duffy, independent LANL contractor (LANL empirical sorption study)
- K. M. Economy, Ecodynamics (PA Culebra transport calculations)
- R. Holt, independent SNL contractor (characterization of clay minerals in the Culebra)
- E. J. Nowak, SNL (Manager, WIPP Chemical & Disposal Room Processes Department 6748)
- H. W. Papenguth, SNL (former Principal Investigator for the dissolved-actinide RRP)
- W. G. Perkins, SNL (Retardation Research Program management)
- M. D. Siegel, SNL (Principal Investigator for the Stanford mechanistic sorption study, brine mixing, and characterization of clay minerals in the Culebra)
- H. W. Stockman, SNL (predictions of actinide oxidation states in the Culebra)
- C. T. Stockman, SNL (predictions of actinide oxidation states in the Culebra)
- M. S. Tierney, SNL (Task Leader for the PA database)
- I. Triay, LANL (Group Leader, Chemical Science and Technology Group, and Principal Investigator for the LANL empirical sorption study)
- R. F. Weiner, SNL (Actinide Source Term Program)

## Observers

- D. Hobart, Carlsbad Administrative and Technical Assistance Contractor (Actinide Source Term Program, Retardation Research Program)
- R. J. Lark, US DOE Carlsbad Area Office

APPENDIX B: RANGES AND PROBABILITY DISTRIBUTIONS OF  
MATRIX  $K_d$ s FOR Pu(V) AND DOLOMITE-RICH  
CULEBRA ROCK

Based on a laboratory study carried out under expected WIPP conditions and previously published results obtained for applications other than the WIPP Project, ASTP personnel have predicted that Pu will speciate as Pu(III) or Pu(IV), but not as Pu(V) nor Pu(VI), in deep (Castile and Salado) brines in the repository. Furthermore, a modeling study of the effects of mixing deep and Culebra brines on the oxidation states of Pu, U, and Np in the Culebra showed that Culebra fluids are poorly poised (see Predictions of Actinide Oxidation States in the Culebra above). Therefore, Pu will not speciate as Pu(V) in the Culebra. However, we could not establish experimentally obtained ranges of matrix  $K_d$ s for Am(III) (see Methods Used to Establish Ranges of Matrix  $K_d$ s above and Appendix C below). Instead, we established experimentally obtained ranges for Pu(V) and used them for Am(III) and Pu(III) by assuming that the  $K_d$ s for Am(III) and Pu(III) are greater than or equal to those for Pu(V).

To establish the *initial* ranges for Pu(V) and the deep brines, we first considered *all* of the data from the 6-week empirical sorption experiments carried out with Brine A and ERDA-6 on the bench top (0.033% CO<sub>2</sub>) by Triay and her group at LANL (see Methods Used to Establish Ranges of Matrix  $K_d$ s for the reasons for considering these data). These runs were: #6004, #6024, #6044, #6064, and #6084 (see Table B-1 below), and #6005, #6025, #6045, #6065, and #6085 (Table B-2). Next, we discarded the data from #6025, #6045, and #6065, the runs in which the difference between the activity of the <sup>239</sup>Pu in a standard and that in a control exceeded 3 $\sigma$ , where  $\sigma$  is the standard deviation (see Methods Used to Establish Ranges of Matrix  $K_d$ s.) Discarding the data from these three runs yielded an *initial* range of 22.7 ml/g (from #6004) to 459 ml/g (#6005) for Pu(V) and the deep brines.

To establish the *initial* ranges for Pu(V) and the Culebra brines, we first considered *all* of Triay's 6-week sorption data obtained with AISinR and H-17 on the bench top (0.033% CO<sub>2</sub>) and in glove boxes with atmospheres containing 0.24 and 1.4% CO<sub>2</sub> (see Methods Used to Establish Ranges of Matrix  $K_d$ s). These were: #6006, #6026, #6046, #6066, #6086, #24006, #24026, #24046, #24066, #24086, #12006, #12026, #12046, #12066, and #12086 (Table B-3), and #6007, #6027, #6047, #6067, #6087, #24007, #24027, #24047, #24067, #24087, #12007, #12027, #12047, #12067, and #12087 (Table B-4). We then discarded the data from #6006, #24006, #24066, and #6007, the runs in which the difference between the activity of the <sup>239</sup>Pu in a standard and that in a control exceeded 3 $\sigma$ , to obtain the *initial* range of 9.61 ml/g (from #12007) to 3,620 ml/g (#12046) for Pu(V) and the Culebra brines.

Next, we compared these initial ranges with the data from the mechanistic sorption study by Brady and his colleagues at SNL and LANL. We used Brady's data to extend Triay's empirical sorption data for the deep brines to the basic conditions expected to result from the use of an MgO backfill in WIPP disposal rooms, *but not* to extend



Triay's data for the Culebra brines to basic conditions (see Methods Used to Establish Ranges of Matrix  $K_{ds}$ ). Brady's data for 0.5 M NaCl, atmospheric  $\text{CO}_2$ , and the highest pH values under these conditions are (to three significant figures) 350 and 411 ml/g at a pH of 9.87 and 9.88, respectively (Table B-5). Because these values are *within* the initial range for Pu(V) and the deep brines (see above), and because we did not use this comparison to extend the initial range for Pu(V) and the Culebra brines to basic conditions, our *revised* ranges for Pu(V) remain 22.7 to 459 ml/g and 9.61 to 3,620 ml/g for the deep and Culebra brines, respectively.

We then compared both of these revised ranges with the data from the transport study with intact Culebra cores by Lucero and his colleagues at SNL. Lucero carried out his experiments under ambient atmospheric conditions; therefore, the  $\text{CO}_2$  content of these experiments was probably similar to that in Triay's bench-top (0.033%  $\text{CO}_2$ ) runs. Because Lucero *did not* observe breakthrough of Pu(V), it was only possible to determine a minimum  $K_d$  for this element. Lucero and his colleagues submitted their results on March 28, 1996, (see Table B-6), then revised them on April 5 and 16, 1996 (Tables B-7 and B-8, respectively). The minimum  $K_{ds}$  reported for experiments C-3, D3, and E-2 (Table B-8) *are consistent with the  $K_{ds}$  reported by Triay for Pu(V) and AISinR in her experiments carried out on the bench top* (0.033%  $\text{CO}_2$ ) (Table B-3). Because these values are consistent with the revised range for Pu(V) and the Culebra brines (see above), and because Lucero did not carry out any experiments with Pu(V) and the deep brines (Table B-8), our *final* ranges for Pu(V) remain 22.7 to 459 ml/g and 9.61 to 3,620 ml/g for the deep and Culebra brines, respectively. However, we rounded these ranges to 20 to 500 ml/g and 10 to 4,000 ml/g, respectively prior to inclusion in Table 1 above.

We recommend that PA personnel use a uniform probability distribution for both of these ranges (see Methods Used to Establish Probability Distributions of Matrix  $K_{ds}$  above).

Furthermore, we recommend that PA use the range of 20 to 500 ml/g (the range for deep brines) for Pu(V) because this range results in less retardation of this element than the range for Culebra brines (see Methods Used for Final Selection of the Range of Matrix  $K_{ds}$  for Use in PA Calculations above).

Finally, we recommend that PA use a range of 20 to 500 ml/g for Pu(III) and Am(III) (see Methods Used to Establish Ranges of Matrix  $K_{ds}$  and Appendix C).



Table B-1. Effects of Initial Radionuclide Concentration and  $P_{CO_2}$  on Matrix  $K_d$ s for Pu(V), Dolomite-Rich Culebra Rock, and Brine A (LANL Empirical Sorption Study). Six-week sorption runs with VPX-25-8. No  $K_d$ s in this table excluded from ranges and distributions because of unacceptable differences between standards and controls. Data current as of April 3, 1996. Table compiled by L. H. Brush on March 23 and 30, 1996, based on information provided by LANL on March 19 and 26, 1996. Table checked by Brush and S. Boone on April 3, 1996. Table revised by Brush on June 7, 1996. Table checked by L. J. Storz on June 10, 1996.

Brine	Range of Initial $^{239}\text{Pu}$ Conc. (M)	$K_d$ (ml/g), 0.033% $\text{CO}_2$	$K_d$ (ml/g), 0.24% $\text{CO}_2$	$K_d$ (ml/g), 1.4% $\text{CO}_2$	$K_d$ (ml/g), 4.1% $\text{CO}_2$
Brine A	$1.98 \times 10^{-7}$ to $2.39 \times 10^{-7}$	22.7, #6004	23.7, #24004	31.9, #12004	28.3 #18004
Brine A	$1.11 \times 10^{-8}$ to $5.28 \times 10^{-8}$	54.9, #6024	261, #24024	38.5, #12024	35.9 #18024
Brine A	$2.38 \times 10^{-8}$ to $3.16 \times 10^{-8}$	28.0, #6044	34.6, #24044	43.9 #12044	39.4 #18044
Brine A	$3.78 \times 10^{-9}$ to $7.03 \times 10^{-9}$	27.2, #6064	30.5, #24064	65.0 #12064	32.1 #18064
Brine A	$3.08 \times 10^{-9}$ to $3.37 \times 10^{-9}$	28.6, #6084	30.5, #24084	31.2 #12084	30.3 #18084

Table B-2. Effects of Initial Radionuclide Concentration and  $P_{CO_2}$  on Matrix  $K_d$ s for Pu(V), Dolomite-Rich Culebra Rock, and ERDA-6 (LANL Empirical Sorption Study). Six-week sorption runs with VPX-25-8.  $K_d$ s in bold font excluded from ranges and distributions because of unacceptable differences between standards and controls. Data current as of April 3, 1996. Table compiled by L. H. Brush on March 23 and 30, 1996, based on information provided by LANL on March 19 and 26, 1996. Table checked by Brush and S. Boone on April 3, 1996. Table revised by Brush on June 7, 1996. Table checked by L. J. Storz on June 10, 1996.

Brine	Range of Initial $^{239}\text{Pu}$ Conc. (M)	$K_d$ (ml/g), 0.033% $\text{CO}_2$	$K_d$ (ml/g), 0.24% $\text{CO}_2$	$K_d$ (ml/g), 1.4% $\text{CO}_2$	$K_d$ (ml/g), 4.1% $\text{CO}_2$
ERDA-6	1.45 x 10 <sup>-9</sup> to 6.01 x 10 <sup>-8</sup>	459, #6005	6,890, #24005	7,070, #12005	151 #18005
ERDA-6	3.88 x 10 <sup>-10</sup> to 1.24 x 10 <sup>-8</sup>	<b>3,920,</b> <b>#6025</b>	<b>6,500,</b> <b>#24025</b>	6,960 #12025	205 #18025
ERDA-6	2.36 x 10 <sup>-10</sup> to 6.35 x 10 <sup>-9</sup>	<b>2,980,</b> <b>#6045</b>	<b>3,040,</b> <b>#24045</b>	7,540 #12045	253 #18045
ERDA-6	1.59 x 10 <sup>-10</sup> to 1.67 x 10 <sup>-9</sup>	<b>677,</b> <b>#6065</b>	1,140, #24065	1,970 #12065	170 #18065
ERDA-6	3.29 x 10 <sup>-11</sup> to 1.20 x 10 <sup>-10</sup>	147, #6085	<b>1,180,</b> <b>#24085</b>	<b>1,460</b> <b>#12085</b>	4,550 #18085

Table B-3. Effects of Initial Radionuclide Concentration and  $P_{CO_2}$  on Matrix  $K_d$ s for Pu(V), Dolomite-Rich Culebra Rock, and AISinR (LANL Empirical Sorption Study). Six-week sorption runs with VPX-25-8.  $K_d$ s in bold font excluded from ranges and distributions because of unacceptable differences between standards and controls. Data current as of April 3, 1996. Table compiled by L. H. Brush on March 23 and 30, 1996, based on information provided by LANL on March 19 and 26, 1996. Table checked by Brush and S. Boone on April 3, 1996. Table revised by Brush on June 7, 1996. Table checked by L. J. Storz on June 10, 1996.

Brine	Range of Initial $^{239}\text{Pu}$ Conc. (M)	$K_d$ (ml/g), 0.033% $\text{CO}_2$	$K_d$ (ml/g), 0.24% $\text{CO}_2$	$K_d$ (ml/g), 1.4% $\text{CO}_2$	$K_d$ (ml/g), 4.1% $\text{CO}_2$
AISinR	$1.76 \times 10^{-9}$ to $9.71 \times 10^{-8}$	<b>348,</b> <b>#6006</b>	<b>62.5,</b> <b>#24006</b>	1,890, #12006	4,100 #18006
AISinR	$4.22 \times 10^{-10}$ to $3.91 \times 10^{-8}$	1,990, #6026	37.2, #24026	1,050 #12026	5,050, #18026
AISinR	$1.91 \times 10^{-10}$ to $1.85 \times 10^{-8}$	221, #6046	39.8, #24046	3,620 #12046	6,260 #18046
AISinR	$1.20 \times 10^{-10}$ to $3.18 \times 10^{-9}$	435, #6066	<b>50.3,</b> <b>#24066</b>	848 #12066	1,910 #18066
AISinR	$8.43 \times 10^{-11}$ to $1.93 \times 10^{-9}$	499, #6086	42.9, #24086	1,070, #12086	1,360 #18086

Table B-4. Effects of Initial Radionuclide Concentration and  $P_{CO_2}$  on Matrix  $K_d$ s for Pu(V), Dolomite-Rich Culebra Rock, and H-17 (LANL Empirical Sorption Study). Six-week sorption runs with VPX-25-8.  $K_d$ s in bold font excluded from ranges and distributions because of unacceptable differences between standards and controls. Data current as of April 3, 1996. Table compiled by L. H. Brush on March 23 and 30, 1996, based on information provided by LANL on March 19 and 26, 1996. Table checked by Brush and S. Boone on April 3, 1996. Table revised by Brush on June 7, 1996. Table checked by L. J. Storz on June 10, 1996.

Brine	Range of Initial $^{239}\text{Pu}$ Conc. (M)	$K_d$ (ml/g), 0.033% $\text{CO}_2$	$K_d$ (ml/g), 0.24% $\text{CO}_2$	$K_d$ (ml/g), 1.4% $\text{CO}_2$	$K_d$ (ml/g), 4.1% $\text{CO}_2$
H-17	$5.94 \times 10^{-8}$ to $3.01 \times 10^{-7}$	<b>157,</b> <b>#6007</b>	89.5, #24007	9.61, #12007	26.7 #18007
H-17	$4.55 \times 10^{-9}$ to $7.16 \times 10^{-8}$	191, #6027	155, #24027	13.3 #12027	33.5 #18027
H-17	$3.80 \times 10^{-9}$ to $3.18 \times 10^{-8}$	332, #6047	183, #24047	<b>14.3</b> <b>#12047</b>	36.6 #18047
H-17	$9.35 \times 10^{-10}$ to $5.48 \times 10^{-9}$	256, #6067	182, #24067	25.2 #12067	43.7 #18067
H-17	$2.01 \times 10^{-10}$ to $2.00 \times 10^{-9}$	235, #6087	637, #24087	93.9 #12087	45.8 #18087



Table B-5. Effects of pH and  $P_{CO_2}$  on Matrix  $K_d$ s for Pu(V) and Pure Dolomite (SNL/LANL Mechanistic Sorption Study). Sorption runs with Norwegian dolomite and 0.5 M NaCl. Data current as of March 31, 1996. Table retyped by L. H. Brush on April 24, 1996. Table checked by Y. Behl on April 28, 1996.

pH (standard units)	$K_d$ (ml/g), atmospheric $CO_2$	$K_d$ (ml/g), 0.5% $CO_2$	$K_d$ (ml/g), 5% $CO_2$
9.88	410.9	NA	NA
9.87	349.56	NA	NA
8.42	0	NA	NA
6.7	-44.928	NA	NA
6.2	34.662	NA	NA
5.81	34.662	NA	NA
5.21	34.662	NA	NA
4.62	128.72	NA	NA
4.05	-113.15	NA	NA
3.51	-44.928	NA	NA
3.11	-310.23	NA	NA

NA: not applicable.



Table B-5. Effects of pH and  $P_{CO_2}$  on Matrix  $K_d$ s for Pu(V) and Pure Dolomite (SNL/LANL Mechanistic Sorption Study) (continued).

pH (standard units)	$K_d$ (ml/g), atmospheric $CO_2$	$K_d$ (ml/g), 0.5% $CO_2$	$K_d$ (ml/g), 5% $CO_2$
6.9	NA	465.69	NA
8.49	NA	3711.1	NA
7.32	NA	1029.4	NA
7.19	NA	1162.5	NA
6.99	NA	968.83	NA
6.88	NA	418.41	NA
6.55	NA	319.12	NA
6.17	NA	570.38	NA
5.28	NA	199.2	NA
3.97	NA	99.265	NA
3.13	NA	99.265	NA

NA: not applicable.

Table B-5. Effects of pH and  $P_{CO_2}$  on Matrix  $K_d$ s for Pu(V) and Pure Dolomite (SNL/LANL Mechanistic Sorption Study) (continued).

pH (standard units)	$K_d$ (ml/g), atmospheric $CO_2$	$K_d$ (ml/g), 0.5% $CO_2$	$K_d$ (ml/g), 5% $CO_2$
6.39	NA	NA	124.82
6.91	NA	NA	499.76
6.89	NA	NA	NR
6.8	NA	NA	499.76
6.75	NA	NA	520.02
6.84	NA	NA	371.73
6.49	NA	NA	423.82
6.07	NA	NA	222.63
5.76	NA	NA	147.77
4.91	NA	NA	22.561
3.62	NA	NA	124.82

NA: not applicable.

NR: not reported.

Table B-6. Minimum Values of R and  $K_d$  for Pu(V) in Intact Culebra Cores (SNL Column Transport Study). Data current as of March 26, 1996. Table compiled by L. H. Brush on March 30, 1996, based on memo by D. A. Lucero, G. O. Brown, and K. G. Budge dated March 28, 1996. Table checked by Brush on March 31, 1996.

Run #	Solid (core)	Brine	Flow rate (ml/min)	Run Time (days)	Ef-fluent Vol. (L)	$R_{min}$	Porosity (%)	$K_{d, min}$ (ml/g)	Range ( $\pm$ ml/g)
C-3	VPX-28-6C	AIS.	0.1	211	30.45	5,200	3.7 <sup>S</sup>	84	NA
D-3	VPX-25-8A	AIS.	0.1	118	17.02	1,140	9.1, <sup>S</sup> 5.3 <sup>D</sup>	46	NA
E-2	VPX-27-7A	AIS.	0.1	61	8.83	405	23, <sup>S</sup> 15.7 <sup>D</sup>	40	NA

AIS: AISinR.

D: dual porosity assumed.

NA: not available yet.

S: single porosity assumed.

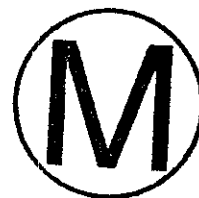


Table B-7. Minimum Values of R and  $K_d$  for Pu(V) in Intact Culebra Cores (SNL Column Transport Study). Data current as of March 26, 1996. Table compiled by L. H. Brush on March 30, 1996, based on memo by D. A. Lucero, G. O. Brown, and K. G. Budge dated March 28, 1996. Table checked by Brush on March 31, 1996. Table revised by Brush on April 6, 1996, based on memo by Lucero and Brown dated April 5, 1996. Table checked by Y Behl on April 8, 1996.



Run #	Solid (core)	Brine	Flow rate (ml/min)	Run Time (days)	Ef-fluent Vol. (L)	$R_{min}$	Porosity (%)	$K_{d, min}$ (ml/g)	Range ( $\pm$ ml/g)
C-3	VPX-28-6C	AIS.	0.1	211	30.45	5,200	3.7 <sup>S</sup>	84	NA
D-3	VPX-25-8A	AIS.	0.1	118	17.02	1,140	9.1 <sup>S</sup>	46	NA
E-2	VPX-27-7A	AIS.	0.1	61	8.83	405	23 <sup>S</sup>	40	NA

AIS: AISinR.

NA: not available yet.

S: single porosity assumed.

Table B-8. Minimum Values of R and  $K_d$  for Pu(V) in Intact Culebra Cores (SNL Column Transport Study). Data current as of March 26, 1996. Table compiled by L. H. Brush on March 30, 1996, based on memo by D. A. Lucero, G. O. Brown, and K. G. Budge dated March 28, 1996. Table checked by Brush on March 31, 1996. Table revised by Brush on April 6, 1996, based on memo by Lucero and Brown dated April 5, 1996. Table checked by Y Behl on April 8, 1996. Table revised by Brush on April 17, 1996, based on memo by Brown dated April 16, 1996.

Run #	Solid (core)	Brine	Flow rate (ml/min)	Run Time (days)	Ef-fluent Vol. (L)	$R_{min}$	Porosity (%)	$K_{d, min}$ (ml/g)	Range ( $\pm$ ml/g)
C-3	VPX-28-6C	AIS.	0.1	211	30.45	5,200	3.7 <sup>S</sup>	84	NA
D-3	VPX-25-8A	AIS.	0.1	118	17.02	1,140	9.1 <sup>S</sup>	45	NA
E-2	VPX-27-7A	AIS.	0.1	61	8.83	405	23 <sup>S</sup>	40	NA

AIS: AISinR.

NA: not available yet.

S: single porosity assumed.



APPENDIX C: RANGES AND PROBABILITY DISTRIBUTIONS OF  
MATRIX  $K_d$ s FOR Am(III) AND DOLOMITE-RICH  
CULEBRA ROCK

For Am, only one oxidation state, Am(III), is possible in the Culebra (see Predictions of Actinide Oxidation States in the Culebra above). Therefore, we attempted to establish experimentally obtained ranges of matrix  $K_d$ s for Am(III), and use them and the oxidation-state analogy to establish ranges for Pu(III).

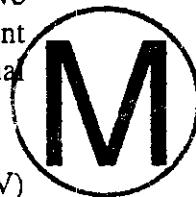
To establish the *initial* ranges for Am(III) and the deep brines, we first considered *all* of the data from the 6-week empirical sorption experiments carried out with Brine A and ERDA-6 on the bench top (0.033% CO<sub>2</sub>) by Triay and her group at LANL (see Methods Used to Establish Ranges of Matrix  $K_d$ s above for the reasons for considering these data). These runs were: #6012, #6032, #6052, #6072, and #6092 (see Table C-1), and #6013, #6033, #6053, #6073, and #6093 (see Table C-2 below). We discarded the data from #6012, #6032, #6013, #6033, #6073, and #6093, the runs in which the difference between the activity of the <sup>243</sup>Am in a standard and that in a control exceeded 3 $\sigma$ , where  $\sigma$  is the standard deviation (see Methods Used to Establish Ranges of Matrix  $K_d$ s.) Even after discarding the results of these six runs, however, the defensibility of the remaining data is questionable because the  $K_d$ s retained for Brine A increase significantly as the final dissolved concentration of <sup>243</sup>Am increases. (We will include these isotherms in the parameter and analysis records packages for these  $K_d$ s. However, this trend is also apparent in Table C-1.) Furthermore, the isotherm obtained by plotting the quantity of radionuclide sorbed by the solid phase or phases versus the final dissolved radionuclide concentration does not appear to pass through the origin. The  $K_d$ s are also proportional to the final dissolved <sup>243</sup>Am concentration in the runs carried out in the glove box with an atmosphere containing 1.4% CO<sub>2</sub>, and, based on the trends observed with *both* retained and discarded data, *appeared* to increase similarly in the runs conducted in the glove boxes with atmospheres containing 0.24 and 4.1% CO<sub>2</sub> (see Table C-1). Moreover, based on the trends observed with *both* retained and discarded data, these  $K_d$ s also *appear* proportional to the final dissolved <sup>243</sup>Am concentration at all four CO<sub>2</sub> concentrations in the runs with ERDA-6 (Table C-2). These trends suggest that sorption of Am by the container walls, precipitation of an Am-bearing solid phase, coprecipitation of Am by another phase, incomplete separation of the aqueous and the solid phases at the end of an experiment, or some combination of these processes occurred in the runs with Am(III). We thought we had eliminated reactions other than sorption by the rock in these experiments because: (1) LANL personnel had filtered the brines sequentially, with a minimum filter size of 0.2  $\mu$ m, after these runs; (2) we had discarded results from the runs in which the difference between the activity of the radionuclide in the standard and that in the control exceeded 3 $\sigma$  before examining these data; (3) the final Am(III) concentrations in these runs were less than the solubilities predicted by FMT for these brines. Triay carried out additional posttest analyses of the brines from her 6-week sorption experiments with Am(III) with 0.033% CO<sub>2</sub> to determine, if possible, what caused these trends, and to redetermine these  $K_d$ s. She did not attempt any additional posttest analyses of the brines from experiments conducted in the glove boxes because

she had removed them from these glove boxes after the original runs, thus exposing them to conditions different from those during the runs. Triay first recounted the brines to determine if mistaken sample identification or improper data entry had caused the trends described above. She then refiltered, centrifuged, and/or ultracentrifuged the brines to remove any suspended particles, and recounted them. Finally, she recalculated the  $K_d$ s using the controls instead of the standards to specify the initial dissolved  $^{243}\text{Am}$  concentration. Despite these efforts, the data continued to display trends similar to those described above.

The 6-week LANL sorption experiments carried out with Am(III) and the Culebra brines (AISinR and H-17) yielded the same trends described above for the deep brines (compare Tables C-3 and C-4 with Tables C-1 and C-2). Therefore, we could not use them to establish a range for Am(III).

We did not use the data from the mechanistic sorption study by Brady and his colleagues at SNL and LANL, nor the column transport study by Lucero and his colleagues at SNL to establish a range for Am(III) for several reasons. First, Brady had used pure Norwegian dolomite and pure NaCl solutions, not actual Culebra dolomite and synthetic Culebra fluids. (Although we used his data to *extend* the initial ranges established with Triay's empirical data to the basic conditions expected to result from the use of an MgO backfill in WIPP disposal rooms, we *did not* believe this would be defensible in the absence of *any* empirical data for actual Culebra dolomite and synthetic Culebra fluids.) Furthermore, Brady's data for Am(III) with atmospheric and 0.5%  $\text{CO}_2$  (see Table C-6), the headspace concentrations corresponding to  $\text{CO}_2$  partial pressures within the range that Siegel now considers likely for groundwaters in the Culebra off-site transport pathway (see Methods Used to Establish Ranges of Matrix  $K_d$ s), were all "high" above a pH of about 5 or 6. ("High" means that insufficient  $^{243}\text{Am}$  remained in solution after these runs to determine a  $K_d$ ). Moreover, although Brady *did* obtain data for Nd(III) with atmospheric and 0.5%  $\text{CO}_2$  at neutral or nearly neutral values of pH (Table C-5), he also obtained them with pure Norwegian dolomite and pure NaCl solutions, not actual Culebra dolomite and synthetic Culebra fluids. Finally, because Lucero *did not* observe breakthrough of Am(III), it is only possible to determine minimum  $K_d$ s for this element (Tables C-7 through C-9). These minimum values are significantly lower than actual Am(III)  $K_d$ s typically obtained for applications other than the WIPP Project (see below).

Therefore, we recommend using the *experimentally obtained* ranges for Pu(V) (see Table 1 and Appendix B above) for Am(III) by assuming that the  $K_d$ s for Am(III) are greater than or equal to those for Pu(V). This assumption is reasonable in view of results such as those in Figure 5 of Canepa (1992). In this case, the Am(III)  $K_d$  obtained for the Yucca Mountain Project is about one order of magnitude higher than that obtained for Pu(V) under the same conditions. (We will cite additional examples of differences between the  $K_d$ s for Am(III) and Pu(V) in future reports and presentations.) We *have not* used the oxidation-state analogy to justify the use of Pu(V) data for Am(III); instead, this approach is based on *differences* in the behavior of these oxidation states. Furthermore, we recommend using the range for Am(III) for Pu(III); for this recommendation, we *have* used the oxidation-state analogy.



## REFERENCE

Canepa, J.A. 1992. *Proceedings of the DOE/Yucca Mountain Site Characterization Project Radionuclide Adsorption Workshop at Los Alamos National Laboratory, September 11-12, 1990*. LA-12325-C. Los Alamos, NM: Los Alamos National Laboratory.



Table C-1. Effects of Initial Radionuclide Concentration and  $P_{CO_2}$  on Matrix  $K_d$ s for Am(III), Dolomite-Rich Culebra Rock, and Brine A (LANL Empirical Sorption Study). Six-week sorption runs with VPX-25-8:  $K_d$ s in bold font excluded from ranges and distributions because of unacceptable differences between standards and controls. Data current as of April 3, 1996. Table compiled by L. H. Brush on March 23 and 30, 1996, based on information provided by LANL on March 19 and 26, 1996. Table checked by Brush and S. Boone on April 3, 1996. Table revised by Brush on June 7, 1996. Table checked by L. J. Storz on June 10, 1996.

Brine	Range of Initial $^{243}\text{Am}$ Conc. (M)	$K_d$ (ml/g), 0.033% $\text{CO}_2$	$K_d$ (ml/g), 0.24% $\text{CO}_2$	$K_d$ (ml/g), 1.4% $\text{CO}_2$	$K_d$ (ml/g), 4.1% $\text{CO}_2$
Brine A	$1.72 \times 10^{-9}$ to $2.95 \times 10^{-9}$	<b>965,</b> <b>#6012</b>	<b>1,040,</b> <b>#24012</b>	1,320, #12012	<b>1,260,</b> <b>#18012</b>
Brine A	$1.13 \times 10^{-9}$ to $1.47 \times 10^{-9}$	<b>927,</b> <b>#6032</b>	<b>1,120,</b> <b>#24032</b>	1,140, #12032	<b>1,070,</b> <b>#18032</b>
Brine A	$4.64 \times 10^{-10}$ to $5.61 \times 10^{-10}$	509, #6052	521, #24052	553, #12052	597, #18052
Brine A	$3.31 \times 10^{-10}$ to $4.14 \times 10^{-10}$	330, #6072	356, #24072	392, #12072	346, #18072
Brine A	$2.65 \times 10^{-10}$ to $3.24 \times 10^{-10}$	67.9, #6092	<b>76.6,</b> <b>#24092</b>	86.8, #12092	77.8, #18092

Table C-2. Effects of Initial Radionuclide Concentration and  $P_{CO_2}$  on Matrix  $K_d$ s for Am(III), Dolomite-Rich Culebra Rock, and ERDA-6 (LANL Empirical Sorption Study). Six-week sorption runs with VPX-25-8.  $K_d$ s in bold font excluded from ranges and distributions because of unacceptable differences between standards and controls. Data current as of April 3, 1996. Table compiled by L. H. Brush on March 23 and 30, 1996, based on information provided by LANL on March 19 and 26, 1996. Table checked by Brush and S. Boone on April 3, 1996. Table revised by Brush on June 7, 1996. Table checked by L. J. Storz on June 10, 1996.

Brine	Range of Initial $^{243}\text{Am}$ Conc. (M)	$K_d$ (ml/g), 0.033% $\text{CO}_2$	$K_d$ (ml/g), 0.24% $\text{CO}_2$	$K_d$ (ml/g), 1.4% $\text{CO}_2$	$K_d$ (ml/g), 4.1% $\text{CO}_2$
ERDA-6	2.18 x 10 <sup>-10</sup> to 4.66 x 10 <sup>-10</sup>	<b>5,620,</b> <b>#6013</b>	<b>9,590,</b> <b>#24013</b>	10,800, #12013	5,230, #18013
ERDA-6	1.57 x 10 <sup>-10</sup> to 7.10 x 10 <sup>-10</sup>	<b>5,100,</b> <b>#6033</b>	<b>4,760,</b> <b>#24033</b>	<b>8,110,</b> <b>#12033</b>	<b>2,080,</b> <b>#18033</b>
ERDA-6	1.06 x 10 <sup>-10</sup> to 2.02 x 10 <sup>-10</sup>	1,650, #6053	1,610, #24053	<b>2,010,</b> <b>#12053</b>	<b>1,210,</b> <b>#18053</b>
ERDA-6	1.22 x 10 <sup>-10</sup> to 1.51 x 10 <sup>-10</sup>	<b>978,</b> <b>#6073</b>	<b>877,</b> <b>#24073</b>	832, #12073	<b>754,</b> <b>#18073</b>
ERDA-6	9.23 x 10 <sup>-11</sup> to 1.16 x 10 <sup>-10</sup>	<b>211,</b> <b>#6093</b>	272, #24093	<b>249,</b> <b>#12093</b>	<b>258,</b> <b>#18093</b>

Table C-3. Effects of Initial Radionuclide Concentration and  $P_{CO_2}$  on Matrix  $K_d$ s for Am(III), Dolomite-Rich Culebra Rock, and AISinR (LANL Empirical Sorption Study). Six-week sorption runs with VPX-25-8.  $K_d$ s in bold font! excluded from ranges and distributions because of unacceptable differences between standards and controls. Data current as of April 3, 1996. Table compiled by L. H. Brush on March 23 and 30, 1996, based on information provided by LANL on March 19 and 26, 1996. Table checked by Brush and S. Boone on April 3, 1996. Table revised by Brush on June 7, 1996. Table checked by L. J. Storz on June 10, 1996.

Brine	Range of Initial $^{243}\text{Am}$ Conc. (M)	$K_d$ (ml/g), 0.033% $\text{CO}_2$	$K_d$ (ml/g), 0.24% $\text{CO}_2$	$K_d$ (ml/g), 1.4% $\text{CO}_2$	$K_d$ (ml/g), 4.1% $\text{CO}_2$
AISinR	$1.14 \times 10^{-9}$ to $4.02 \times 10^{-9}$	<b>1,790,</b> <b>#6014</b>	730, #24014	<b>637,</b> <b>#12014</b>	<b>507,</b> <b>#18014</b>
AISinR	$6.95 \times 10^{-10}$ to $2.29 \times 10^{-9}$	<b>1,660,</b> <b>#6034</b>	<b>594,</b> <b>#24034</b>	<b>676,</b> <b>#12034</b>	<b>504,</b> <b>#18034</b>
AISinR	$1.92 \times 10^{-10}$ to $4.47 \times 10^{-10}$	934, #6054	760, #24054	<b>437,</b> <b>#12054</b>	<b>436,</b> <b>#18054</b>
AISinR	$1.27 \times 10^{-10}$ to $2.89 \times 10^{-10}$	<b>653,</b> <b>#6074</b>	640, #24074	344, #12074	<b>334,</b> <b>#18074</b>
AISinR	$1.26 \times 10^{-10}$ to $1.64 \times 10^{-10}$	190, #6094	145, #24094	133, #12094	156, #18094



Table C-4. Effects of Initial Radionuclide Concentration and  $P_{CO_2}$  on Matrix  $K_d$ s for Am(III), Dolomite-Rich Culebra Rock, and H-17 (LANL Empirical Sorption Study). Six-week sorption runs with VPX-25-8.  $K_d$ s in bold font excluded from ranges and distributions because of unacceptable differences between standards and controls. Data current as of April 3, 1996. Table compiled by L. H. Brush on March 23 and 30, 1996, based on information provided by LANL on March 19 and 26, 1996. Table checked by Brush and S. Boone on April 3, 1996. Table revised by Brush on June 7, 1996. Table checked by L. J. Storz on June 10, 1996.



Brine	Range of Initial $^{243}\text{Am}$ Conc. (M)	$K_d$ (ml/g), 0.033% $\text{CO}_2$	$K_d$ (ml/g), 0.24% $\text{CO}_2$	$K_d$ (ml/g), 1.4% $\text{CO}_2$	$K_d$ (ml/g), 4.1% $\text{CO}_2$
H-17	$6.35 \times 10^{-10}$ to $1.69 \times 10^{-9}$	<b>1,590,</b> <b>#6015</b>	<b>1,310,</b> <b>#24015</b>	<b>688,</b> <b>#12015</b>	<b>547,</b> <b>#18015</b>
H-17	$4.42 \times 10^{-10}$ to $1.77 \times 10^{-9}$	<b>1,140,</b> <b>#6035</b>	<b>1,120,</b> <b>#24035</b>	<b>622,</b> <b>#12035</b>	<b>484,</b> <b>#18035</b>
H-17	$2.27 \times 10^{-10}$ to $3.60 \times 10^{-10}$	<b>870,</b> <b>#6055</b>	836, #24055	499, #12055	<b>633,</b> <b>#18055</b>
H-17	$1.57 \times 10^{-10}$ to $3.16 \times 10^{-10}$	<b>826,</b> <b>#6075</b>	626, #24075	418, #12075	<b>383,</b> <b>#18075</b>
H-17	$1.43 \times 10^{-10}$ to $3.36 \times 10^{-10}$	76.1, #6095	187, #24095	189, #12095	<b>155,</b> <b>#18095</b>

Table C-5. Effects of pH and  $P_{CO_2}$  on Matrix  $K_d$ s for Nd(III) and Pure Dolomite (SNL/LANL Mechanistic Sorption Study). Sorption runs with Norwegian dolomite and 0.05 M NaCl. Data current as of March 31, 1996. Table retyped by L. H. Brush on April 24, 1996. Table checked by Y. Behl on April 28, 1996.

pH (standard units)	$K_d$ (ml/g), atmospheric $CO_2$	$K_d$ (ml/g), 0.5% $CO_2$	$K_d$ (ml/g), 5% $CO_2$
9.08	2864.3	NA	NA
8.41	1619.2	NA	NA
7.52	1225.2	NA	NA
6.72	1141.4	NA	NA
6.49	571.49	NA	NA
6.19	497.91	NA	NA
5.74	546.24	NA	NA
5.25	272.78	NA	NA
4.63	241.5	NA	NA
4.2	279.24	NA	NA
3.75	202.2	NA	NA
3.35	141.3	NA	NA

NA: not applicable.



Table C-5. Effects of pH and  $P_{CO_2}$  on Matrix  $K_d$ s for Nd(III) and Pure Dolomite (SNL/LANL Mechanistic Sorption Study) (continued).

pH (standard units)	$K_d$ (ml/g), atmospheric $CO_2$	$K_d$ (ml/g), 0.5% $CO_2$	$K_d$ (ml/g), 5% $CO_2$
7.08	NA	538.93	NA
6.81	NA	403.05	NA
6.45	NA	261.86	NA
6.26	NA	386.81	NA
5.92	NA	149.45	NA
5.18	NA	84.721	NA
4.35	NA	55.485	NA
3.64	NA	51.358	NA

NA: not applicable.

Table C-5. Effects of pH and  $P_{CO_2}$  on Matrix  $K_d$ s for Nd(III) and Pure Dolomite (SNL/LANL Mechanistic Sorption Study) (continued).

pH (standard units)	$K_d$ (ml/g), atmospheric $CO_2$	$K_d$ (ml/g), 0.5% $CO_2$	$K_d$ (ml/g), 5% $CO_2$
6.33	NA	NA	226.71
6.24	NA	NA	179.19
6.15	NA	NA	182.28
6.01	NA	NA	169.89
5.88	NA	NA	168.9
5.76	NA	NA	111.58
5.54	NA	NA	72.6
5.21	NA	NA	206.36
3.42	NA	NA	34.636

NA: not applicable.



Table C-6. Effects of pH and  $P_{CO_2}$  on Matrix  $K_d$ s for Am(III) and Pure Dolomite (SNL/LANL Mechanistic Sorption Study). Sorption runs with Norwegian dolomite and 0.5 M NaCl. Data current as of March 31, 1996. Table retyped by L. H. Brush on April 24, 1996. Table checked by Y. Behl on April 28, 1996.

pH (standard units)	$K_d$ (ml/g), atmospheric $CO_2$	$K_d$ (ml/g), 0.5% $CO_2$	$K_d$ (ml/g), 5% $CO_2$
9.88	High	NA	NA
9.87	High	NA	NA
8.42	High	NA	NA
6.7	High	NA	NA
6.2	High	NA	NA
5.81	High	NA	NA
5.21	High	NA	NA
4.62	791.15	NA	NA
4.05	630.75	NA	NA
3.51	285.41	NA	NA
3.11	92.603	NA	NA

NA: not applicable.



Table C-6. Effects of pH and  $P_{CO_2}$  on Matrix  $K_d$ s for Am(III) and Pure Dolomite (SNL/LANL Mechanistic Sorption Study) (continued).

pH (standard units)	$K_d$ (ml/g), atmospheric $CO_2$	$K_d$ (ml/g), 0.5% $CO_2$	$K_d$ (ml/g), 5% $CO_2$
6.9	NA	High	NA
8.49	NA	High	NA
7.32	NA	High	NA
7.19	NA	High	NA
6.99	NA	High	NA
6.88	NA	High	NA
6.55	NA	High	NA
6.17	NA	High	NA
5.28	NA	1130.9	NA
3.97	NA	65.441	NA
3.13	NA	158.09	NA

NA: not applicable.

Table C-6. Effects of pH and  $P_{CO_2}$  on Matrix  $K_d$ s for Am(III) and Pure Dolomite (SNL/LANL Mechanistic Sorption Study) (continued).

pH (standard units)	$K_d$ (ml/g), atmospheric $CO_2$	$K_d$ (ml/g), 0.5% $CO_2$	$K_d$ (ml/g), 5% $CO_2$
6.39	NA	NA	High
6.91	NA	NA	High
6.89	NA	NA	High
6.8	NA	NA	High
6.75	NA	NA	High
6.84	NA	NA	High
6.49	NA	NA	High
6.07	NA	NA	High
5.76	NA	NA	1934.3
4.91	NA	NA	333.78
3.62	NA	NA	-10.908

NA: not applicable.

Table C-7 Minimum Values of R and  $K_d$  for Am(III) in Intact Culebra Cores (SNL Column Transport Study). Data current as of March 26, 1996. Table compiled by L. H. Brush on March 30, 1996, based on memo by D. A. Lucero, G. O. Brown, and K. G. Budge dated March 28, 1996. Table checked by Brush on March 31, 1996.



Run #	Solid (core)	Brine	Flow rate (ml/min)	Run Time (days)	Ef-fluent Vol. (L)	$R_{min}$	Porosity (%)	$K_{d, min}$ (ml/g)	Range ( $\pm$ ml/g)
C-3	VPX-28-6C	AIS.	0.1	211	30.45	1,420	3.7 <sup>S</sup>	11	NA
D-3	VPX-25-8A	AIS.	0.1	118	17.02	350	9.1, <sup>S</sup> 5.3 <sup>D</sup>	14	NA
E-2	VPX-27-7A	AIS.	0.1	61	8.83	200	23, <sup>S</sup> 15.7 <sup>D</sup>	20	NA

AIS: AISinR.

D: dual porosity assumed.

NA: not available yet.

S: single porosity assumed.

Table C-8. Minimum Values of R and  $K_d$  for Am(III) in Intact Culebra Cores (SNL Column Transport Study). Data current as of March 26, 1996. Table compiled by L. H. Brush on March 30, 1996, based on memo by D. A. Lucero, G. O. Brown, and K. G. Budge dated March 28, 1996. Table checked by Brush on March 31, 1996. Table revised by Brush on April 6, 1996, based on memo by Lucero and Brown dated April 5, 1996. Table checked by Y. Behl on April 8, 1996.

Run #	Solid (core)	Brine	Flow rate (ml/min)	Run Time (days)	Ef-fluent Vol. (L)	$R_{min}$	Porosity (%)	$K_{d, min}$ (ml/g)	Range ( $\pm$ ml/g)
C-3	VPX-28-6C	AIS.	0.1	211	30.45	1,420	3.7 <sup>S</sup>	11	NA
D-3	VPX-25-8A	AIS.	0.1	118	17.02	350	9.1 <sup>S</sup>	14	NA
E-2	VPX-27-7A	AIS.	0.1	61	8.83	200	23 <sup>S</sup>	20	NA



AIS: AISinR.

NA: not available yet.

S: single porosity assumed.

Table C-9. Minimum Values of R and  $K_d$  for Am(III) in Intact Culebra Cores (SNL Column Transport Study). Data current as of March 26, 1996. Table compiled by L. H. Brush on March 30, 1996, based on memo by D. A. Lucero, G. O. Brown, and K. G. Budge dated March 28, 1996. Table checked by Brush on March 31, 1996. Table revised by Brush on April 6, 1996, based on memo by Lucero and Brown dated April 5, 1996. Table checked by Y. Behl on April 8, 1996. Table revised by Brush on April 17, 1996, based on memo by Brown dated April 16, 1996.

Run #	Solid (core)	Brine	Flow rate (ml/min)	Run Time (days)	Ef-fluent Vol. (L)	$R_{min}$	Porosity (%)	$K_{d, min}$ (ml/g)	Range ( $\pm$ ml/g)
C-3	VPX-28-6C	AIS.	0.1	211	30.45	1,420	3.7 <sup>S</sup>	23	NA
D-3	VPX-25-8A	AIS.	0.1	118	17.02	350	9.1 <sup>S</sup>	14	NA
E-2	VPX-27-7A	AIS.	0.1	61	8.83	200	23 <sup>S</sup>	20	NA

AIS: AISinR.

NA: not available yet.

S: single porosity assumed.

APPENDIX D: RANGES AND PROBABILITY DISTRIBUTIONS OF  
MATRIX  $K_d$ s FOR U(VI) AND DOLOMITE-RICH  
CULEBRA ROCK

Based on experimental results, ASTP personnel have predicted that U will speciate as U(IV) or U(VI) in deep (Castile and Salado) brines in WIPP disposal rooms. Furthermore, a modeling study of the effects of mixing deep and Culebra brines on the oxidation states of Pu, U, and Np in the Culebra showed that Culebra fluids are poorly poised (see Predictions of Actinide Oxidation States in the Culebra above). Therefore, we established experimentally obtained ranges of matrix  $K_d$ s for U(VI) and used the experimentally obtained ranges for Th(IV) (see Appendix E below) and the oxidation-state analogy to establish ranges for U(IV) (and Np(IV)).

To establish the *initial* ranges for U(VI) and the deep brines, we first considered *all* of the data from the 6-week empirical sorption experiments carried out with Brine A and ERDA-6 on the bench top (0.033% CO<sub>2</sub>) by Triay and her group at LANL (see Methods Used to Establish Ranges of Matrix  $K_d$ s above for the reasons for considering these data). These runs were: #6008, #6028, #6048, #6068, and #6088 (see Table D-1 below), and #6009, #6029, #6049, #6069, and #6089 (Table D-2). Next, we discarded the data from #6008, #6028, #6048, #6068, and #6009, the runs in which the difference between the activity of the <sup>233</sup>U in a standard and that in a control exceeded 3 $\sigma$ , where  $\sigma$  is the standard deviation (see Methods Used to Establish Ranges of Matrix  $K_d$ s). Discarding the data from these five runs yielded an *initial* range of 3.76 ml/g (from #6029) to 21.8 ml/g (#6088) for U(VI) and the deep brines.

To establish the *initial* ranges for U(VI) and the Culebra brines, we first considered *all* of Triay's 6-week sorption data obtained with AISinR and H-17 on the bench top (0.033% CO<sub>2</sub>) and in glove boxes with atmospheres containing 0.24 and 1.4% CO<sub>2</sub> (see Methods Used to Establish Ranges of Matrix  $K_d$ s). These were: #6010, #6030, #6050, #6070, #6090, #24010, #24030, #24050, #24070, #24090, #12010, #12030, #12050, #12070, and #12090 (Table D-3), and #6011, #6031, #6051, #6071, #6091, #24011, #24031, #24051, #24071, #24091, #12011, #12031, #12051, #12071, and #12091 (Table D-4). We then discarded the data from #6010, #6050, #6070, #24010, #24030, #12010, #6011, #6031, #6051, #6071, #12011, and #12051, the runs in which the difference between the activity of the <sup>233</sup>U in a standard and that in a control exceeded 3 $\sigma$ , to obtain the *initial* range of -1.66 ml/g (from #12091) to 68.7 ml/g (#24091) for U(VI) and the Culebra brines. However, we set the lower limit of this range equal to 0 ml/g because there is no reason why a  $K_d$  could have a value less than 0.

Next, we compared these initial ranges with the data from the mechanistic sorption study by Brady and his colleagues at SNL and LANL. We used Brady's data to extend Triay's empirical sorption data for the deep brines to the basic conditions expected to result from the use of an MgO backfill in WIPP disposal rooms, *but not* to extend Triay's data for the Culebra brines to basic conditions (see Methods Used to Establish Ranges of Matrix  $K_d$ s). Brady's data for 0.5 M NaCl, atmospheric CO<sub>2</sub>, and the highest

pH values under these conditions are (to three significant figures) 10.6 and 34.7 ml/g at a pH of 9.87 and 9.88, respectively (Table D-5). Because these values are *greater than the upper limit* of the initial range for U(VI) and the deep brines (see above), we extended this range to obtain a *revised* range for U(VI) and deep brines of 3.76 ml/g to 34.7 ml/g. Because we did not use this comparison to extend the initial range for U(VI) and the Culebra brines to basic conditions, this *revised* range remains 0 to 68.7 ml/g.

We then compared both of these revised ranges with the data from the transport study with intact Culebra cores by Lucero and his colleagues at SNL. Lucero carried out his experiments under ambient atmospheric conditions; therefore, the CO<sub>2</sub> content of these experiments was probably similar to that in the LANL bench-top (0.033% CO<sub>2</sub>) runs. Lucero *did* observe breakthrough of U(VI) in his experiments. Therefore, it was possible to determine actual K<sub>d</sub>s for this element. Lucero and his colleagues submitted their results on March 28, 1996, (see Table D-6), then revised them on April 5 and 16, 1996 (Tables D-7 and D-8, respectively). The K<sub>d</sub> reported for Experiment C-7 with the deep brine ERDA-6 (Table D-8) is *less than the lower limit of the revised range of K<sub>d</sub>s for U(VI) and the deep brines obtained from the empirical and mechanistic sorption studies* (see above). Therefore, we extended this range to obtain a *final* range for U(VI) and deep brines of 0.029 ml/g to 34.7 ml/g, and rounded it to 0.03 to 30 ml/g prior to inclusion in Table 1 above. Because Lucero's K<sub>d</sub>s for U(VI) and the Culebra brine AISinR (B-3, B-6, C-2, D-5, and D-6 in Table D-8) are *within* the revised range for U(VI) and the Culebra brines (see above), our *final* range remains 0 to 68.7 ml/g, rounded to 0 to 70 ml/g for inclusion in Table 1.

We recommend that PA personnel use a uniform probability distribution for both of these ranges (see Methods Used to Establish Probability Distributions of Matrix K<sub>d</sub>s above).

Finally, we recommend that PA use the range of 0.03 to 30 ml/g (the range for deep brines) for U(VI) because this range results in less retardation of this element than the range for Culebra brines (see Methods Used for Final Selection of the Range of Matrix K<sub>d</sub>s for Use in PA Calculations above).

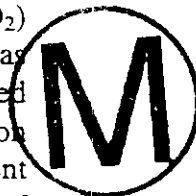


Table D-1. Effects of Initial Radionuclide Concentration and  $P_{CO_2}$  on Matrix  $K_d$ s for U(VI), Dolomite-Rich Culebra Rock, and Brine A (LANL Empirical Sorption Study). Six-week sorption runs with VPX-25-8.  $K_d$ s in bold font excluded from ranges and distributions because of unacceptable differences between standards and controls. Data current as of April 3, 1996. Table compiled by L. H. Brush on March 23 and 30, 1996, based on information provided by LANL on March 19 and 26, 1996. Table checked by Brush and S. Boone on April 3, 1996. Table revised by Brush on June 7, 1996. Table checked by L. J. Storz on June 10, 1996.



Brine	Range of Initial $^{233}U$ Conc. (M)	$K_d$ (ml/g), 0.033% $CO_2$	$K_d$ (ml/g), 0.24% $CO_2$	$K_d$ (ml/g), 1.4% $CO_2$	$K_d$ (ml/g), 4.1% $CO_2$
Brine A	$1.65 \times 10^{-6}$ to $2.81 \times 10^{-6}$	<b>12.5,</b> <b>#6008</b>	<b>4.77,</b> <b>#24008</b>	<b>1.16,</b> <b>#12008</b>	0.709, #18008
Brine A	$7.89 \times 10^{-7}$ to $1.05 \times 10^{-6}$	<b>16.8,</b> <b>#6028</b>	2.86, #24028	1.21, #12028	2.67, #18028
Brine A	$1.85 \times 10^{-7}$ to $2.72 \times 10^{-7}$	<b>19.9,</b> <b>#6048</b>	5.23, #24048	1.47, #12048	2.46, #18048
Brine A	$7.60 \times 10^{-8}$ to $1.09 \times 10^{-7}$	<b>16.6,</b> <b>#6068</b>	6.81, #24068	0.933, #12068	2.30, #18068
Brine A	$2.14 \times 10^{-8}$ to $4.16 \times 10^{-8}$	21.8, #6088	4.70, #24088	-5.41, #12088	1.44, #18088

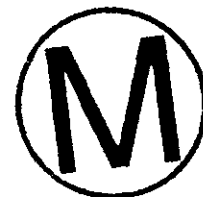
Table D-2. Effects of Initial Radionuclide Concentration and  $P_{CO_2}$  on Matrix  $K_d$ s for U(VI), Dolomite-Rich Culebra Rock, and ERDA-6 (LANL Empirical Sorption Study). Six-week sorption runs with VPX-25-8.  $K_d$ s in bold font excluded from ranges and distributions because of unacceptable differences between standards and controls. Data current as of April 3, 1996. Table compiled by L. H. Brush on March 23 and 30, 1996, based on information provided by LANL on March 19 and 26, 1996. Table checked by Brush and S. Boone on April 3, 1996. Table revised by Brush on June 7, 1996. Table checked by L. J. Storz on June 10, 1996.

Brine	Range of Initial $^{233}U$ Conc. (M)	$K_d$ (ml/g), 0.033% $CO_2$	$K_d$ (ml/g), 0.24% $CO_2$	$K_d$ (ml/g), 1.4% $CO_2$	$K_d$ (ml/g), 4.1% $CO_2$
ERDA-6	$2.62 \times 10^{-6}$ to $2.99 \times 10^{-6}$	<b>0.542,</b> <b>#6009</b>	1.29, #24009	<b>4.13,</b> <b>#12009</b>	3.75, #18009
ERDA-6	$8.61 \times 10^{-7}$ to $9.87 \times 10^{-7}$	3.76, #6029	1.52, #24029	5.92, #12029	<b>3.17,</b> <b>#18029</b>
ERDA-6	$2.14 \times 10^{-7}$ to $2.56 \times 10^{-7}$	3.86, #6049	2.38, #24049	7.25, #12049	3.22, #18049
ERDA-6	$8.40 \times 10^{-8}$ to $9.28 \times 10^{-8}$	3.88, #6069	4.35, #24069	6.24, #12069	4.76, #18069
ERDA-6	$2.31 \times 10^{-8}$ to $2.87 \times 10^{-8}$	6.55, #6089	2.11, #24089	7.04, #12089	1.04, #18089

Table D-3. Effects of Initial Radionuclide Concentration and  $P_{CO_2}$  on Matrix  $K_d$ s for U(VI), Dolomite-Rich Culebra Rock, and AISinR (LANL Empirical Sorption Study). Six-week sorption runs with VPX-25-8.  $K_d$ s in bold font excluded from ranges and distributions because of unacceptable differences between standards and controls. Data current as of April 3, 1996. Table compiled by L. H. Brush on March 23 and 30, 1996, based on information provided by LANL on March 19 and 26, 1996. Table checked by Brush and S. Boone on April 3, 1996. Table revised by Brush on June 7, 1996. Table checked by L. J. Storz on June 10, 1996.

Brine	Range of Initial $^{233}U$ Conc. (M)	$K_d$ (ml/g), 0.033% $CO_2$	$K_d$ (ml/g), 0.24% $CO_2$	$K_d$ (ml/g), 1.4% $CO_2$	$K_d$ (ml/g), 4.1% $CO_2$
AISinR	$2.86 \times 10^{-6}$ to $3.04 \times 10^{-6}$	<b>2.56,</b> <b>#6010</b>	<b>0.351,</b> <b>#24010</b>	<b>0.550,</b> <b>#12010</b>	<b>1.67,</b> <b>#18010</b>
AISinR	$9.57 \times 10^{-7}$ to $1.06 \times 10^{-6}$	2.62, <b>#6030</b>	<b>2.69,</b> <b>#24030</b>	2.05, <b>#12030</b>	<b>0.756,</b> <b>#18030</b>
AISinR	$2.63 \times 10^{-7}$ to $2.87 \times 10^{-7}$	<b>3.74,</b> <b>#6050</b>	0.389, <b>#24050</b>	1.65, <b>#12050</b>	<b>3.73,</b> <b>#18050</b>
AISinR	$8.22 \times 10^{-8}$ to $9.50 \times 10^{-8}$	<b>4.02,</b> <b>#6070</b>	3.16, <b>#24070</b>	1.03, <b>#12070</b>	<b>0.341,</b> <b>#18070</b>
AISinR	$2.60 \times 10^{-8}$ to $2.79 \times 10^{-8}$	7.51, <b>#6090</b>	0.117, <b>#24090</b>	1.73, <b>#12090</b>	1.88, <b>#18090</b>

Table D-4. Effects of Initial Radionuclide Concentration and  $P_{CO_2}$  on Matrix  $K_d$ s for U(VI), Dolomite-Rich Culebra Rock, and H-17 (LANL Empirical Sorption Study). Six-week sorption runs with VPX-25-8.  $K_d$ s in bold font excluded from ranges and distributions because of unacceptable differences between standards and controls. Data current as of April 3, 1996. Table compiled by L. H. Brush on March 23 and 30, 1996, based on information provided by LANL on March 19 and 26, 1996. Table checked by Brush and S. Boone on April 3, 1996. Table revised by Brush on June 7, 1996. Table checked by L. J. Storz on June 10, 1996.



Brine	Range of Initial $^{233}U$ Conc. (M)	$K_d$ (ml/g), 0.033% $CO_2$	$K_d$ (ml/g), 0.24% $CO_2$	$K_d$ (ml/g), 1.4% $CO_2$	$K_d$ (ml/g), 4.1% $CO_2$
H-17	2.76 x 10 <sup>-6</sup> to 2.97 x 10 <sup>-6</sup>	<b>3.63,</b> <b>#6011</b>	0.313, #24011	<b>-0.745,</b> <b>#12011</b>	-0.104, #18011
H-17	1.11 x 10 <sup>-6</sup> to 1.16 x 10 <sup>-6</sup>	<b>5.55,</b> <b>#6031</b>	1.30, #24031	0.157, #12031	0.530, #18031
H-17	2.72 x 10 <sup>-7</sup> to 2.92 x 10 <sup>-7</sup>	<b>6.97,</b> <b>#6051</b>	3.03, #24051	<b>-1.83,</b> <b>#12051</b>	2.26, #18051
H-17	8.73 x 10 <sup>-8</sup> to 9.86 x 10 <sup>-8</sup>	<b>5.12,</b> <b>#6071</b>	1.90, #24071	1.50, #12071	-1.22, #18071
H-17	6.89 x 10 <sup>-9</sup> to 2.83 x 10 <sup>-8</sup>	10.2, #6091	68.7, #24091	-1.66, #12091	2.96, #18091

Table D-5. Effects of pH and  $P_{CO_2}$  on Matrix  $K_d$ s for U(VI) and Pure Dolomite (SNL/LANL Mechanistic Sorption Study). Sorption runs with Norwegian dolomite and 0.5 M NaCl. Data current as of March 31, 1996. Table retyped by L. H. Brush on April 24, 1996. Table checked by Y. Behl on April 28, 1996.

pH (standard units)	$K_d$ (ml/g), atmospheric $CO_2$	$K_d$ (ml/g), 0.5% $CO_2$	$K_d$ (ml/g), 5% $CO_2$
9.88	34.662	NA	NA
9.87	10.6	NA	NA
8.42	7691.2	NA	NA
6.7	4794.1	NA	NA
6.2	3345.6	NA	NA
5.81	5685.5	NA	NA
5.21	2476.5	NA	NA
4.62	2476.5	NA	NA
4.05	2621.3	NA	NA
3.51	2342.8	NA	NA
3.11	1897.1	NA	NA

NA: not applicable.



Table D-5. Effects of pH and  $P_{CO_2}$  on Matrix  $K_d$ s for U(VI) and Pure Dolomite (SNL/LANL Mechanistic Sorption Study) (continued).

pH (standard units)	$K_d$ (ml/g), atmospheric $CO_2$	$K_d$ (ml/g), 0.5% $CO_2$	$K_d$ (ml/g), 5% $CO_2$
6.9	NA	775.74	NA
8.49	NA	-112.13	NA
7.32	NA	44.55	NA
7.19	NA	123.88	NA
6.99	NA	286.76	NA
6.88	NA	849.72	NA
6.55	NA	1114	NA
6.17	NA	455.52	NA
5.28	NA	1774.6	NA
3.97	NA	1611.4	NA
3.13	NA	4222.7	NA

NA: not applicable.



Table D-5. Effects of pH and  $P_{CO_2}$  on Matrix  $K_d$ s for U(VI) and Pure Dolomite (SNL/LANL Mechanistic Sorption Study) (continued).

pH (standard units)	$K_d$ (ml/g), atmospheric $CO_2$	$K_d$ (ml/g), 0.5% $CO_2$	$K_d$ (ml/g), 5% $CO_2$
6.39	NA	NA	475.59
6.91	NA	NA	69.799
6.89	NA	NA	0
6.8	NA	NA	0
6.75	NA	NA	69.799
6.84	NA	NA	69.799
6.49	NA	NA	296.73
6.07	NA	NA	1517.2
5.76	NA	NA	2056.6
4.91	NA	NA	3075.4
3.62	NA	NA	1674.5

NA: not applicable.

Table D-6. Measured Values of R and Calculated Values of  $K_d$  for U(VI) in Intact Culebra Cores (SNL Column Transport Study). Values in bold font to be excluded from ranges and distributions because fits to elution data were inferior to those assuming single porosity and dual porosity with fracture retardation. Data current as of March 30, 1996. Table compiled by L. H. Brush on March 30, 1996, based on memo by D. A. Lucero, G. O. Brown, and K. G. Budge dated March 28, 1996. Table checked by Brush on March 31, 1996.



Run #	Solid (core)	Brine	Flow rate (ml/min)	Run Time (days)	Ef-fluent Vol. (L)	R	Porosity (%)	$K_d$ (ml/g)	Range ( $\pm$ ml/g)
B-3	VPX-26-11A	AIS.	0.1	NA	NA	3.4; <sup>S</sup>	9.8 <sup>S</sup>	.084 <sup>S</sup>	.022 <sup>S</sup>
						<b>1,</b> <b>18.3;</b> <sup>N</sup>	5.2 <sup>DN</sup>	<b>0.68</b> <sup>DN</sup>	<b>.67</b> <sup>DN</sup>
						3.1, 5.2 <sup>DF</sup>	5.2 <sup>DF</sup>	.039 <sup>DF</sup>	0.03 <sup>DF</sup>
B-6	VPX-26-11A	AIS.	0.05	NA	NA	13.1; <sup>S</sup>	4.8 <sup>S</sup>	0.25 <sup>S</sup>	0.07 <sup>S</sup>
						<b>1,</b> <b>NA;</b> <sup>DN</sup>	NA <sup>DN</sup>	NA <sup>DN</sup>	NA <sup>DN</sup>
						NA, NA <sup>DF</sup>	NA <sup>DF</sup>	NA <sup>DF</sup>	NA <sup>DF</sup>
C-2	VPX-28-6C	AIS.	0.1	21	2	10.4; <sup>S</sup>	5.7 <sup>S</sup>	0.23 <sup>S</sup>	0.08 <sup>S</sup>
						<b>1,</b> <b>260;</b> <sup>DN</sup>	3.5 <sup>DN</sup>	<b>3.9</b> <sup>DN</sup>	<b>7</b> <sup>DN</sup>
						12.0, 0.6 <sup>DF</sup>	3.5 <sup>DF</sup>	0.17 <sup>DF</sup>	0.06 <sup>DF</sup>
C-7	VPX-28-6C	ER.-6	0.1	13	2	2.7; <sup>S</sup>	3.9 <sup>S</sup>	.029 <sup>S</sup>	.022 <sup>S</sup>
						<b>1,</b> <b>0.6;</b> <sup>DN</sup>	2.1 <sup>DN</sup>	<b>.069</b> <sup>DN</sup>	<b>0.13</b> <sup>DN</sup>
						2.7, 0.76 <sup>DF</sup>	2.1 <sup>DF</sup>	.016 <sup>DF</sup>	.005 <sup>DF</sup>

Table D-6. Measured Values of R and Calculated Values of  $K_d$  for U(VI) in Intact Culebra Cores (SNL Column Transport Study) (continued)

Run #	Solid (core)	Brine	Flow rate (ml/min)	Run Time (days)	Ef-fluent Vol. (L)	R	Porosity (%)	$K_d$ (ml/g)	Range ( $\pm$ ml/g)
D-5	VPX-25-8A	AIS.	0.1	13	2	21; <sup>S</sup> 1, 184; <sup>DN</sup> NA, NA <sup>DF</sup>	17.3 <sup>S</sup> 7.1 <sup>DN</sup> 7.1 <sup>DF</sup>	1.50 <sup>S</sup> 5.6 <sup>DN</sup> NA <sup>DF</sup>	0.38 <sup>S</sup> 5.5 <sup>DN</sup> NA <sup>DF</sup>
D-6	VPX-25-8A	AIS.	0.05	60	2	10.1; <sup>S</sup> 1, NA; <sup>DN</sup> 12.3, 71 <sup>DF</sup>	15.5 <sup>S</sup> 7.1 <sup>DN</sup> 7.1 <sup>DF</sup>	0.61 <sup>S</sup> NA <sup>DN</sup> 0.35 <sup>DF</sup>	0.15 NA <sup>DN</sup> 0.19 <sup>DF</sup>

AIS: AISinR.

DF: dual porosity and fracture retardation assumed.

DN: dual porosity and no fracture retardation assumed.

ER.-6: ERDA-6.

NA: not available yet.

S: single porosity assumed.



Table D-7. Measured Values of R and Calculated Values of  $K_d$  for U(VI) in Intact Culebra Cores (SNL Column Transport Study). Data current as of March 30, 1996. Table compiled by L. H. Brush on March 30, 1996, based on memo by D. A. Lucero, G. O. Brown, and K. G. Budge dated March 28, 1996. Table checked by Brush on March 31, 1996. Table revised by Brush on April 6, 1996, based on memo by Lucero and Brown dated April 5, 1996. Table checked by Y. Behl on April 8, 1996.

Run #	Solid (core)	Brine	Flow rate (ml/min)	Run Time (days)	Ef-fluent Vol. (L)	R	Porosity (%)	$K_d$ (ml/g)	Range ( $\pm$ ml/g)
B-3	VPX-26-11A	AIS.	0.1	NA	NA	3.4 <sup>S</sup>	9.8 <sup>S</sup>	0.084 <sup>S</sup>	NA <sup>S</sup>
B-6	VPX-26-11A	AIS.	0.05	NA	NA	13 <sup>S</sup>	4.8 <sup>S</sup>	0.25 <sup>S</sup>	NA <sup>S</sup>
C-2	VPX-28-6C	AIS.	0.1	21	2	10.4 <sup>S</sup>	5.7 <sup>S</sup>	0.23 <sup>S</sup>	NA <sup>S</sup>
C-7	VPX-28-6C	ER.-6	0.1	13	2	2.7 <sup>S</sup>	3.9 <sup>S</sup>	0.029 <sup>S</sup>	NA <sup>S</sup>
D-5	VPX-25-8A	AIS.	0.1	13	2	21 <sup>S</sup>	17.3 <sup>S</sup>	1.5 <sup>S</sup>	NA <sup>S</sup>
D-6	VPX-25-8A	AIS.	0.05	60	2	10 <sup>S</sup>	15.5 <sup>S</sup>	0.61 <sup>S</sup>	NA <sup>S</sup>

AIS: AISinR.

ER.-6: ERDA-6.

NA: not available yet.

S: single porosity assumed.



Table D-8. Measured Values of R and Calculated Values of  $K_d$  for U(VI) in Intact Culebra Cores (SNL Column Transport Study). Data current as of March 30, 1996. Table compiled by L. H. Brush on March 30, 1996, based on memo by D. A. Lucero, G. O. Brown, and K. G. Budge dated March 28, 1996. Table checked by Brush on March 31, 1996. Table revised by Brush on April 6, 1996 based on memo by Lucero and Brown dated April 5, 1996. Table checked by Y. Behl on April 8, 1996. Table revised by Brush on April 17, 1996, based on memo by Brown dated April 16, 1996.

Run #	Solid (core)	Brine	Flow rate (ml/min)	Run Time (days)	Ef-fluent Vol. (L)	R	Porosity (%)	$K_d$ (ml/g)	Range ( $\pm$ ml/g)
B-3	VPX-26-11A	AIS.	0.1	NA	NA	3.4 <sup>S</sup>	9.8 <sup>S</sup>	0.10 <sup>S</sup>	NA <sup>S</sup>
B-6	VPX-26-11A	AIS.	0.05	NA	NA	13 <sup>S</sup>	4.8 <sup>S</sup>	0.25 <sup>S</sup>	NA <sup>S</sup>
C-2	VPX-28-6C	AIS.	0.1	21	2	10.4 <sup>S</sup>	5.7 <sup>S</sup>	0.23 <sup>S</sup>	NA <sup>S</sup>
C-7	VPX-28-6C	ER.-6	0.1	13	2	2.7 <sup>S</sup>	3.9 <sup>S</sup>	0.029 <sup>S</sup>	NA <sup>S</sup>
D-5	VPX-25-8A	AIS.	0.1	13	2	21 <sup>S</sup>	17.3 <sup>S</sup>	1.5 <sup>S</sup>	NA <sup>S</sup>
D-6	VPX-25-8A	AIS.	0.05	60	2	10 <sup>S</sup>	15.5 <sup>S</sup>	0.61 <sup>S</sup>	NA <sup>S</sup>

AIS: AISinR.

ER.-6: ERDA-6.

NA: not available yet.

S: single porosity assumed.

APPENDIX E: RANGES AND PROBABILITY DISTRIBUTIONS OF  
MATRIX  $K_d$ s FOR Th(IV) AND DOLOMITE-RICH  
CULEBRA ROCK

For Th, only one oxidation state, Th(IV), is possible in the Culebra (see Predictions of Actinide Oxidation States in the Culebra above). Therefore, we established an experimentally obtained range of matrix  $K_d$ s for Th(IV), and used it and the oxidation-state analogy to establish ranges for Pu(IV), U(IV), and Np(IV).

To establish the *initial* ranges for Th(IV) and the deep brines, we first considered *all* of the data from the 6-week empirical sorption experiments carried out with Brine A and ERDA-6 on the bench top (0.033% CO<sub>2</sub>) by Triay and her group at LANL (see Methods Used to Establish Ranges of Matrix  $K_d$ s above for the reasons for considering these data). These runs were: #7011A and #7011B (see Table E-1 below), and #7007A, #7007B, #7008A, #7008B, #7009A, #7009B, #7010A, and #7010B (Table E-2). Next, we discarded the data from #7011A and #7011B, the runs in which the difference between the activity of the <sup>230</sup>Th in a standard and that in a control exceeded 3 $\sigma$ , where  $\sigma$  is the standard deviation (see Methods Used to Establish Ranges of Matrix  $K_d$ s). Discarding the data from these two runs yielded an *initial* range of 864 ml/g (from #7010A) to 15,000 ml/g (#7008B) for Th(IV) and the deep brines.

For the *initial* ranges for Th(IV) and the Culebra brines, we first considered *all* of Triay's 6-week sorption data obtained with AISinR and H-17 on the bench top (0.033% CO<sub>2</sub>) and in glove boxes with atmospheres containing 0.24 and 1.4% CO<sub>2</sub> (see Methods Used to Establish Ranges of Matrix  $K_d$ s). These were: #7012A, #7012B, #7054A, #7054B, #7026A, #7026B, #7040A, and #7040B (Table E-3), and #7013A, #7013B, #7055A, #7055B, #7027A, #7027B, #7041A, and #7041B (Table E-4). Unfortunately, we had to discard the data from *all* of these the runs because the difference between the activity of the <sup>230</sup>Th in a standard and that in a control exceeded 3 $\sigma$ . Therefore, we assumed that the *initial* range of 864 to 15,000 ml/g for Th(IV) and the deep brines does not differ significantly from that for Th(IV) and the Culebra brines.

Next, we attempted to compare these initial ranges with the data from the mechanistic sorption study by Brady and his colleagues at SNL and LANL. However, Brady *did not* obtain any usable results for Th because of one or more of the following reasons: (1) the walls of the containers used to prepare Th-bearing solutions sorbed essentially all of it prior to his experiments; (2) essentially all of the Th precipitated on the walls of these containers prior to his runs; (3) the walls of his apparatus sorbed essentially all of the Th during his runs; (4) essentially all of the Th precipitated on the dolomite and/or the apparatus during his runs. Therefore, our *revised* ranges for Th(IV) remained 864 to 15,000 ml/g for *both* the deep and Culebra brines.

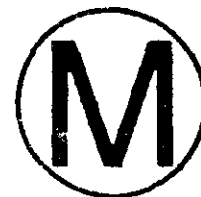
We then compared the revised range with the data from the transport study with intact Culebra cores by Lucero and his colleagues at SNL. Lucero carried out his experiments under ambient atmospheric conditions; therefore, the CO<sub>2</sub> content of these

experiments was probably similar to that in the LANL bench-top (0.033% CO<sub>2</sub>) runs. Because Lucero *did not* observe breakthrough of Th(IV), it was only possible to determine a minimum K<sub>d</sub> for this element. Furthermore, the minimum K<sub>d</sub>s calculated for Th are significantly lower than those calculated for Pu and Am, the other elements for which Lucero did not observe breakthrough (compare Tables B-8, C-9, and E-6), because: (1) the detection limit of γ-spectrometric analysis (one of the two methods used in this study) for <sup>228</sup>Th in the effluent is much higher than those for <sup>241</sup>Pu and <sup>241</sup>Am because of the low yield of the <sup>228</sup>Th γ emission; (2) although <sup>228</sup>Th emits α particles detectable by LSC (the other analytical method used in this study), its daughter products have interfering α emissions; (3) lowering the detection limit for <sup>228</sup>Th by observing the decay of its daughters, such as <sup>224</sup>Ra, was not possible because of interference by identical daughters produced by the decay of <sup>232</sup>U, which was used in all of the cores. Lucero and his colleagues submitted their results on March 28, 1996, (Table E-5), then revised them on April 5, 1996 (Table E-6). The minimum K<sub>d</sub>s reported for experiments C-2, C-5, and D-2 (Table E-6) *are consistent with the revised range obtained from the empirical and mechanistic sorption studies* (see above). Therefore, our *final* range remains 864 to 15,000 ml/g, rounded to 900 to 20,000 ml/g prior to inclusion in Table 1 above.

We recommend that PA personnel use a uniform probability distribution for this range (see Methods Used to Establish Probability Distributions of Matrix K<sub>d</sub>s above).

Finally, based on the oxidation-state analogy, we recommend that PA use a range of 900 to 20,000 ml/g for Pu(IV), U(IV), and Np(IV) (see Table 1).

Table E-1. Effects of Initial Radionuclide Concentration and  $P_{CO_2}$  on Matrix  $K_d$ s for Th(IV), Dolomite-Rich Culebra Rock, and Brine A (LANL Empirical Sorption Study). Six -week sorption runs with VPX-25-8.  $K_d$ s in bold font excluded from ranges and distributions because of unacceptable differences between standards and controls. Data current as of April 3, 1996. Table compiled by L. H. Brush on March 30 and April 3, 1996, based on information provided by LANL on March 28 and April 1, 1996. Table checked by Brush and S. Boone on April 3, 1996.



Brine	Initial $^{230}\text{Th}$ Conc. (M)	$K_d$ (ml/g), 0.033% $\text{CO}_2$	$K_d$ (ml/g), 0.24% $\text{CO}_2$	$K_d$ (ml/g), 1.4% $\text{CO}_2$	$K_d$ (ml/g), 4.1% $\text{CO}_2$
Brine A	ND	ND	ND	ND	ND
Brine A	ND	ND	ND	ND	ND
Brine A	ND	ND	ND	ND	ND
Brine A	ND	ND	ND	ND	ND
Brine A	ND	ND	ND	ND	ND
Brine A	ND	ND	ND	ND	ND
Brine A	NA	<b>313, #7011A</b>	<b>205, #7053A</b>	<b>338, #7025A</b>	<b>694, #7039A</b>
Brine A	NA	<b>250, #7011B</b>	<b>227, #7053B</b>	<b>352, #7025B</b>	<b>706, #7039B</b>
Brine A	ND	ND	ND	ND	ND
Brine A	ND	ND	ND	ND	ND

NA: not available yet.

ND: not determined.

Table E-2. Effects of Initial Radionuclide Concentration and  $P_{CO_2}$  on Matrix  $K_d$ s for Th(IV), Dolomite-Rich Culebra Rock, and ERDA-6 (LANL Empirical Sorption Study). Six-week sorption runs with VPX-25-8.  $K_d$ s in bold font excluded from ranges and distributions because of unacceptable differences between standards and controls. Data current as of April 3, 1996. Table compiled by L. H. Brush on March 30 and April 3, 1996, based on information provided by LANL on March 28 and April 1, 1996. Table checked by Brush and S. Boone on April 3, 1996.



Brine	Initial $^{230}\text{Th}$ Conc. (M)	$K_d$ (ml/g), 0.033% $\text{CO}_2$	$K_d$ (ml/g), 0.24% $\text{CO}_2$	$K_d$ (ml/g), 1.4% $\text{CO}_2$	$K_d$ (ml/g), 4.1% $\text{CO}_2$
ERDA-6	ND	ND	ND	ND	ND
ERDA-6	ND	ND	ND	ND	ND
ERDA-6	NA	5,340, #7007A	<b>6,600,</b> <b>#7049A</b>	12,900, #7021A	4,600, #7035A
ERDA-6	NA	5,270, #7007B	<b>8,950,</b> <b>#7049B</b>	15,900, #7021B	7,060, #7035B
ERDA-6	NA	6,650, #7008A	<b>8,720,</b> <b>#7050A</b>	8,670, #7022A	<b>7,340,</b> <b>#7036A</b>
ERDA-6	NA	15,000, #7008B	<b>6,450,</b> <b>#7050B</b>	7,780, #7022B	<b>9,620,</b> <b>#7036B</b>
ERDA-6	NA	2,180, #7009A	1,640, #7051A	14,100, #7023A	6,810, #7037A
ERDA-6	NA	2,820, #7009B	3,740, #7051B	7,270, #7023B	45,600, #7037B
ERDA-6	NA	864, #7010A	1,930, #7052A	High, #7024A	364, #7038A
ERDA-6	NA	1,300, #7010B	1,780, #7052B	1,130, #7024B	2,850, #7038B

NA: not available yet.

ND: not determined.

Table E-3. Effects of Initial Radionuclide Concentration and  $P_{CO_2}$  on Matrix  $K_d$ s for Th(IV), Dolomite-Rich Culebra Rock, and AISinR (LANL Empirical Sorption Study). Six-week sorption runs with VPX-25-8.  $K_d$ s in bold font excluded from ranges and distributions because of unacceptable differences between standards and controls. Data current as of April 3, 1996. Table compiled by L. H. Brush on March 30 and April 3, 1996, based on information provided by LANL on March 28 and April 1, 1996. Table checked by Brush and S. Boone on April 3, 1996.

Brine	Initial $^{230}\text{Th}$ Conc. (M)	$K_d$ (ml/g), 0.033% $\text{CO}_2$	$K_d$ (ml/g), 0.24% $\text{CO}_2$	$K_d$ (ml/g), 1.4% $\text{CO}_2$	$K_d$ (ml/g), 4.1% $\text{CO}_2$
AISinR	ND	ND	ND	ND	ND
AISinR	ND	ND	ND	ND	ND
AISinR	ND	ND	ND	ND	ND
AISinR	ND	ND	ND	ND	ND
AISinR	ND	ND	ND	ND	ND
AISinR	ND	ND	ND	ND	ND
AISinR	NA	<b>High, #7012A</b>	<b>10,800, #7054A</b>	<b>4,580, #7026A</b>	<b>57,100, #7040A</b>
AISinR	NA	<b>High, #7012B</b>	<b>16,900, #7054B</b>	<b>7,080, #7026B</b>	<b>High, #7040B</b>
AISinR	ND	ND	ND	ND	ND
AISinR	ND	ND	ND	ND	ND

NA: not available yet.

ND: not determined.

Table E-4. Effects of Initial Radionuclide Concentration and  $P_{CO_2}$  on Matrix  $K_d$ s for Th(IV), Dolomite-Rich Culebra Rock, and H-17 (LANL Empirical Sorption Study). Six-week sorption runs with VPX-25-8.  $K_d$ s in bold font excluded from ranges and distributions because of unacceptable differences between standards and controls. Data current as of April 3, 1996. Table compiled by L. H. Brush on March 30 and April 3, 1996, based on information provided by LANL on March 28 and April 1, 1996. Table checked by Brush and S. Boone on April 3, 1996.

Brine	Initial $^{230}\text{Th}$ Conc. (M)	$K_d$ (ml/g), 0.033% $\text{CO}_2$	$K_d$ (ml/g), 0.24% $\text{CO}_2$	$K_d$ (ml/g), 1.4% $\text{CO}_2$	$K_d$ (ml/g), 4.1% $\text{CO}_2$
H-17	ND	ND	ND	ND	ND
H-17	ND	ND	ND	ND	ND
H-17	ND	ND	ND	ND	ND
H-17	ND	ND	ND	ND	ND
H-17	ND	ND	ND	ND	ND
H-17	ND	ND	ND	ND	ND
H-17	NA	<b>12,100, #7013A</b>	<b>7,580, #7055A</b>	<b>High, #7027A</b>	<b>14,500, #7041A</b>
H-17	NA	<b>High, #7013B</b>	<b>High, #7055B</b>	<b>23,700, #7027B</b>	<b>14,300, #7041B</b>
H-17	ND	ND	ND	ND	ND
H-17	ND	ND	ND	ND	ND

NA: not available yet.

ND: not determined.

Table E-5. Minimum Values of R and  $K_d$  for Th(IV) in Intact Culebra Cores (SNL Column Transport Study). Data current as of March 26, 1996. Table compiled by L. H. Brush on March 30, 1996, based on memo by D. A. Lucero, G. O. Brown, and K. G. Budge dated March 28, 1996. Table checked by Brush on March 31, 1996.

Run #	Solid (core)	Brine	Flow rate (ml/min)	Run Time (days)	Ef-fluent Vol. (L)	$R_{min}$	Porosity (%)	$K_{d, min}$ (ml/g)	Range ( $\pm$ ml/g)
C-2	VPX-28-6C	AIS.	0.1	237	34.15	35	5.7, <sup>S</sup> 3.5 <sup>D</sup>	0.87	NA
C-5	VPX-28-6C	ER.-6	0.1	146	20.98	22	3.9, <sup>S</sup> 2.3 <sup>D</sup>	0.36	NA
D-2	VPX-25-8A	AIS.	0.1	133	19.12	8.5	8.2, <sup>S</sup> 5.5 <sup>D</sup>	0.25	NA

AIS: AISinR.

D: dual porosity assumed.

ER.-6: ERDA-6.

NA: not available yet.

S: single porosity assumed.



Table E-6. Minimum Values of R and  $K_d$  for Th(IV) in Intact Culebra Cores (SNL Column Transport Study). Data current as of March 26, 1996. Table compiled by L. H. Brush on March 30, 1996, based on memo by D. A. Lucero, G. O. Brown, and K. G. Budge dated March 28, 1996. Table checked by Brush on March 31, 1996. Table revised by Brush on April 6, 1996, based on memo by Lucero and Brown dated April 5, 1996. Table checked by Y. Behl on April 8, 1996.

Run #	Solid (core)	Brine	Flow rate (ml/min)	Run Time (days)	Ef-fluent Vol. (L)	$R_{min}$	Poro-sity (%)	$K_{d, min}$ (ml/g)	Range ( $\pm$ ml/g)
C-2	VPX-28-6C	AIS.	0.1	237	34.15	35	5.7 <sup>S</sup>	0.87	NA
C-5	VPX-28-6C	ER.-6	0.1	146	20.98	22	3.9 <sup>S</sup>	0.36	NA
D-2	VPX-25-8A	AIS.	0.1	133	19.12	8.5	8.2 <sup>S</sup>	0.25	NA

AIS: AISinR.

ER.-6: ERDA-6.

NA: not available yet.

S: single porosity assumed.



APPENDIX F: RANGES AND PROBABILITY DISTRIBUTIONS OF  
MATRIX  $K_d$ s FOR Np(V) AND DOLOMITE-RICH  
CULEBRA ROCK

Based on experimental results, ASTP personnel have predicted that Np will speciate as Np(IV) or Np(V), but not as Np(VI), in deep (Castile and Salado) brines in WIPP disposal rooms. Furthermore, a modeling study of the effects of mixing deep and Culebra brines on the oxidation states of Pu, U, and Np in the Culebra showed that Culebra fluids are poorly poised (see Predictions of Actinide Oxidation States in the Culebra above). Therefore; we established experimentally obtained ranges of matrix  $K_d$ s for Np(V) and used the experimentally obtained ranges for Th(IV) (see Appendix E above) and the oxidation-state analogy to establish ranges for Np(IV) (and U(IV)).

For the *initial* ranges for Np(V) and the deep brines, we first considered *all* of the data from the 6-week empirical sorption experiments carried out with Brine A and ERDA-6 on the bench top (0.033% CO<sub>2</sub>) by Triay and her group at LANL (see Methods Used to Establish Ranges of Matrix  $K_d$ s above for the reasons for considering these data). These runs were: #6020, #6040, #6060, and #6080 (see Table F-1 below), and #6021, #6041, #6061, #6081 (Table F-2). Next, we discarded the data from #6040, #6021, and #6041, the runs in which the difference between the activity of the <sup>237</sup>Np in a standard and that in a control exceeded 3 $\sigma$ , where  $\sigma$  is the standard deviation (see Methods Used to Establish Ranges of Matrix  $K_d$ s). Discarding the data from these three runs yielded an *initial* range of 8.64 ml/g (from #6020) to 47.7 ml/g (#6061) for Np(V) and the deep brines.

For the *initial* ranges for Np(V) and the Culebra brines, we first considered *all* of Triay's 6-week sorption data obtained with AISinR and H-17 on the bench top (0.033% CO<sub>2</sub>) and in glove boxes with atmospheres containing 0.24 and 1.4% CO<sub>2</sub> (see Methods Used to Establish Ranges of Matrix  $K_d$ s). These were: #6022, #6042, #6062, #6082 #24022, #24042 #24062, #24082, #12022, #12042, #12062, and #12082 (Table F-3), and #6023, #6043, #6063, #6083, #24023, #24043, #24063, #24083, #12023, #12043, #12063, and #12083 (Table F-4). We then discarded the data from #24042 and #24082, the runs in which the difference between the activity of the <sup>237</sup>Np in a standard and that in a control exceeded 3 $\sigma$ , to obtain the *initial* range of 2.09 ml/g (from #12022) to 163 ml/g (#6042) for Np(V) and the Culebra brines.

Next, we compared these initial ranges with the data from the mechanistic sorption study by Brady and his colleagues at SNL and LANL. We used Brady's data to extend Triay's empirical sorption data for the deep brines to the basic conditions expected to result from the use of an MgO backfill in WIPP disposal rooms, *but not* to extend Triay's data for the Culebra brines to basic conditions (see Methods Used to Establish Ranges of Matrix  $K_d$ s). Brady's data for 0.5 M NaCl, atmospheric CO<sub>2</sub>, and the highest pH values under these conditions are (to three significant figures) 892 and 938 ml/g at a pH of 9.87 and 9.88, respectively (Table F-5). Because these values are *greater than the upper limit* of the initial range for Np(V) and the deep brines (see above), we extended

this range to obtain a *revised* range for Np(V) and deep brines of 8.64 to 938 ml/g. Because we did not use this comparison to extend the initial range for Np(V) and the Culebra brines to basic conditions, this *revised* range remains 2.09 to 163 ml/g.

We then compared both of these revised ranges with the data from the transport study with intact Culebra cores by Lucero and his colleagues at SNL. Lucero carried out his experiments under ambient atmospheric conditions; therefore, the CO<sub>2</sub> content of these experiments was probably similar to that in the LANL bench-top (0.033% CO<sub>2</sub>) runs. Lucero *did* observe breakthrough of Np(V) in his experiments. Therefore, it was possible to determine actual K<sub>ds</sub> for this element. Lucero and his colleagues submitted their results on March 28, 1996, (see Table F-6), then revised them on April 5, 1996 (Table F-7). The K<sub>d</sub> reported for Experiment C-7 with the deep brine ERDA-6 (Table F7) *is less than the lower limit of the revised range of K<sub>ds</sub> for Np(V) and the deep brines obtained from the empirical and mechanistic sorption experiments* (see above). Therefore, we extended this range to obtain a *final* range for Np(V) and deep brines of 2.0 to 938 ml/g, and rounded it to 2 to 900 ml/g prior to inclusion in Table 1 above. Because Lucero's K<sub>ds</sub> for Np(V) and the Culebra brine AISinR (C-6, D-2, and D4 in Table F-7), *are also less than the lower limit of the revised range for Np(V) and the Culebra brines obtained from the sorption studies* (see above), we extended this range to obtain a *final* range of 1.0 to 163 ml/g, rounded to 1 to 200 ml/g (Table 1).

We recommend that PA personnel use a uniform probability distribution for both of these ranges (see Methods Used to Establish Probability Distributions of Matrix K<sub>ds</sub> above).

Furthermore, we recommend that PA use the range of 1 to 200 ml/g (the range for Culebra brines) for Np(V) because this range results in less retardation of this element than the range for deep brines (see Methods Used for Final Selection of the Range of Matrix K<sub>ds</sub> for Use in PA Calculations above).

Table F-1. Effects of Initial Radionuclide Concentration and  $P_{CO_2}$  on Matrix  $K_d$ s for Np(V), Dolomite-Rich Culebra Rock, and Brine A (LANL Empirical Sorption Study). Six-week sorption runs with VPX-25-8.  $K_d$ s in bold font excluded from ranges and distributions because of unacceptable differences between standards and controls. Data current as of April 3, 1996. Table compiled by L. H. Brush on March 23 and 30, 1996, based on information provided by LANL on March 19 and 26, 1996. Table checked by Brush and S. Boone on April 3, 1996. Table revised by Brush on June 7, 1996. Table checked by L. J. Storz on June 10, 1996.



Brine	Range of Initial $^{237}\text{Np}$ Conc. (M)	$K_d$ (ml/g), 0.033% $\text{CO}_2$	$K_d$ (ml/g), 0.24% $\text{CO}_2$	$K_d$ (ml/g), 1.4% $\text{CO}_2$	$K_d$ (ml/g), 4.1% $\text{CO}_2$
Brine A	ND	ND	ND	ND	ND
Brine A	$6.80 \times 10^{-7}$ to $9.26 \times 10^{-6}$	8.64, #6020	5.05, #24020	224, #12020	380, #18020
Brine A	$3.86 \times 10^{-6}$ to $4.52 \times 10^{-6}$	<b>16.1,</b> #6040	<b>31.9,</b> #24040	11.8, #12040	8.91, #18040
Brine A	$6.09 \times 10^{-7}$ to $6.56 \times 10^{-7}$	20.3, #6060	<b>150,</b> #24060	21.3, #12060	21.9, #18060
Brine A	$2.16 \times 10^{-7}$ to $2.58 \times 10^{-7}$	37.5, #6080	32.5, #24080	36.7, #12080	27.0, 18080

ND: not determined.

Table F-2. Effects of Initial Radionuclide Concentration and  $P_{CO_2}$  on Matrix  $K_d$ s for Np(V), Dolomite-Rich Culebra Rock, and ERDA-6 (LANL Empirical Sorption Study). Six-week sorption runs with VPX-25-8.  $K_d$ s in bold font excluded from ranges and distributions because of unacceptable differences between standards and controls. Data current as of April 3, 1996. Table compiled by L. H. Brush on March 23 and 30, 1996, based on information provided by LANL on March 19 and 26, 1996. Table checked by Brush and S. Boone on April 3, 1996. Table revised by Brush on June 7, 1996. Table checked by L. J. Storz on June 10, 1996.



Brine	Range of Initial $^{237}\text{Np}$ Conc. (M)	$K_d$ (ml/g), 0.033% $\text{CO}_2$	$K_d$ (ml/g), 0.24% $\text{CO}_2$	$K_d$ (ml/g), 1.4% $\text{CO}_2$	$K_d$ (ml/g), 4.1% $\text{CO}_2$
ERDA-6	ND	ND	ND	ND	ND
ERDA-6	4.43 x 10 <sup>-7</sup> to 9.85 x 10 <sup>-7</sup>	<b>218,</b> <b>#6021</b>	<b>241,</b> <b>#24021</b>	562, #12021	<b>508,</b> <b>#18021</b>
ERDA-6	4.81 x 10 <sup>-7</sup> to 1.46 x 10 <sup>-6</sup>	<b>55.2,</b> <b>#6041</b>	<b>181,</b> <b>#24041</b>	153, #12041	<b>117,</b> <b>#18041</b>
ERDA-6	1.70 x 10 <sup>-7</sup> to 5.58 x 10 <sup>-7</sup>	47.7, #6061	<b>280,</b> <b>#24061</b>	163, #12061	29.9, #18061
ERDA-6	8.59 x 10 <sup>-9</sup> to 2.78 x 10 <sup>-7</sup>	31.7, #6081	<b>14,000,</b> <b>#24081</b>	<b>High!</b> <b>#12081</b>	<b>High!</b> <b>#18081</b>

ND: not determined.

Table F-3. Effects of Initial Radionuclide Concentration and  $P_{CO_2}$  on Matrix  $K_d$ s for Np(V), Dolomite-Rich Culebra Rock, and AISinR (LANL Empirical Sorption Study). Six-week sorption runs with VPX-25-8.  $K_d$ s in bold font excluded from ranges and distributions because of unacceptable differences between standards and controls. Data current as of April 3, 1996. Table compiled by L. H. Brush on March 23 and 30, 1996, based on information provided by LANL on March 19 and 26, 1996. Table checked by Brush and S. Boone on April 3, 1996. Table revised by Brush on June 7, 1996. Table checked by L. J. Storz on June 10, 1996.

Brine	Range of Initial $^{237}\text{Np}$ Conc. (M)	$K_d$ (ml/g), 0.033% $\text{CO}_2$	$K_d$ (ml/g), 0.24% $\text{CO}_2$	$K_d$ (ml/g), 1.4% $\text{CO}_2$	$K_d$ (ml/g), 4.1% $\text{CO}_2$
AISinR	ND	ND	ND	ND	ND
AISinR	$7.62 \times 10^{-6}$ to $8.72 \times 10^{-6}$	5.12, #6022	3.70, #24022	2.09, #12022	2.19, #18022
AISinR	$6.06 \times 10^{-7}$ to $4.53 \times 10^{-6}$	163, #6042	<b>11.9,</b> <b>#24042</b>	2.35, #12042	2.23, #18042
AISinR	$5.26 \times 10^{-7}$ to $8.08 \times 10^{-7}$	20.4, #6062	9.64, #24062	4.06, #12062	4.83, #18062
AISinR	$2.39 \times 10^{-7}$ to $3.81 \times 10^{-7}$	32.9, #6082	<b>46.7,</b> <b>#24082</b>	9.89, #12082	10.4, #18082

ND: not determined.



Table F-4. Effects of Initial Radionuclide Concentration and  $P_{CO_2}$  on Matrix  $K_d$ s for Np(V), Dolomite-Rich Culebra Rock, and H-17 (LANL Empirical Sorption Study). Six-week sorption runs with VPX-25-8. No  $K_d$ s in this table excluded from ranges and distributions because of unacceptable differences between standards and controls. Data current as of April 3, 1996. Table compiled by L. H. Brush on March 23 and 30, 1996, based on information provided by LANL on March 19 and 26, 1996. Table checked by Brush and S. Boone on April 3, 1996. Table revised by Brush on June 7, 1996. Table checked by L. J. Storz on June 10, 1996.

Brine	Range of Initial $^{237}\text{Np}$ Conc. (M)	$K_d$ (ml/g), 0.033% $\text{CO}_2$	$K_d$ (ml/g), 0.24% $\text{CO}_2$	$K_d$ (ml/g), 1.4% $\text{CO}_2$	$K_d$ (ml/g), 4.1% $\text{CO}_2$
H-17	ND	ND	ND	ND	ND
H-17	$2.88 \times 10^{-7}$ to $9.88 \times 10^{-6}$	52.4, #6023	19.0, #24023	2.96, #12023	1.40, #18023
H-17	$3.30 \times 10^{-6}$ to $4.93 \times 10^{-6}$	15.8, #6043	13.3, #24043	3.23, #12043	2.37, #18043
H-17	$3.44 \times 10^{-7}$ to $8.87 \times 10^{-7}$	40.1, #6063	25.8, #24063	47.1, #12063	4.61, #18063
H-17	$2.16 \times 10^{-7}$ to $8.19 \times 10^{-6}$	44.2, #6083	8.02, #24083	3.79, #12083	6.60, #18083

ND: not determined.

Table F-5. Effects of pH and  $P_{CO_2}$  on Matrix  $K_d$ s for Np(V) and Pure Dolomite (SNL/LANL Mechanistic Sorption Study). Sorption runs with Norwegian dolomite and 0.5 M NaCl. Data current as of March 31, 1996. Table retyped by L. H. Brush on April 24, 1996. Table checked by Y. Behl on April 28, 1996.

pH (standard units)	$K_d$ (ml/g), atmospheric $CO_2$	$K_d$ (ml/g), 0.5% $CO_2$	$K_d$ (ml/g), 5% $CO_2$
9.88	938.1	NA	NA
9.87	891.95	NA	NA
8.42	324.37	NA	NA
6.7	59.493	NA	NA
6.2	59.493	NA	NA
5.81	-6.7249	NA	NA
5.21	59.493	NA	NA
4.62	59.493	NA	NA
4.05	59.493	NA	NA
3.51	59.493	NA	NA
3.11	-6.7249	NA	NA



NA: not applicable.

Table F-5. Effects of pH and  $P_{CO_2}$  on Matrix  $K_d$ s for Np(V) and Pure Dolomite (SNL/LANL Mechanistic Sorption Study) (continued).

pH (standard units)	$K_d$ (ml/g), atmospheric $CO_2$	$K_d$ (ml/g), 0.5% $CO_2$	$K_d$ (ml/g), 5% $CO_2$
6.9	NA	82.353	NA
8.49	NA	623.53	NA
7.32	NA	352.94	NA
7.19	NA	248.87	NA
6.99	NA	248.87	NA
6.88	NA	159.66	NA
6.55	NA	82.353	NA
6.17	NA	159.66	NA
5.28	NA	82.353	NA
3.97	NA	82.353	NA
3.13	NA	159.66	NA

NA: not applicable.

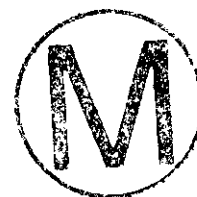


Table F-5. Effects of pH and  $P_{CO_2}$  on Matrix  $K_d$ s for Np(V) and Pure Dolomite (SNL/LANL Mechanistic Sorption Study) (continued).

pH (standard units)	$K_d$ (ml/g), atmospheric $CO_2$	$K_d$ (ml/g), 0.5% $CO_2$	$K_d$ (ml/g), 5% $CO_2$
6.39	NA	NA	-56.83
6.91	NA	NA	100.36
6.89	NA	NA	0
6.8	NA	NA	100.36
6.75	NA	NA	100.36
6.84	NA	NA	100.36
6.49	NA	NA	100.36
6.07	NA	NA	15.721
5.76	NA	NA	15.721
4.91	NA	NA	100.36
3.62	NA	NA	15.721

NA: not applicable.



Table F-6. Measured Values of R and Calculated Values of  $K_d$  for Np(V) in Intact Culebra Cores (SNL Column Transport Study). Values in bold font to be excluded from ranges and distributions because fits to elution data were inferior to those assuming single porosity and dual porosity with fracture retardation. Data current as of March 30, 1996. Table compiled by L. H. Brush on March 30, 1996, based on memo by D. A. Lucero, G. O. Brown, and K. G. Budge dated March 28, 1996. Table checked by Brush on March 31, 1996.

Run #	Solid (core)	Brine	Flow rate (ml/min)	Run Time (days)	Ef-fluent Vol. (L)	R	Porosity	$K_d$ (ml/g)	Range ( $\pm$ ml/g)
C-5	VPX-28-6C	ER.-6	0.1	13	2	30.8; <sup>S</sup>	3.9 <sup>S</sup>	0.51 <sup>S</sup>	0.29 <sup>S</sup>
						<b>1,</b> <b>166;</b> <sup>DN</sup>	2.3 <sup>DN</sup>	<b>1.65</b> <sup>DN</sup>	<b>1.0</b> <sup>DN</sup>
						7.0, 103 <sup>DF</sup>	2.3 <sup>DF</sup>	0.06 <sup>DF</sup>	0.03 <sup>DF</sup>
C-6	VPX-28-6C	AIS.	0.1	13	2	58.5; <sup>S</sup>	4.5 <sup>S</sup>	1.12 <sup>S</sup>	0.26 <sup>S</sup>
						<b>1,</b> <b>301;</b> <sup>DN</sup>	1.85 <sup>DN</sup>	<b>2.4</b> <sup>DN</sup>	<b>1.4</b> <sup>DN</sup>
						22, 158 <sup>DF</sup>	1.85 <sup>DF</sup>	.169 <sup>DF</sup>	.048 <sup>DF</sup>
C-7	VPX-28-6C	ER.-6	0.1	13	2	119; <sup>S</sup>	3.9 <sup>S</sup>	2.0 <sup>S</sup>	0.8 <sup>S</sup>
						<b>1,</b> <b>910;</b> <sup>DN</sup>	2.1 <sup>DN</sup>	<b>8.3</b> <sup>DN</sup>	<b>11.9</b> <sup>DN</sup>
						169, 0 <sup>DF</sup>	2.1 <sup>DF</sup>	1.53 <sup>DF</sup>	38 <sup>DF</sup>
D-2	VPX-25-8A	AIS.	0.1	12	2	47; <sup>S</sup>	8.2 <sup>S</sup>	1.64 <sup>S</sup>	0.58 <sup>S</sup>
						<b>1,</b> <b>1670;</b> <sup>N</sup>	5.5 <sup>DN</sup>	<b>40</b> <sup>DN</sup>	<b>6</b> <sup>DN</sup>
						6.6, NA <sup>DF</sup>	5.5 <sup>DF</sup>	NA <sup>DF</sup>	NA <sup>DF</sup>

Table F-6. Measured Values of R and Calculated Values of  $K_d$  for Np(V) in Intact Culebra Cores (SNL Column Transport Study) (continued).

Run #	Solid (core)	Brine	Flow rate (ml/min)	Run Time (days)	Ef-fluent Vol. (L)	R	Porosity	$K_d$ (ml/g)	Range ( $\pm$ ml/g)
D-4	VPX-25-8A	AIS.	0.1	13	2	39; <sup>S</sup> 1, 340; <sup>DN</sup> 17.5, 154 <sup>DF</sup>	10.0 <sup>S</sup> 4.8 <sup>DN</sup> 4.8 <sup>DF</sup>	1.65 <sup>S</sup> 7.1 <sup>DN</sup> 0.34 <sup>DF</sup>	0.22 <sup>S</sup> 4.2 <sup>DN</sup> 0.07 <sup>DF</sup>

AIS: AISinR.

DF: dual porosity and fracture retardation assumed.

DN: dual porosity and no fracture retardation assumed.

ER.-6: ERDA-6.

NA: not available yet.

S: single porosity assumed.

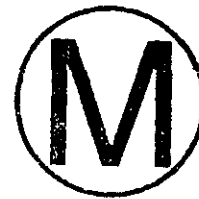


Table F-7. Measured Values of R and Calculated Values of  $K_d$  for Np(V) in Intact Culebra Cores (SNL Column Transport Study). Data current as of March 30, 1996. Table compiled by L. H. Brush on March 30, 1996, based on memo by D. A. Lucero, G. O. Brown, and K. G. Budge dated March 28, 1996. Table checked by Brush on March 31, 1996. Table revised by Brush on April 6, 1996, based on memo by Lucero and Brown dated April 5, 1996. Table checked by Y. Behl on April 8, 1996.



Run #	Solid (core)	Brine	Flow rate (ml/min)	Run Time (days)	Ef-fluent Vol. (L)	R	Porosity	$K_d$ (ml/g)	Range ( $\pm$ ml/g)
C-6	VPX-28-6C	AIS.	0.1	13	2	59 <sup>S</sup>	4.5 <sup>S</sup>	1.1 <sup>S</sup>	NA
C-7	VPX-28-6C	ER.-6	0.1	13	2	120 <sup>S</sup>	3.9 <sup>S</sup>	2.0 <sup>S</sup>	NA
D-2	VPX-25-8A	AIS.	0.1	12	2	47 <sup>S</sup>	8.2 <sup>S</sup>	1.6 <sup>S</sup>	NA
D-4	VPX-25-8A	AIS.	0.1	13	2	39 <sup>S</sup>	10.0 <sup>S</sup>	1.6 <sup>S</sup>	NA

AIS: AISinR.

ER.-6: ERDA-6.

NA: not available yet.

S: single porosity assumed.



APPENDIX G: EFFECTS OF ORGANIC LIGANDS ON RANGES AND PROBABILITY DISTRIBUTIONS OF MATRIX  $K_{ds}$  FOR Pu(V), Am(III), U(VI), Th(IV), Np(V), AND DOLOMITE-RICH CULEBRA ROCK

Triay and her group at LANL carried out two sets of experiments on the effects of four organic ligands (acetate, citrate, ethylenediaminetetraacetic acid or EDTA, and lactate) on the  $K_{ds}$  for dissolved Pu(V), Am(III), U(VI), Th(IV), and Np(V) under conditions expected in the Culebra. Brush (1990) concluded that these and six other organic and two inorganic ligands could affect the solubilities of the actinide elements in TRU waste. Therefore, he estimated the concentrations of these 12 ligands in three quantities of brine that could resaturate WIPP disposal rooms after filling and sealing. Since 1990, the ASTP has reduced the number of organic ligands of concern from twelve to four (acetate, citrate, EDTA, and oxalate). Triay carried out experiments with acetate, citrate, EDTA, and lactate because the ASTP had not eliminated lactate from consideration yet, and because Triay concluded that oxalate would be extremely insoluble given the dissolved Ca concentrations expected in WIPP brines. Triay conducted the first set of runs with ERDA-6 and H17, and acetate, citrate, EDTA, and lactate all present at concentrations as close as possible to the "minimum" and "maximum" concentrations estimated by Brush (1990) (see Table G-1 below). Soon after Triay started their preliminary experiments, Weiner (1996) used the quantities of acetate, citrate, EDTA, and oxalate in TRU waste estimated by Drez (1996) to predict the concentrations of these organic ligands in brines in the repository (Table G-1).

Tables G-2, G-3, G-4, G-5, and G-6 give the results of the preliminary experiments with ERDA-6 and H-17, and Pu(V), Am(III), U(VI), Th(IV), and Np(V), respectively. At low concentrations, acetate, citrate, EDTA, and lactate have little or no effect on the  $K_{ds}$  for these elements (compare the results for "low-concentration organics" to those for "none," the runs without any organic ligands present.) In fact, for Pu(V) and ERDA-6 in contact with ambient atmospheric or (about 0.033%)  $\text{CO}_2$ ; Am(III), ERDA-6, and 0.033%  $\text{CO}_2$ ; and U(VI), ERDA-6, and 0.033%  $\text{CO}_2$ , low concentrations of these organic ligands actually *increase* the  $K_{ds}$  relative to those obtained without any organic ligands. However, at high concentrations, these organic ligands significantly *decrease* the  $K_{ds}$  for all of these elements. Note that the low and the high concentrations of acetate, citrate, and EDTA used in these preliminary runs bracket the predicted concentrations of these organic ligands (Table G-1).

Triay used ERDA-6 and H-17, which contain 19 and 74.1 mM Mg, respectively, for this set of experiments. However, ASTP personnel have predicted the effects of acetate, citrate, EDTA, and oxalate on the solubilities of the actinide elements by assuming that all of these organic ligands will dissolve in intergranular Salado brine as it accumulates in WIPP disposal rooms. Novak (1996) used FMT to predict that the Mg concentration in SPC brine (Brine A modified by omitting minor and trace constituents, and used by the ASTP to simulate Salado brine in several experimental and modeling studies) will be 454 mM after equilibration with halite, anhydrite, the actinide elements and the organic ligands in TRU waste, and an MgO backfill. This Mg concentration is significantly higher than that of ERDA-6 before or after equilibration with this backfill (19 and 48 mM, respectively) and significantly higher than that of H-17 (74.1 mM). Because we hoped that competition among Mg and Pu, Am, U, Th, and Np for the binding sites on these organic ligands

would mitigate the effects of these organics on the  $K_d$ s for these elements, Triay carried out an additional set of experiments with acetate, citrate, EDTA, and lactate at low, intermediate, and high concentrations (see Table G-1) and with Brine A modified to simulate the composition of Salado brine after equilibration with an MgO backfill.

Table G-7 shows the results of these experiments. Low concentrations of organics significantly decreased the  $K_d$ s for Th relative to those obtained without any organics, but had much less effect on the  $K_d$ s for the other elements. Intermediate concentrations of organics significantly decreased the  $K_d$ s for all of the elements except U(VI). High concentrations significantly decreased the  $K_d$ s for all five of these elements.

However, we *have not* revised the ranges and probability distributions of  $K_d$ s for Pu, Am, U, Th, and Np shown in Table 1 (see above) because large quantities of other metals (see below) will be present to form complexes with these organic ligands, thus preventing them from forming complexes with the actinide elements and decreasing the  $K_d$ s for the actinides in the Culebra. (These other metals will also prevent these organic ligands from increasing the solubilities of the actinide elements in WIPP disposal rooms.) These other metals include Fe, large quantities which will be present in WIPP disposal rooms in steel waste containers (drums and boxes) and as steels, stainless steels, and other Fe-base materials in the waste; Mg, large quantities of which will be emplaced in the repository as an MgO backfill to remove microbially produced  $\text{CO}_2$  (but will be present as  $\text{MgCO}_3$  and/or  $\text{Mg}(\text{OH})_2$ , and magnesium oxychloride after reaction with  $\text{CO}_2$  and/or brine); and Cr, Mn, Ni, Pb, and V, which will be present in lesser but still sufficient quantities in steel drums and boxes, and in steels, stainless steels, and other Fe-base alloys in the waste, and in other waste constituents. Preliminary modeling of the equilibria among dissolved and solid-phase Pu and Am, Fe, Mg, and Ni, and EDTA imply that, under the conditions expected in WIPP disposal rooms, Ni would form complexes with 99.8% of the EDTA expected to be present in the repository, thus preventing it from complexing significant quantities of Pu and Am. A detailed description of these calculations, and any additional modeling or laboratory studies of these competitive equilibria, will appear elsewhere.

## REFERENCES



- Brush, L.H. 1990. *Test Plan for Laboratory and Modeling Studies of Repository and Radionuclide Chemistry for the Waste Isolation Pilot Plant*. SAND90-0266. Albuquerque, NM: Sandia National Laboratories.
- Drez, P.E. 1996. "Final Preliminary Estimates of Complexing Agents in TRU Solidified Waste Forms Scheduled for Disposal in WIPP." Unpublished memorandum to J. Harvill, March 20, 1996. Albuquerque, NM: Drez Environmental Associates.
- Novak, C.F., and R.C. Moore. 1996. "Estimates of Dissolved Concentrations for +III, +IV, +V, and +VI Actinides in a Salado and a Castile Brine under Anticipated Repository Conditions." Unpublished memorandum to M. D. Siegel, March 28, 1996. Albuquerque, NM: Sandia National Laboratories.

Weiner, R. 1996. "Dissolved Ligand Concentrations." Unpublished memorandum to C. F. Novak, March 27, 1996. Albuquerque, NM: Sandia National Laboratories.



Table G-1. Concentrations of Organic Ligands in Experiments with ERDA-6, H-17, and Modified Brine A, and Predicted Concentrations of Organic Ligands in Brines in WIPP Disposal Rooms. Table compiled by L. H. Brush on May 10, 1996, based on information provided by LANL on April 25, 1996. Table checked by L. J. Storz on May 17, 1996.

Organic Ligand	Low Conc.	High Conc.	Low Conc.	Intermediate	High Conc.	Predicted Conc. in WIPP (mM)
	(ERDA-6 and H-17) (mM)	(ERDA-6 and H-17) (mM)	(Modified Brine A) (mM)	Conc. (Modified Brine A) (mM)	(Modified Brine A) (mM)	
Acetate	0.195 (ERDA-6)	19.5172 (ERDA-6)	0.489	4.89	48.9	1.062
	0.195 (H-17)	19.5172 (H-17)				
Citrate	0.0340 (ERDA-6)	3.4002 (ERDA-6)	0.03417	0.3417	3.417	0.465
	0.0340 (H-17)	3.4002 (H-17)				
EDTA	0.000146 (ERDA-6)	0.0146 (ERDA-6)	0.00011	0.0011	0.011	0.00416
	0.000146 (H-17)	0.0146 (H-17)				
Lactate	0.00761 (ERDA-6)	0.7610 (ERDA-6)	0.02088	0.2088	2.088	Not predicted
	0.00796 (H-17)	0.7956 (H-17)				
Oxalate	NU	NU	NU	NU	NU	7.404

NU: Not used because LANL expected Ca-oxalate to precipitate from these brines at very low oxalate concentrations.

Table G-2. Effects of Brine, Organic Ligands, and  $P_{CO_2}$  on Matrix  $K_d$ s for Pu(V) and Dolomite-Rich Culebra Rock (LANL Empirical Sorption Study): One-week sorption runs with H-19, B-4, Box 7.  $K_d$ s in bold font excluded from ranges and distributions because of unacceptable differences between standards and controls. Still counting new controls for underlined samples. Data current as of May 30, 1996. Table compiled by L. H. Brush on May 16, 1996, based on information provided by LANL on May 15, 1996. Table checked by L. J. Storz on May 16 and 17, 1996. Table revised by Brush on May 31 and June 1, 1996, based on information provided by LANL on May 30 and 31, 1996. Table checked by L. J. Storz on June 10, 1996.



Brine	Additive	$K_d$ , (ml/g), 0.033% $CO_2$	$K_d$ (ml/g), 4.1% $CO_2$
ERDA-6	None	157, #JRF O-131	<u>217</u> , #JRF O-181
ERDA-6	None	158, #JRF O-132	<u>223</u> , #JRF O-182
ERDA-6	Avg. without organics	158	<u>220</u>
ERDA-6	Low-conc. organics	787, #JRF O-139	171, #JRF O-189
ERDA-6	Low-conc. organics	142, #JRF O-140	184, #JRF O-190
ERDA-6	Avg. w. low-conc. org.	464	178
ERDA-6	High-conc. organics	6.44, #JRF O-137	10.3, #JRF O-187
ERDA-6	High-conc. organics	7.48, #JRF O-138	9.10, #JRF O-188
ERDA-6	Avg. w. high-conc. org.	6.96	9.70

Table G-2. Effects of Brine, Organic Ligands, and  $P_{CO_2}$  on Matrix  $K_d$ s for Pu(V) and Dolomite-Rich Culebra Rock (LANL Empirical Sorption Study) (continued).

Brine	Additive	$K_d$ (ml/g), 0.033% $CO_2$	$K_d$ (ml/g), 4.1% $CO_2$
H-17	None	18.4, #JRF O-31	<u>8.51,</u> <u>#JRF O-81</u>
H-17	None	19.8, #JRF O-32	<u>9.19,</u> <u>#JRF O-82</u>
H-17	Avg. without organics	19.1	<u>8.85</u>
H-17	Low-conc. organics	9.50, #JRF O-39	4.45, #JRF O-89
H-17	Low-conc. organics	17.0, #JRF O-40	7.73, #JRF O-90
H-17	Avg. w. low-conc. org.	13.2	6.14
H-17	High-conc. organics	1.39, #JRF O-37	0.315, #JRF O-87
H-17	High-conc. organics	0.934, #JRF O-38	0.515, #JRF O-88
H-17	Avg. w. high-conc. org.	1.16	0.415



Table G-3. Effects of Brine, Organic Ligands, and  $P_{CO_2}$  on Matrix  $K_d$ s for Am(III) and Dolomite-Rich Culebra Rock (LANL Empirical Sorption Study). One-week sorption runs with H-19, B-4, Box 7.  $K_d$ s in bold font excluded from ranges and distributions because of unacceptable differences between standards and controls. Still counting new controls for underlined samples. Data current as of May 30, 1996. Table compiled by L. H. Brush on May 16, 1996, based on information provided by LANL on May 15, 1996. Table checked by L. J. Storz on May 16 and 17, 1996. Table revised by Brush on May 31 and June 1, 1996, based on information provided by LANL on May 30 and 31, 1996. Table checked by L. J. Storz on June 10, 1996.

Brine	Additive	$K_d$ , (ml/g), 0.033% $CO_2$	$K_d$ , (ml/g), 4.1% $CO_2$
ERDA-6	None	199, #JRF O-141	<u>2,890</u> , #JRF O-191
ERDA-6	None	1,220, #JRF O-142	<u>2,160</u> , #JRF O-192
ERDA-6	Avg. without organics	710	<u>2,520</u>
ERDA-6	Low-conc. organics	1,390 #JRF O-161	1,680, #JRF O-199
ERDA-6	Low-conc. organics	1,470, #JRF O-171	1,880, #JRF O-200
ERDA-6	Avg. w. low-conc. org.	1,430	1,780
ERDA-6	High-conc. organics	<b>10.6</b> , #JRF O-147	7.40, #JRF O-197
ERDA-6	High-conc. organics	<b>7.84</b> , #JRF O-151	5.05, #JRF O-198
ERDA-6	Avg. w. high-conc. org.	9.22	6.22

Table G-3. Effects of Brine, Organic Ligands, and  $P_{CO_2}$  on Matrix  $K_d$ s for Am(III) and Dolomite-Rich Culebra Rock (LANL Empirical Sorption Study) (continued).

Brine	Additive	$K_d$ (ml/g), 0.033% $CO_2$	$K_d$ (ml/g), 4.1% $CO_2$
H-17	None	533, #JRF O-41	<u>379,</u> <u>#JRF O-91</u>
H-17	None	549, #JRF O-42	<u>391,</u> <u>#JRF O-92</u>
H-17	Avg. without organics	541	<u>385</u>
H-17	Low-conc. organics	503, #JRF O-49	311, #JRF O-99
H-17	Low-conc. organics	497, #JRF O-50	299, #JRF O-100
H-17	Avg. w. low-conc. org.	500	305
H-17	High-conc. organics	7.79, #JRF O-47	3.58, #JRF O-97
H-17	High-conc. organics	7.37, #JRF O-48	3.75, #JRF O-98
H-17	Avg. w. high-conc. org.	7.58	3.66

Table G-4. Effects of Brine, Organic Ligands, and  $P_{CO_2}$  on Matrix  $K_d$ s for U(VI) and Dolomite-Rich Culebra Rock (LANL Empirical Sorption Study). One-week sorption runs with H19, B-4, Box 7.  $K_d$ s in bold font excluded from ranges and distributions because of unacceptable differences between standards and controls. Still counting new controls for underlined samples. Negative  $K_d$ s set to 0.00 before determining the mean. Data current as of May 30, 1996. Table compiled by L. H. Brush on May 16, 1996, based on information provided by LANL on May 15, 1996. Table checked by L. J. Storz on May 16 and 17, 1996. Table revised by Brush on May 31 and June 1, 1996, based on information provided by LANL on May 30 and 31, 1996. Table checked by L. J. Storz on June 10, 1996.



Brine	Additive	$K_d$ , (ml/g), 0.033% $CO_2$	$K_d$ , (ml/g), 4.1% $CO_2$
ERDA-6	None	-0.148, #JRF O-111	<u>-0.296</u> , #JRF O-159
ERDA-6	None	0.220, #JRF O-112	<u>0.275</u> , #JRF O-160
ERDA-6	Avg. without organics	0.110	<u>0.138</u>
ERDA-6	Low-conc. organics	<u>1.83</u> , #JRF O-119	<u>-0.0367</u> , #JRF O-168
ERDA-6	Low-conc. organics	<u>-0.371</u> , #JRF O-120	<u>-0.933</u> , #JRF O-169
ERDA-6	Avg. w. low-conc. org.	<u>0.915</u>	<u>0.00</u>
ERDA-6	High-conc. organics	<u>-0.631</u> , #JRF O-117	<u>-0.475</u> , #JRF O-166
ERDA-6	High-conc. organics	<u>-0.638</u> , #JRF O-118	<u>-0.948</u> , #JRF O-167
ERDA-6	Avg. w. high-conc. org.	<u>0.000</u>	<u>0.00</u>

Table G-4. Effects of Brine, Organic Ligands, and  $P_{CO_2}$  on Matrix  $K_d$ s for U(VI) and Dolomite-Rich Culebra Rock (LANL Empirical Sorption Study) (continued).

Brine	Additive	$K_d$ (ml/g), 0.033% $CO_2$	$K_d$ (ml/g), 4.1% $CO_2$
H-17	None	-2.11, #JRF O-11	<u>-1.69,</u> <u>#JRF O-61</u>
H-17	None	-1.79, #JRF O-12	<u>-0.323,</u> <u>#JRF O-62</u>
H-17	Avg. without organics	0.00	<u>0.00</u>
H-17	Low-conc. organics	-1.27, #JRF O-19	-0.601, #JRF O-69
H-17	Low-conc. organics	-1.67, #JRF O-20	-1.44, #JRF O-70
H-17	Avg. w. low-conc. org.	0.00	0.00
H-17	High-conc. organics	-1.77, #JRF O-17	-1.81, #JRF O-67
H-17	High-conc. organics	-1.51, #JRF O-18	-1.67, #JRF O-68
H-17	Avg. w. high-conc. org.	0.00	0.00

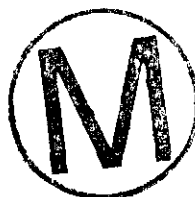
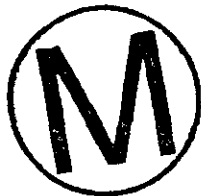


Table G-5. Effects of Brine, Organic Ligands, and  $P_{CO_2}$  on Matrix  $K_d$ s for Th(IV) and Dolomite-Rich Culebra Rock (LANL Empirical Sorption Study). One-week sorption runs with H-19, B-4, Box 7.  $K_d$ s in bold font excluded from ranges and distributions because of unacceptable differences between standards and controls. Still counting new controls for underlined samples. Data current as of May 30, 1996. Table compiled by L. H. Brush on May 16, 1996, based on information provided by LANL on May 16, 1996. Table checked by L. J. Storz on May 16 and 17, 1996. Table revised by Brush on May 31 and June 1, 1996, based on information provided by LANL on May 30 and 31, 1996. Table checked by L. J. Storz on June 10, 1996.



Brine	Additive	$K_d$ , (ml/g), 0.033% $CO_2$	$K_d$ , (ml/g), 4.1% $CO_2$
ERDA-6	None	<b>120,</b> #JRF O-101	<b><u>153,</u></b> <b><u>#JRF O-148</u></b>
ERDA-6	None	<b>98.6,</b> #JRF O-102	<b><u>169,</u></b> <b><u>#JRF O-149</u></b>
ERDA-6	Avg. without organics	<b>109</b>	<b><u>161</u></b>
ERDA-6	Low-conc. organics	<b>101,</b> #JRF O-109	<b>157,</b> #JRF O-157
ERDA-6	Low-conc. organics	<b>99.9,</b> #JRF O-110	<b>166,</b> #JRF O-158
ERDA-6	Avg. w. low-conc. org.	<b>100</b>	<b>162</b>
ERDA-6	High-conc. organics	<b>30.0,</b> #JRF O-107	<b>55.0,</b> #JRF O-155
ERDA-6	High-conc. organics	<b>32.8,</b> #JRF O-108	<b>63.2,</b> #JRF O-156
ERDA-6	Avg. w. high-conc. org.	<b>31.4</b>	<b>59.1</b>

Table G-5. Effects of Brine, Organic Ligands, and  $P_{CO_2}$  on Matrix  $K_d$ s for Th(IV) and Dolomite-Rich Culebra Rock (LANL Empirical Sorption Study) (continued).

Brine	Additive	$K_d$ (ml/g), 0.033% $CO_2$	$K_d$ (ml/g), 4.1% $CO_2$
H-17	None	15.0, #JRF O-1	<u>12.0</u> , #JRF O-51
H-17	None	16.6, #JRF O-2	<u>11.3</u> , #JRF O-52
H-17	Avg. without organics	15.8	<u>11.6</u>
H-17	Low-conc. organics	13.8, #JRF O-9	9.72, #JRF O-59
H-17	Low-conc. organics	14.4, #JRF O-10	9.20, #JRF O-60
H-17	Avg. w. low-conc. org.	14.1	9.46
H-17	High-conc. organics	5.72, #JRF O-7	0.874, #JRF O-57
H-17	High-conc. organics	8.04, #JRF O-8	1.06, #JRF O-58
H-17	Avg. w. high-conc. org.	6.88	0.967



Table G-6. Effects of Brine, Organic Ligands, and  $P_{CO_2}$  on Matrix  $K_d$ s for Np(V) and Dolomite-Rich Culebra Rock (LANL Empirical Sorption Study). One-week sorption runs with H-19, B-4, Box 7.  $K_d$ s in bold font excluded from ranges and distributions because of unacceptable differences between standards and controls. Still counting new controls for underlined samples. Data current as of May 30, 1996. Table compiled by L. H. Brush on May 16, 1996, based on information provided by LANL on May 15, 1996. Table checked by L. J. Storz on May 16 and 17, 1996. Table revised by Brush on May 31 and June 1, 1996, based on information provided by LANL on May 30 and 31, 1996. Table checked by L. J. Storz on June 10, 1996.

Brine	Additive	$K_d$ , (ml/g), 0.033% $CO_2$	$K_d$ , (ml/g), 4.1% $CO_2$
ERDA-6	None	<b>96.5,</b> #JRF O-121	<b><u>136,</u></b> #JRF O-170
ERDA-6	None	<b>87.6,</b> #JRF O-122	<b><u>148,</u></b> #JRF O-172
ERDA-6	Avg. without organics	<b>92.0</b>	<b><u>142</u></b>
ERDA-6	Low-conc. organics	<b><u>83.6,</u></b> #JRF O-129	<b><u>175,</u></b> #JRF O-179
ERDA-6	Low-conc. organics	<b><u>79.1,</u></b> #JRF O-130	<b><u>147,</u></b> #JRF O-180
ERDA-6	Avg. w. low-conc. org.	<b><u>81.4</u></b>	<b><u>161</u></b>
ERDA-6	High-conc. organics	<b><u>63.9,</u></b> #JRF O-127	<b><u>131,</u></b> #JRF O-177
ERDA-6	High-conc. organics	<b><u>63.3,</u></b> #JRF O-128	<b><u>113,</u></b> #JRF O-178
ERDA-6	Avg. w. high-conc. org.	<b><u>63.6</u></b>	<b><u>122</u></b>



Table G-6. Effects of Brine, Organic Ligands, and  $P_{CO_2}$  on Matrix  $K_d$ s for Np(V) and Dolomite-Culebra Rock (LANL Empirical Sorption Study) (continued).

Brine	Additive	$K_d$ (ml/g), 0.033% $CO_2$	$K_d$ (ml/g), 4.1% $CO_2$
H-17	None	5.17, #JRF O-21	<u>0.905,</u> <u>#JRF O-71</u>
H-17	None	4.37, #JRF O-22	<u>1.06,</u> <u>#JRF O-72</u>
H-17	Avg. without organics	4.77	<u>0.983</u>
H-17	Low-conc. organics	4.86, #JRF O-29	1.33, #JRF O-79
H-17	Low-conc. organics	4.44, #JRF O-30	0.694, #JRF O-80
H-17	Avg. w. low-conc. org.	4.65	1.01
H-17	High-conc. organics	1.45, #JRF O-27	-0.236, #JRF O-77
H-17	High-conc. organics	1.67, #JRF O-28	-0.433, #JRF O-78
H-17	Avg. w. high-conc. org.	1.56	0.00

Table G-7. Effects of Organic Ligands on Matrix  $K_d$ s (ml/g) for Pu(V), Am(III), U(VI), Th(IV), and Np(V), Dolomite-Rich Culebra Rock, and Modified Brine A (LANL Empirical Sorption Study). One-week sorption runs with H-19, B-4, Box 7.  $K_d$ s in bold font excluded from ranges and distributions because of unacceptable differences between standards and controls. Data current as of May 30, 1996. Table compiled by L. H. Brush on May 16, 1996, based on information provided by LANL on May 15, 1996. Table checked by L. J. Storz on May 16, 1996. Table revised by Brush on May 31, 1996, based on information provided by LANL on May 30, 1996. Table checked by L. J. Storz on June 10, 1996.

Element and Oxidation State					
Additive	Pu(V)	Am(III)	U(VI)	Th(IV)	Np(V)
None	8.73, #JRF-233	<b>528</b> , #JRF-243	<b>19.3</b> , #JRF-213	<b>11,300</b> , #JRF-203	22.7, #JRF-223
None	10.1, #JRF-234	<b>501</b> , #JRF-244	<b>19.1</b> , #JRF-214	<b>10,700</b> , #JRF-204	17.1, #JRF-224
Avg. without organics	9.42	<b>514</b>	<b>19.2</b>	<b>11,000</b>	19.9
Low-conc. organics	<b>7.69</b> , #JRF-239	355, #JRF-249	12.4, #JRF-219	1.70, #JRF-209	11.9, #JRF-229
Low-conc. organics	<b>8.84</b> , #JRF-240	325, #JRF-250	17.2, #JRF-220	6.47, #JRF-210	10.5, #JRF-230
Avg. w. low-conc. organics	<b>8.26</b>	340	14.8	4.08	11.2
Intermed.-conc. organics	<b>5.03</b> , #JRF-237	67.6, #JRF-247	16.6, #JRF-217	<b>1.05</b> , #JRF-207	6.25, #JRF-227
Intermed.-conc. organics	<b>5.06</b> , #JRF-238	36.7, #JRF-248	16.8, #JRF-218	<b>6.29</b> , #JRF-208	5.89, #JRF-228
Avg. w. inter.-conc. org.	<b>5.04</b>	52.2	16.7	<b>3.67</b>	6.07

Table G-7. Effects of Organic Ligands on Matrix  $K_{ds}$  (ml/g) for Pu(V), Am(III), U(VI), Th(IV), and Np(V), Dolomite-Rich Culebra Rock, and Modified Brine A (LANL Empirical Sorption Study) (continued).

Additive	Element and Oxidation State				
	Pu(V)	Am(III)	U(VI)	Th(IV)	Np(V)
High-conc. organics	2.55, #JRF-235	2.34, #JRF-245	10.1, #JRF-215	0.469, #JRF-205	1.93, #JRF-225
High-conc. organics	2.22, #JRF-236	2.05, #JRF-246	8.01, #JRF-216	0.467, #JRF-206	2.49, #JRF-226
Avg. w. high-conc. org.	2.38	2.20	9.06	0.468	2.21

---

**Title 40 CFR Part 191  
Compliance Certification  
Application  
for the  
Waste Isolation Pilot Plant**



**MASS Attachment 15-2**

---

**THIS PAGE INTENTIONALLY LEFT BLANK**



WFO 26385



Sandia National Laboratories

Operated for the U.S. Department of Energy by Sandia Corporation

Albuquerque, New Mexico 87185-1328

date: April 8, 1996

to: Distribution

from:   
Jim Ramsey, MS-1328 (6749)



INFORMATION ONLY

subject: Numerical Implementation of the Colloid Transport Conceptual Model

Following several meetings between members of departments 6748 and 6749 we have developed a conceptual model of colloid-facilitated isotope transport in the Culebra and a numerical means of implementing it. Because the modeling effort will be vastly different than past performance assessments, we felt it would be appropriate to document the numerical approach and circulate it for comments before we begin the CCA calculations. If your name appears on the distribution list, your opinions are valued. Both positive and negative comments will be appreciated.

Colloid transport will be modeled with the dual porosity transport simulator SECOTP2D. This model was not developed to transport colloids so there are some serious limitations concerning the transport processes we can include in the analysis. The most serious limitation is that dissolved actinides in the Culebra can not sorb to colloids, nor can sorbed actinides detach into the dissolved state. I can think of no way to incorporate or even investigate the impact of this process without substantial code development or bringing in a new code specifically designed for colloids. Unfortunately, that is not going to happen in the allotted time frame.

Therefore, we are proposing to include colloid-facilitated transport in the CCA analysis, but only by modeling the transport of actinide bearing colloids contained in brine transported from the repository to the Culebra. Actinides sorbed to a colloid will be assumed to remain fixed to that colloid for the duration of the simulation. By restricting actinide / colloid interactions and limiting the retardation mechanisms, colloid-facilitated transport can be modeled with SECOTP2D.

The governing equation solved by SECOTP2D for the transport of the kth isotope through the fracture continuum is given as;

$$\nabla[\phi D \nabla C_k - V C_k] = \phi R_k \frac{\partial C_k}{\partial t} + \phi(R\lambda C)_k + \phi(R\lambda C)_{k-1} - Q_k - \Gamma_k \quad (1)$$

Equation 1 can also be used to describe transport of the kth colloid by defining  $C_k$  as the colloid concentration  $[M/L^3]$  rather than the isotope concentration. Many of the remaining parameters also need to be redefined with respect to the colloid being modeled. The following are the colloid fracture continuum transport parameter required by SECOTP2D;

C	Colloid Concentration	$[M/L^3]$
D	Hydrodynamic Dispersion Tensor	$[L^2/T]$
V	Darcy velocity - fluid flux rate / bulk cross-sectional area	$[L/T]$
$\phi$	Fracture Porosity - fracture pore volume / bulk volume	$[-]$
R	Colloid Retardation Coefficient	$[-]$
$\lambda$	Colloid Decay Constant	$[1/T]$
Q	Colloid Source/Sink Term	$[M/TL^3]$
$\Gamma$	Matrix/Fracture Mass Transfer Term	$[M/TL^3]$
t	Time	$[T]$

SECOTP2D computes mass transfer between the matrix and the fracture assuming molecular diffusion is the only transport mechanism. Therefore,  $\Gamma$  is defined as,

$$\Gamma_k = \frac{\phi}{b} \left( \phi' D' \frac{\partial C'_k}{\partial \chi} \Big|_{\chi=L} \right) \quad (2)$$

where,  $\chi$  is a spatial coordinate originating at the center of the matrix block,  $b$  is half the fracture aperture,  $L$  is half the matrix block length,  $\phi'$  is the matrix porosity,  $C'_k$  the matrix concentration of the kth colloid, and  $D'$  the matrix diffusion coefficient defined as,

$$D' = D^* \tau' \quad (3)$$

where,  $D^*$  is the molecular diffusion coefficient and  $\tau'$  is the matrix tortuosity.

To evaluate the concentration gradient at the fracture wall ( $\chi = L$ ), it is necessary to solve a transport equation in the matrix. The governing transport equation solved by SECOTP2D in the matrix is,

$$\frac{\partial}{\partial \chi} \left( \phi' D' \frac{\partial C'_k}{\partial \chi} \right) = \phi' R'_k \frac{\partial C'_k}{\partial t} + \phi' (R' \lambda C')_k + \phi' (R' \lambda C')_{k-1} \quad (4)$$

with the boundary conditions,

$$D' \frac{\partial C'_k}{\partial \chi}(0, t) = 0 \quad (5)$$

$$C'_k(L, t) = C_k \quad (6)$$

The prime in Equations 4, 5, and 6 denotes matrix properties.

The use of Equations 1 through 6 describes the transport of isotope bearing colloids introduced into the problem domain by the source term,  $Q$ . The solution to this set of equations will allow one to calculate the integrated release of colloids across the land withdrawal boundary. By knowing the initial isotope concentration on the colloids, the integrated colloid release can be converted to an integrated isotope release. Isotope decay can also be accounted for with simple post processing.

With SECOTP2D we can model colloid sorption in both the matrix and fracture using the retardation coefficients  $R$  and  $R'$ . For colloids that are too large to diffuse into the matrix, the matrix tortuosity,  $\tau$ , in Equation 3 can be set to zero. This will prevent colloids from diffusing into the matrix but still allow colloid diffusion within the fractures.

Colloid filtration in the fractures can be modeled using the decay constant  $\lambda$ , defined by,

$$\lambda = \gamma \bar{V} \quad (7)$$

where,  $\gamma [L^{-1}]$  is the filter coefficient, and  $\bar{V}$  is a representative colloid velocity. Several researchers (Herzig et al., 1970; Dieulin, 1982; Ibaraki and Sudicky, 1995) have used a similar approach.  $\bar{V}$  will be determined from the travel time,  $t_p [T]$ , computed by particle tracking software, and the travel distance of the particle,  $l_p [L]$ ,

$$\bar{V} = \frac{l_p}{t_p} \quad (8)$$

Unfortunately, we cannot model sorption and filtration at the same time for a single colloid. This is apparent in Equations 1 and 4 where the decay constant is applied to both sorbed and dissolved species through the retardation coefficient. Obviously, sorbed colloids will not be filtered out. Hence, only the dominant retardation mechanism of each colloid (sorption or filtration) will be accounted for in the analysis.

Colloid filtration in the matrix is a topic I am also concerned about. Technically speaking, the velocity in the matrix is assumed be zero and therefore  $\lambda$  should also be zero. I'm certain arguments could be made to include matrix filtration based on pore size differences, brownian motion, ect. However, it is my opinion (more of a guess actually) that for colloids where filtration is the dominate retardation mechanism, the fractures alone will substantially filter out colloids. Therefore, I propose we do not permit matrix filtration and avoid this debate altogether.

In summary, a particular colloid will be modeled in one of two ways depending on the colloids dominate retardation mechanism. If sorption is the dominate mechanism, the colloid will be treated nearly the same as a dissolved actinide, see Table 1. However, if filtration is the dominate retardation mechanism, matrix diffusion will be disabled and the decay constant will be used to filter out colloids. Of course other combinations are possible should a particular colloid require special consideration.

Table 1: Anticipated Transport Mechanisms

Dominate Retardation Mechanism	Filtration	Matrix Diffusion	Matrix Retardation	Fracture Retardation
Sorption	Off	On	On	Off
Filtration	On	Off	Off	Off

## Distribution:

MS-1324 Tom Corbet  
 MS-1324 Lucy Meigs  
 MS-1324 Jim McCord  
 MS-1326 Jack Gauthier  
 MS-1328 Mike Wallace  
 MS-1328 Rebecca Blaine  
 MS-1328 Alex Treadway  
 MS-1328 Bob MacKinnon  
 MS-1328 J.T. Schneider  
 MS-1341 Hans Papenguth  
 MS-1341 George Perkins  
 MS-1343 Kurt Larson

SWCF-A:WBS1.2.07.5.3:PDD:QA:GENERAL



---

**Title 40 CFR Part 191  
Compliance Certification  
Application  
for the  
Waste Isolation Pilot Plant**

**MASS Attachment 15-3**



**THIS PAGE INTENTIONALLY LEFT BLANK**

WPO 37533

Sandia National Laboratories

Albuquerque, New Mexico 87185-1341

date: May 11, 1996

to: M. S. Tierney, MS-1328 (Org. 6741)

L. H. Brush

from: L. H. Brush, MS-1341 (Org. 6748)

INFORMATION ONLY

subject: Revised Free-Solution Tracer Diffusion Coefficients ( $D_{sol}$ s) for Dissolved Pu, Am, U, Th, Np, Cm, and Ra in Boreholes and the Culebra for Use in the PA Calculations to Support the WIPP CCA

This memorandum revises the free-solution tracer diffusion coefficients ( $D_{sol}$ s) recommended by Brush (1996) for use in the long-term performance-assessment (PA) calculations to support the Waste Isolation Pilot Plant (WIPP) Compliance Certification Application (CCA). After submission of this memorandum, C. T. Stockman suggested a better way of using the  $D_{sol}$ s for Pu, U, and Np in the PA calculations (see below).

Brush (1996) modified the  $D_{sol}$ s for Pu, U, and Np from Brush (1987) (see Table 1) slightly to be consistent with the oxidation states of Pu, U, and Np predicted for WIPP disposal rooms and assumed for boreholes and the Culebra. Actinide Source Term Program and the Dissolved Actinide Retardation Research Program personnel have predicted that Pu will speciate as Pu(III) or Pu(IV), but not as Pu(V) nor Pu(VI), U will speciate as U(IV) or U(VI), and Np will speciate as Np(IV) or Np(V), but not as Np(VI), in WIPP disposal rooms, boreholes, and the Culebra. Because Brush (1996) believed that PA personnel required fixed values of  $D_{sol}$  for Pu, U, and Np for the calculations to support the WIPP CCA, he recommend that PA use the mean of the  $D_{sol}$ s for Am(III) and Th(IV) compiled by Brush (1987) for Pu, the mean of the  $D_{sol}$ s for Th(IV) and U(VI) from Brush (1987) for U, and the mean of the  $D_{sol}$ s for Th(IV) and Np(V) from Brush (1987) for Np.

However, Stockman suggested that PA personnel sample  $D_{sol}$ s for Pu, U, and Np the same way they will sample the oxidation states for these elements in WIPP disposal rooms and the Culebra for predictions of solubilities and  $K_{ds}$ , respectively. PA will sample solubilities and  $K_{ds}$  for *either* Pu(III), U(IV), and Np(IV), *or* Pu(IV), U(VI), and Np(V) in any given vector. PA will specify the oxidation states of these elements by sampling "oxstat," a parameter with a uniform distribution of 0 to 1. If the sampled value of oxstat is 0.5 or less, PA will use the solubilities predicted for Pu(III), U(IV), and Np(IV). If oxstat is greater than 0.5, PA will use solubilities for Pu(IV), U(VI), and Np(V). Therefore, I recommend that, if oxstat is 0.5 or less, PA use the  $D_{sol}$ s for

Am(III), Th(IV), and Th(IV) compiled by Brush (1987) for Pu(III), U(IV), and Np(IV), respectively, for that vector (see Table 2). If oxstat is greater than 0.5, I recommend that PA use the  $D_{sol}$ s for Th(IV), U(VI), and Np(V) from Brush (1987) for Pu(IV), U(VI), and Np(V), respectively.

#### REFERENCES

Brush, L.H. 1987. *Feasibility of Disposal of High-Level Radioactive Wastes into the Seabed: Review of Laboratory Investigations of Radionuclide Migration through Deep-Sea Sediments*. SAND87-2438. Albuquerque, NM: Sandia National Laboratories.

Brush, L.H. "Free-Solution Tracer Diffusion Coefficients ( $D_{sol}$ s for Dissolved Pu, Am, U, Th, Np, Cm, and Ra in Boreholes and the Culebra for Use in the PA Calculations to Support the WIPP CCA." Unpublished memorandum to M.S. Tierney, May 2, 1996. Albuquerque, NM: Sandia National Laboratories.

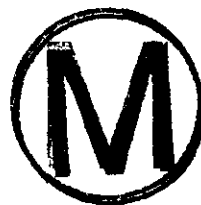


Table 1. Values of  $D_{sol}$  from Brush (1987). Table includes only the elements needed for the PA calculations to support the WIPP CCA. Table retyped by L. H. Brush on May 2, 1996. Table checked by L. J. Storz on May 2, 1996.

Element	Species for Which $D_{sol}$ Was Determined	Temperature at Which $D_{sol}$ Was Determined (C)	$D_{sol}$ , $cm^2/sec$
Pu	$Pu^{4+}$ , $PuO_2^+$	4	$3 \times 10^{-6}$
Am	$Am^{3+}$	4	$3 \times 10^{-6}$
U	$UO_2^{2+}$	25	$4.26 \times 10^{-6}$
Th	$Th^{4+}$	18	$1.53 \times 10^{-6}$
Np	$NpO_2^+$	4	$3 \times 10^{-6}$
Cm	$Cm^{3+}$	4	$3 \times 10^{-6}$
Ra	$Ra^{2+}$	0	$4.02 \times 10^{-6}$

Values for  $Pu^{4+}$  and  $PuO_2^+$ ,  $Am^{3+}$ , and  $NpO_2^+$  from Higgo et al. (1987); values for  $UO_2^{2+}$ ,  $Th^{4+}$ , and  $Ra^{2+}$  from Li and Gregory (1974); value for  $Am^{3+}$  applied to  $Cm^{3+}$  by oxidation-state analogy.

Table 2. Revised Values of  $D_{sol}$  for Use in the PA Calculations to Support the WIPP CCA. Table compiled by L. H. Brush on May 11, 1996. Table checked by L. J. Storz on May 13, 1996.

Element	Oxidation State for Which $D_{sol}$ Was Estimated	$D_{sol}$ , $cm^2/sec$
Pu	Pu(III)	$3 \times 10^{-6}$
	Pu(IV)	$1.53 \times 10^{-6}$
Am	Am(III)	$3 \times 10^{-6}$
U	U(IV)	$1.53 \times 10^{-6}$
	U(VI)	$4.26 \times 10^{-6}$
Th	Th(IV)	$1.53 \times 10^{-6}$
Np	Np(IV)	$1.53 \times 10^{-6}$
	Np(V)	$3 \times 10^{-6}$
Cm	Cm(III)	$3 \times 10^{-6}$
Ra	Ra(II)	$4.02 \times 10^{-6}$



Distribution:

MS 1320 E. J. Nowak (Org. 6831)  
MS 1320 R. V. Bynum (Org. 6831)  
MS 1320 H. W. Papenguth (Org. 6748)  
MS 1320 W. G. Perkins (Org. 6748)  
MS 1320 M. D. Siegel (Org. 6748)  
MS 1324 P. B. Davies (Org. 6115)  
MS 1324 A. R. Lappin (Org. 6115)  
MS 1324 L. C. Meigs (Org. 6115)  
MS 1328 H. Jow (Org. 6741)  
MS 1328 D. R. Anderson (Org. 6749)  
MS 1328 M. A. Martell (Org. 6749)  
MS 1328 J. L. Ramsey (Org. 6749)  
MS 1328 C. T. Stockman (Org. 6749)  
MS 1335 M. S. Y. Chu (Org. 6801)  
MS 1337 W. D. Weart (Org. 6000)  
MS 1341 J. T. Holmes (Org. 6748)  
MS 1341 L. H. Brush (Org. 6748)  
MS 1341 R. C. Moore (Org. 6748)  
MS 1341 C. F. Novak (Org. 6748)  
MS 1341 L. J. Storz (Org. 6748)  
MS 1341 Y. Wang (Org. 6748)  
MS1341 K. W. Larson (Org. 6751)  
MS 1343 R. F. Weiner (Org. 6751)  
MS 1395 L. E. Shephard (Org. 6800)  
MS 1395 M. G. Marietta (Org. 6821)  
MS 1330 SWCF (Org. 6352), WBS 1.1.10.3.1 (2)

100

**THIS PAGE INTENTIONALLY LEFT BLANK**



---

**Title 40 CFR Part 191  
Compliance Certification  
Application  
for the  
Waste Isolation Pilot Plant**



**MASS Attachment 15-4**

---

**THIS PAGE INTENTIONALLY LEFT BLANK**



wpo 37455

INFORMATION ONLY

# Sandia National Laboratories

Albuquerque, New Mexico 87185-1341

date: April 25, ~~1995~~ <sup>1996</sup> *Kul*

to: Mike Wallace, MS 1328, Dept. 6749 (Re/Spec)

from: Kurt Larson, MS 1341, Dept. 6751 *Kurt Larson*

subject: Mining Transmissivity Multiplier - Area to be mined.

The EPA's 40 CFR 194 specifically requires the DOE to evaluate the consequences of mining in the McNutt Potash Member on the performance of the WIPP. 40 CFR 194 and supporting and supplemental information provides guidance for determining what gets mined both inside the Land Withdrawal Area (LWA) and outside the LWA.

Westinghouse Waste Isolation Division (WID) has completed an analysis consistent with regulatory guidance to determine which areas of the McNutt Potash Zone should be assumed to be mined inside and outside the LWA. This analysis is reported in Attachment 1 to a letter titled "Future Mining Events in the Performance Assessment" sent to Mel Marietta from Bryan Howard dated April 3, 1996. This document has been introduced into the SWCF.

Performance assessment should use Figure 5 in the WID document as the basis for areas assumed to be mined outside the LWA. Two regions reported on Figure 5 should be assumed to be mined: the region labeled "Extent of Mining Outside the Controlled Area" and denoted with a fine cross-hatch; and the extent of existing mines, which have been excluded from this category. It appears that the existing mines are lumped in with the categories "Known Potash Leases within the Delaware Basin" and "Known Potash Leases Outside the Delaware Basin." Therefore, for accurate representation of the extent of current mines, I suggest using both Figure 5 and the Roswell District BLM (1993) base map of potash resources and reserves titled "Preliminary Map showing Distribution of Potash Resources, Carlsbad Mining District [sic], Eddy and Lea Counties, New Mexico", which clearly shows the current extent of mines.

For mining within the LWA, use Figure 8 of the WID attachment without modification.

It is understood in these recommendations that the extent of mining impact in the Culebra will be determined based on these suggestions, and the applicable angle of draw, which will enlarge somewhat the areas of impact. Further, it is understood that the region affected in the Culebra must be rendered at a resolution consistent with the gridding of the Culebra for groundwater and transport modeling.

**Distribution:**

Sharla Bertram	MS 1341
Lori Dotson	MS 1341
Peter Swift	MS 1341
Kurt Larson	Day File



~~SWCF:WBS1:2:07:1:PDD:QA:Non-Salado:Mining-Transmissivity-Multiplier-(WPO-#36489)-(2)~~

---

**Title 40 CFR Part 191  
Compliance Certification  
Application  
for the  
Waste Isolation Pilot Plant**

**MASS Attachment 15-5**



**THIS PAGE INTENTIONALLY LEFT BLANK**



INFORMATION ONLY



Westinghouse  
Electric Corporation

Government and Environmental  
Services Company

WS:96:03105  
DA:96:11017

Waste Isolation Division

Box 2078  
Carlsbad New Mexico 88221

April 3, 1996

Mr. Mel Marietta, Manager  
WIPP Project Compliance Department  
Sandia National Laboratories  
115 N. Main Street  
Carlsbad, NM 88220



Subject: FUTURE MINING EVENTS IN THE PERFORMANCE ASSESSMENT

Dear Mr. Marietta:

Per our discussion, this submittal updates our earlier package provided to you on February 29, 1996 (DA:96:11004, attached). The revised information includes changes made to incorporate comments received from Mr. Kurt Larson of your staff.

The map in Figure 5 of the attachment has been revised with additional information by including areas where potash has already been mined and areas currently considered barren of potash by the Bureau of Land Management.

Our earlier recommendation to use Figure 8 to incorporate the effects of mining in WIPP Performance Assessment remains the same.

Should you have any further questions, please contact me at (505) 234-8380, or Mr. R. F. Kehrman at (505) 234-8690.

Sincerely,

B. A. Howard, Manager  
Long-Term Regulatory Compliance

hmp

Attachments

cc: without map

D. R. Anderson, SNL-AL  
G. T. Basabilvazo, CAO  
J. E. Bean, SNL-AL  
M. S. Y. Chu, SNL-AL  
J. H. Maes, CAO  
J. A. Mewhinney, CAO

Distribution: 4/8/96 *ah*  
Mike Wallace, 6749  
Kurt Larson, 6751  
Peter Swift, 6821  
Tom Corbet, 6115  
Wendell Weart, 6000

SWCF-A: 1.4.3.3; NQ COM

## EXTENT OF MINING POSITION PAPER

Revision 1

### 1.0 INTRODUCTION

In 40 CFR Part 194, the Environmental Protection Agency's recently published standard for the certification of WIPP's compliance to 40 CFR Part 191, they (the EPA) have specified that the DOE must consider the impact of mining in the analysis of the long-term performance of the disposal system. The specific requirement being imposed by the EPA is stated in 40 CFR Part 194<sup>1</sup>, section 32(a), (b), and (c) as follows:

- 
- (a) *Performance assessments shall consider natural processes and events, mining, deep drilling, and shallow drilling that may affect the disposal system during the regulatory time frame.*
  - (b) *Assessments of mining effects may be limited to changes in the hydraulic conductivity of the hydrogeologic units of the disposal system from excavation mining for natural resources. Mining shall be assumed to occur with a one in 100 probability in each century of the regulatory time frame. Performance assessments shall assume that mineral deposits of those resources, similar in quality and type to those resources currently extracted from the Delaware Basin, will be completely removed from the controlled area during the century in which such mining is randomly calculated to occur. Complete removal of such mineral resources shall be assumed to occur only once during the regulatory time frame.*
  - (c) *Performance assessments shall include an analysis of the effects on the disposal system of any activities that occur in the vicinity of the disposal system prior to disposal and are expected to occur in the vicinity of the disposal system soon after disposal. Such activities shall include, but shall not be limited to, existing boreholes and the development of any existing leases that can be reasonably expected to be developed in the near future, including boreholes and leases that may be used for fluid injection activities.*

The phrase "*Performance assessments shall assume that mineral deposits of those resources, similar in quality and type to those resources currently extracted from the Delaware Basin, will be completely removed from the controlled area*" in section (b) and the phrase "*any activities that occur in the vicinity of the disposal system prior to disposal and are expected to occur in the vicinity of the disposal system soon after disposal*" in section (c) require a definition of an area within the controlled area (b) and outside the controlled area (c) for the purposes of analysis. Defining the requisite areas to satisfy these requirements is the subject of this paper.

The EPA provides extensive discussion of how the impacts of mining are to be considered in the supplemental information provided with the new standard. However, the EPA only gives limited guidance on how to determine the extent of mining that must be considered. This is an important factor, because the extent of mining determines whether or not the effect of subsidence will directly affect the performance of the disposal system. In the Supplemental Information provided with the rule, the EPA states: "*Some natural resources in the vicinity of the WIPP can be extracted by mining. These natural resources lie within the geologic formations found at shallower depths than the tunnels and shafts of the repository and do not lie vertically above the repository. Were mining of these resources to occur, this could alter the hydrologic properties of overlying formations ...*" Following this statement, the Agency proceeds to provide a methodology to bound such considerations based on their analysis of the effects of subsidence. Subsequently, the EPA states that "*The final rule specifies those assumptions and methods that shall be used in performance assessments to account for the effects of mining.*" As a basis for the assumptions that are specified in the rule, the EPA points out their intent that "*the historical record of the*

---

<sup>1</sup>U. S. Environmental Protection Agency, 1996, "Criteria for the Certification and Re-Certification of the Waste Isolation Pilot Plant's compliance With the 40 CFR Part 191 Disposal Regulations; Final Rule", *Federal Register*, Vol. 61, No. 28, pp 5224, February 9, 1996.

*past 100 years' mining activity in the Delaware Basin provides a reasonable basis for predicting the nature of future mining activity.*" The EPA applied the historical record in two ways. First, it used the record to determine a frequency for mining as specified in the rule, and second, it used the record to address the physical characteristics of the mining activity. Only this second aspect is of concern in this paper.

With regard to the physical characteristics of the mining activity, the agency imposes assumptions and limitations that assure consistency with the future states requirements elsewhere in 40 CFR Part 194. Specifically, in the supplemental information, the agency states that *"the size and shape of the mine"* should conform with *"existing mineral deposits that are similar in type and quality to those extracted in the Delaware Basin."* The EPA provides the following rationale for this requirement: *"The Agency basis for this requirement was their consideration of the physical nature of mining activities that are currently underway in the Delaware Basin. First, the Agency assumed that the size and shape of a mine will be dictated by the size and shape of the mineral deposits that are to be extracted with no two mines being alike. The mineral deposits that will be mined in the future may consist of minerals of current economic interest, or of materials not useful or valuable in present-day terms. Without knowledge of what these future resources might be, any attempt to predict the size and shape of the associated mineral deposits would be speculative, as would any attempt to determine the size and shape of the mines used to extract them. The Agency further recognized that individual mines are of highly irregular shape and there is every reason to believe that deposits of minerals that are mined in the future will also vary in size and be highly irregular in shape. The Agency believes that no logical mathematical scheme exists that could be used to predict the potentially wide variety of sizes and highly irregular shapes. In light of the speculativeness and mathematical difficulty, the Agency has chosen to use existing mineral deposits as "stand-ins" to be used to determine the size and shape of the unknown mineral deposits that might be mined in the future. Thus, the final rule requires performance assessments to assume that all the presently known mineral resources lying within the controlled area will be extracted at the single point in time determined by the method in the final rule, discussed above."* In other words, because implementing this requirement can lead to a great deal of speculation which the EPA seeks to prevent, the DOE should use the existing minerals as the basis for demonstrating compliance with this requirement. The only minerals of interest are the potash minerals that occur in the McNutt Potash Member of the Salado.

The discussion in the Supplemental Information clearly equates "presently known mineral resources lying within the controlled area" to "existing mineral deposits lying within the controlled area that are of similar quality and typw to those minerals currently extracted" (see the last two paragraphs on 61 FR 5229). The entire controlled area is overlain by potash mineralization. Both the thickness and purity vary spatially. The EPA recognized that the current practice within the potash mining area is to recover those resources that can be extracted economically. The challenge for the DOE is to assign a boundary to the extent of mining that is consistent with the certification criterion, thus accomplishing the EPA's goals.

In order to assign a suitable boundary, the DOE can turn to further text in the supplemental information. In the section titled "Changes to the proposed rule," EPA clarifies that they intend for the DOE to use current practices as the standard for this analysis. Specifically, the EPA states: *"Additionally, the requirements of the final rule specify the method for determining the size and shape, location and point in time at which mining occurs. The Agency specified these items to provide clarification on how mining should be considered and to avoid unbounded speculation that would result from the high uncertainty regarding whether, where and how mining would occur in the Land Withdrawal area. EPA's decision was based on a desire to include mining in performance assessment in a realistic fashion without recourse to such unconstrained speculation. To this end, the final rule has specified that mining will continue at the same rate as it has over the past 100 years, that the area to be mined is the area that contains mineral deposits of similar type and quality to those that are currently extracted in the Delaware Basin, and that only the major impacts on the disposal system of mining need be considered. EPA believes this is consistent with the future states assumptions of section 25 as they apply to the future*



activities of man."

This clarification certainly indicates that the EPA did not intend that "all" potash be considered. Instead, only those considered to be resources consistent with current usage of the term. Applying the EPA's guidance raises the question "whose estimate of resources should be used?" As stated above, the EPA's intent of their requirement is to use current conditions to provide estimates for future conditions. The current knowledge regarding resources consists of two parts: 1) the overall resource and 2) that portion that is economically developable today. The first part is reflected in maps and analyses published by several agencies such as the Bureau of Land Management (BLM), the U.S. Bureau of Mines (USBM), the U.S. Geological Survey (USGS), and the New Mexico Bureau of Mines and Mineral Resources (NMBMMR). Determining the second part is somewhat more difficult to determine since it changes periodically as the economics of potash changes. Mining companies file mine development maps and plans with regulatory agencies as a means of indicating their plans for development of potash. These maps and plans are proprietary and are not available to the public. As a substitute for actual mining plans, the current lease map can be used as an indication of what the potash industry as a whole considers to be ore that can be extracted. Identifying leased areas outside the controlled area is relatively straightforward. However, since there are no leases within the WIPP site boundary, it is necessary to look at both the published analyses and estimates, the potash development history and the areas that were considered at one time to be viable potash properties because they were previously leased for production.

## 2.0 BACKGROUND

The development of potash in southeastern New Mexico dates back to 1926, with the first commercial shipment occurring in 1931. At one time, eleven different companies were exploring for potash in the region. A large portion of the potash minerals lie within properties owned by the Federal Government and administered by the BLM. The BLM administers these resources under the federal Mineral and Leasing Act of 1920 and the Federal Land Policy and Management Act. Management policy is codified as 43 CFR Part 3000. Part of the BLM's responsibility is resolving disputes between the oil and gas industry and the potash industry over priority use of leases. These disputes develop because, according to Olsen, 1993<sup>2</sup>, "... exploiting petroleum and potash at the same location would create unacceptable safety risks for underground mining and would create petroleum production difficulties." Conflicts began before 1939 when the first federal order designating the potash area banned oil and gas leasing. Much of the conflict was resolved in 1987 when the oil and gas and potash industries signed the "Statement of Agreement between the Potash and Oil and Gas Industries on concurrent Operations in the Potash Area". The state of New Mexico incorporated the principles of the agreement into their order R-111-P. The BLM has proposed rule changes to incorporate R-111-P into the federal system, however, the change is still pending. Typically, the BLM resolves any resource development issues in favor of potash.

One key to understanding the BLM's decision process is the concept of the Potash Enclave. The enclave is an area within the boundaries established by the Secretary of Interior Order which defines the area available for potash leasing. To qualify for enclave status, lands must contain ore that meets minimal leasing criterion based on boreholes that are up to 1.5 miles apart. (The 1993 enclave map<sup>3</sup> will be superimposed on the lease map in Figure 1 when the digitization of the enclave map is completed.) The long-standing policy of the BLM (since 1975) is to deny requests to drill oil and gas wells from surface locations within the enclave. However, the current policy uses the concept of drilling islands within the enclave for oil and gas resources that may not be available from outside the enclave. Drilling islands are

---

<sup>2</sup>Olsen, James A., 1993, "Federal Management of the Potash Area in Southeastern New Mexico", in *Carlsbad Region, New Mexico and West Texas*, by D. W. Love et al., New Mexico Geological Society 44th Annual Field Conference, October 6-9, 1993.

<sup>3</sup>U. S. Bureau of Land Management, 1993, "Preliminary Map Showing Distributions of Potash Resources, Carlsbad Mining District, Eddy & Lea Counties, New Mexico", U.S. Bureau of Land Management, Roswell, NM.

permitted within the enclave when certain conditions are met as defined in the BLM's regulations<sup>4</sup>. Currently, the BLM enforces either a 0.25 mile barrier for oil wells and a 0.5 mile barrier for gas wells in the vicinity of existing operating mines or a barrier that is equal to 110 percent of the depth to the mine.

The BLM maintains estimates of potash resources and reserves based on information provided by the U.S. Geological Survey, the DOE, and operating companies. The operating company data are generally held by the BLM as proprietary and are not available to the public. In addition, operators are required to file mine development plans with the BLM. These, too, are proprietary and are not available for inspection.

Estimates of the active life of mining in the area have been prepared at various times. The most recent are shown below and were collected by the EPA for the Background Information Document supporting the 40 CFR Part 194 Final Rulemaking<sup>5</sup>. The EPA's information reflects mining both within the Delaware Basin and outside the Delaware Basin. In the following table, the resources of Eddy Potash and Horizon Potash lie outside the Delaware Basin; those of New Mexico Potash, IMC, and Mississippi Chemical lie both outside and within the Delaware Basin; and those of Western-Ag lie within the Delaware Basin.

Active Potash Mines in New Mexico Showing Estimated Capacity, Average Ore Grade, and Mine Life at the Average 1992 Price of \$81.14/st product



Operator	County	Product Capacity (st/yr <sup>1</sup> )	Ore Grade (% K <sub>2</sub> O)	Mine Life (yrs)
Eddy Potash Inc. <sup>2</sup>	Eddy	550,000	18	4
Horizon Potash Co.	Eddy	450,000	12	6
IMC Fertilizer, Inc.	Eddy	1,000,000 <sup>3</sup>	11 <sup>3</sup>	33
Mississippi Chemical	Eddy	300,000	15	125
New Mexico Potash <sup>2</sup>	Eddy	450,000	14	25
Western Ag-Minerals <sup>4</sup>	Eddy	400,000	8 <sup>5</sup>	30

Data from J.P. Searis, U.S. Bureau of Mines, oral communication, 1993.

<sup>1</sup> May not be operating at full capacity.

<sup>2</sup> Owned by Trans-Resource, Inc.

<sup>3</sup> Muriate, langbeinite, and sulfate combined.

<sup>4</sup> Owned by Rayrock Resources of Canada.

<sup>5</sup> Langbeinite only.

Certain public information is available and has been consulted for this paper. This includes property title abstracts for the sections of land within the controlled area (which is the area inside the WIPP site boundary), BLM lease maps, BLM reserve maps, and a mineral evaluation report prepared by the NMBMMR at the request of the DOE. In addition, a map of current oil well drilling within the enclave was used.

## 2.1 Background on leased areas outside the WIPP controlled area

The current lease holdings within the potash area<sup>6</sup> are shown in Figure 1. Typically, potash leases are obtained as the result of exploration and as the reward for discovery. While numerous interest have historically owned potash leases in the area, these have been consolidated through acquisition into the

<sup>4</sup>U.S. Department of Interior Secretarial Order dated October 28, 1986 designating the Oil-Potash Area, 51 FR 39425.

<sup>5</sup>U.S. Environmental Protection Agency, 1996, Background Information Document, 40 CFR Part 194, Chapter 9, Table 9-2.

<sup>6</sup>U. S. Bureau of Land Management, 1995, "Preliminary Lease Map of the Carlsbad Mining District, Eddy and Lea Counties, New Mexico".

eight holding companies shown in Figure 1. Five of these companies are currently mining in the area. One of the holding companies is an oil company.

Under current federal regulations, all mine operators are required to file a life of mine reserves (LMR) document with the BLM. This document, which is held as proprietary by the BLM, defines the proposed extent of mining that a company plans. The LMR is used by the BLM in resolving leasing conflicts between oil and gas interests and potash interests. Figure 2 illustrates the distribution of oil and gas wells within the Delaware Basin in the vicinity of the WIPP<sup>7</sup>. For the most part, the wells within the potash area are in locations determined to be barren by the Bureau of Land Management and, consequently, not likely to conflict with potash development.

Another area of interest is the leased area directly north of the WIPP site. This area is shown as being leased to both a potash company and an oil company. Priority for use of this area is currently under litigation. It is likely that as long as the oil interest holds the lease, no mining will occur.

## 2.2 Background on potash within the WIPP controlled area

There are no active potash leases within the controlled area. A historical leasing chronology of this area is provided in Table 1. Those leases in Sections 15, 17, and 18 were allowed to expire by their holders. The others (Sections 16, 22, 27, 32, and 34) were acquired by the DOE in 1988 and in 1990. Based on information recorded in title abstracts, prospecting occurred on all sections within the controlled area as evidenced by the information in Table 1.

In 1995, the DOE requested that the NMBMMR<sup>8</sup> re-evaluate the natural resource information available for the controlled area and the area within one mile of the controlled area. This report focused on oil and gas and potash resources and used existing data to update resource estimates used in the 1980 WIPP Environmental Impact Statement. Figures 3 and 4 are the potash reserve estimates for this area. The heavy line marks the ore grade-thickness product that is considered to be economic by local potash companies. The dashed line depicts the ore grade-thickness product that is generally considered by the BLM to be lease grade and thereby qualify a property for inclusion in the potash enclave. These are referred to as "Lease Grade Reserves" and are defined in the 1986 Secretarial Order as criterion for inclusion in the enclave. The following table summarizes these values based on the NMBMMR assessment.

Reserve Type	Langbeinite (Figure 3)		Sylvite (Figure 4)	
	BLM Lease Grade	16 contour	4% K <sub>2</sub> O at 4'	40 contour
Economic-mining	37.5 contour		55 contour	

The assumptions that were used in the NMBMMR assessment are valid for today's potash economy and the projections made in that report. One assumption is that the potash within the immediate vicinity of the controlled area could (and would) be mined by extending existing facilities. If, sometime in the future, after the cessation of active controls, the ore within the controlled area were mined, such an activity would require a new infrastructure which would drastically alter the economics of mining.

<sup>7</sup>Westinghouse Electric Corporation, 1996, Preliminary Map of Oil Wells in the Delaware Basin, Based on Data Collected by Petroleum Information Service Through June, 1995", Westinghouse Electric Corporation, Carlsbad, NM.

<sup>8</sup>NMBMMR, 1995, "Economic Mineral Resources at the Waste Isolation Pilot Plant (WIPP) Site", New Mexico bureau of Mines and Mineral Resources, Socorro, NM, March 31, 1995.

### 3.0 DISCUSSION

Based on the information in the standard and the supplemental information, and on discussions with the EPA regarding their intent for the analysis of mining, the following criteria can be established for describing the anticipated areal extent for mining.

- Criterion 1: **Quantifiable evidence of resources upon which to base future estimates:** The standard requires the resources currently being extracted from the Delaware basin be "stand-ins" for characterizing future resources that may be subject to mining.
- Criterion 2: **Quantifiable experience in extraction:** The standard assumes that mining in the future will be the same as it is today.
- Criterion 3: **Quantifiable limit on quality:** EPA only requires consideration of resources that are of similar quality to those being mined today. "Quality" in this context refers to ore of sufficient grade and thickness to make mining economical.

In addition, several assumptions and givens are needed to formulate an extent of future mining.

- Assumption 1: Mining within the controlled area is independent (from a feasibility viewpoint) of mining outside the controlled area. It is likely that all economically extractable potash outside the controlled area will be removed by the end of the active control period. This situation is assumed not to affect the chance of mining within the controlled area.<sup>9</sup>
- Assumption 2: Mining inside the controlled area will not occur within the first 100 years after decommissioning. Since this is the active control period, mining will be deterred.
- Assumption 3: Mining technology will be the same. This means that methods used today will be used in the future and those methods that are not economic today will be avoided in the future.
- Assumption 4: Only those potash zones being mined today will be mined in the future. Currently uneconomical zones will not be mined; however, all currently economic potash will be extracted from the ore zones being mined today.
- Assumption 5: The economics of mining today and not the presence of minerals will dictate the extent of mining. Specifically, the current economic extraction contour will be used as the indicator of the extent of future mining.
- Assumption 6: The presence of the two hydrocarbon holes within the controlled area will have no impact on the future development of mineral resources. Without this simplifying assumption significant portions of the minable reserves would be thrown out.<sup>10</sup>

---

<sup>9</sup>This assumption is conservative since, in reality, based on the NMBMMR report, the construction of a mine and mill results in a net financial loss from mining within the WIPP and the one mile area around the WIPP. The case of constructing a mine and mill for mining the reserves within the controlled area alone was not run by the NMBMMR, however, the reduction on minable resources associated with the smaller area would only exacerbate the loss.

<sup>10</sup>In reality, the presence of these bore holes and the assumptions with regard to future drilling have the potential to significantly reduce the extent of mining in the future if one assumes that requirements for buffer areas between drilling and mining are imposed in the future as they are today.

Assumption 7: The term "quality" in Section 194.32(b) is interpreted to refer to the economics of mining. That is, the phrase "resources of similar quality" means "resources of similar grade and thickness". Specifically, this is the 37.5 grade-thickness contour for langbeinite and the 55 grade-thickness contour for sylvite.

Assumption 8: Beginning in 1993, there are no more than 50 years of minable potash reserves in the Delaware Basin portion of the Potash Area. Even though one company reports up to 125 years of active mining, most of that company's reserves are north of the Delaware Basin.

Finally, data sources need to be summarized since they form the basis for determining what areas meet the criteria. Three primary sources of potash data exist. These are the NMBMMR study, the BLM map, and the leasing histories.

- The NMBMMR report provides a snapshot (as of 1995) of those resources that are economic to recover under the assumptions made in the assessment.
- The BLM map shows the extent of resources that are of lease quality and that have been offered for development.
- The leasing history shows those areas that have been traditionally considered worth retaining by companies for future development in the area<sup>11</sup>.

In addition, a fourth source of data that is important is the hydrocarbon drilling record associated with the area outside the controlled area. Since buffer zones are required between drilled areas and present or future mined areas as discussed above, this factor will be used to reduce the amount of leased area outside the controlled area that may be mined in the foreseeable future.

#### 4.0 RECOMMENDATIONS

The recommended extent of mining for the area outside the controlled area is depicted in Figure 5. This area represents the currently leased area less areas that are precluded from mining by the presence of existing hydrocarbon holes. Hydrocarbon hole barriers are set at either 0.25 miles for shallow oil, 0.5 mile for holes deeper than 5000 feet, or 110 percent of the depth to the mine. The use of leases is justified since the actual grade-thickness information is not available (since it is proprietary information) and the BLM lease grade map bounds the economic mining areas. In addition, areas that are known to be barren of resource grade potash and are not leased as shown in Figure 1 have been excluded. (Note, once the BLM map is digitized, mined out areas can also be excluded as well as leased areas that are barren.) No effort was made to distinguish between the various ore zones on this map. An average mine height of 6 feet should be used.

Three possible interpretations for the extent of mining inside the controlled area are shown in Figures 6, 7, and 8. These have been compiled from the three sources mentioned above. Figure 6 shows the most conservative interpretation based on the BLM lease map. This map, however, includes a significant volume of potash that is not minable under today's economic conditions. Figure 7 shows areas that have been previously leased for potash mining. Note that Section 32 has been deleted since it is shown to be essentially barren of lease grade potash on the BLM lease grade map in Figure 6. This area is most consistent with the approach used to identify the extent of mining outside the controlled area. However,

---

<sup>11</sup>Leasing history is particularly important within the controlled area since there are no current leases to indicate what a mining company would consider for mining or what may be included in a life of mine plan. Such leases did exist recently. However, as indicated in Table 1, the DOE purchased these leases as part of the process of preserving the controlled area.

the lease approach was used outside the controlled area due to the lack of sufficient data to draw a more precise boundary. Figure 8 depicts a more precise area based on the most current interpretation of what are economically viable potash leases. Figure 8 is the recommended area for use in the analysis<sup>12</sup>. Because of the detail available in the background information, the area has been divided into sections that may be mined for langbeinite, sections that may be mined for sylvite, and sections may be mined for both. The parameters for mining should be as depicted in the following table, based on information in the NMBMMR report.

	Mining Method	Mine layout	Mine height	Extraction Ratio
Langbeinite (4th ore zone)	Conventional	Room and pillar	4 to 8 feet	60 percent
Sylvite (10th ore zone)	Continuous	Long panel	4 to 5 feet	80 percent

The area in Figure 8 is based on the "55" and "37.5" contours in the NMBMMR report.



---

<sup>12</sup>The contours in the NMBMMR report are the result of a specific contouring program used by the investigator. Other interpretations are possible using different packages or by contouring without the use of software. This paper simply accepts the work done by the NMBMMR as a valid representation of the data. Other equally valid representations may exist and may be of interest in the evaluation of the impacts of mining.

**TABLE 1: HISTORY OF POTASH PROSPECTING AND LEASING ON THE WIPP  
SITE  
TOWNSHIP 22 SOUTH RANGE 31 EAST**

<u>SECTION</u>	<u>SERIAL NO.</u>	<u>DATE OF ACTION</u>	<u>STATUS</u>
15: All	LC047600(Pot. Per.)	5/26/33	Canceled 9/30/36
All	LC065503(Pot. Per.)	3/7/50	Canceled 5/29/54
All	NM011422(Pot. Per.)	1/27/54	Canceled 6/30/54
All	NM011812(Pot. Per.)	11/21/57	Expired 11/21/59
All	NM075014(Pot. Per.)	5/3/60	Lease issued 7/1/64
16: All	M-14957-1(Pot. Les.)	2/4/67	DOE Acquired Lease 3/4/88
17: All	LC065504(Pot. Per.)	1/16/50	Canceled 5/29/52
All	NM011813(Pot. Per.)	4/7/58	Expired 4/7/60
All	NM094314(Pot. Per.)	8/1/60	Lease Issued 7/31/64, Lease Relinquished 12/22/72
18: All	LC065506(Pot. Per.)	12/14/54	Expired 12/14/56
Lots 1,2,3,4 E $\frac{1}{2}$ W $\frac{1}{2}$ , E $\frac{1}{4}$	NM057290(Pot. Per.)	10/28/59	Lease Issued 1/1/64, Lease Relinquished 12/22/72
19: All	NM08285(Pot. Per.)	9/18/56	Lease Expired 9/18/60
Lots 1,2,3,4 W $\frac{1}{2}$ E $\frac{1}{2}$ , E $\frac{1}{4}$ W $\frac{1}{4}$ , SE $\frac{1}{4}$ SE $\frac{1}{4}$	NM02535(Pot. Per.)	6/1/67	Lease Terminated 8/31/68
20: All	NM08285(Pot. Per.)	9/18/56	Lease Expired 9/18/60
All	NM0384583(Pot. Per.)	12/1/63	Lease Expired 1/9/68
21: All	NM08285(Pot. Per.)	9/18/56	Lease Expired 9/18/60
All	NM384583(Pot. Per.)	12/1/63	Lease Expired 1/9/68
22: SW $\frac{1}{4}$ SE $\frac{1}{4}$ , NW $\frac{1}{4}$ SE $\frac{1}{4}$	LC045236 (Pot. Per.)	5/23/32	Canceled 6/2/36
NW $\frac{1}{4}$ SE $\frac{1}{4}$	NM08285(Pot. Per.)	9/18/56	Lease Expired 9/18/60
All	NM0384584(Pot. Per.)	9/1/63	Leased 11/1/67, Lease Acquired by DOE

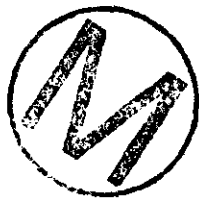


**TABLE 1: HISTORY OF POTASH PROSPECTING AND LEASING ON THE WIPP  
SITE  
TOWNSHIP 22 SOUTH RANGE 31 EAST (Continued)**

<u>SECTION</u>	<u>SERIAL NO.</u>	<u>DATE OF ACTION</u>	<u>STATUS</u>
27: NW¼	LC047927(Pot. Per.)	5/14/48	Canceled 6/13/51
NW¼	NM0214(Pot. Per.)	10/27/55	Expired 10/27/57
NW¼	NM08285(Pot. Per.)	9/18/56	Expired 9/18/60
NE¼	NM038266(Pot. Per.)	7/29/59	Expired 7/29/61
27: SW¼,SE¼	NM0221(Pot. Per.)	4/23/56	Expired 4/23/58
SW¼,SE¼	NM045331(Pot. Per.)	7/29/59	Expired 7/29/61
All	NM0384584(Pot. Per.)	9/1/63	Leased 11/1/67, Lease Acquired by DOE
28: All	NM0384583(Pot. Per.)	12/1/63	Lease Expired 1/9/68
29: All	NM0384583(Pot. Per.)	12/1/63	Expired 11/30/67
30: Lots 1,2,3,4 E½W¼, SE¼	NM038136(Pot. Per.)	7/29/59	Lease Expired 9/13/61
Lots 1,2,3,4 NE¼, E½W¼, W¼SE¼	NM0359163(Pot. Per.)	6/1/63	Expired 5/31/67
Lots 1,2,3,4 NE¼, E½W¼, W¼SE¼	NM 2535(Pot. Per.)	6/1/67	Lease Terminated 8/31/68
31: All	LC045662(Pot. Per.)	10/11/32	Canceled 6/2/36
All	LC066113(Pot. Per.)	1/5/55	Expired 1/5/57
Lots 1,2,3,4 E½W¼, E¼ (All)	NM038136(Pot. Per.)	7/29/59	Expired 9/13/61
32: All	M-14957(Pot. Les)	2/4/67	Lease Acquired by DOE 3/4/88



**TABLE 1: HISTORY OF POTASH PROSPECTING AND LEASING ON THE WIPP  
SITE  
TOWNSHIP 22 SOUTH RANGE 31 EAST (Continued)**

<u>SECTION</u>	<u>SERIAL NO.</u>	<u>DATE OF ACTION</u>	<u>STATUS</u>
33: All	LC045661(Pot. Per.)	10/21/32	Canceled 3/23/37
All	NM0359161(Pot. Per.)	6/1/63	Expired 5/31/67
All	NM02534(Pot. Per.)	9/1/67	Terminated 8/31/68
All	NM10409(Pot. Per.)	2/1/70	Expired 1/31/72
34: NE¼, NW¼, NE¼SW½	LC047602(Pot. Per.)	5/26/33	Canceled 9/30/36
NW¼,SW¼	NM0384584(Pot. Per.)	9/1/63	Leased 11/1/67, Lease Acquired by DOE

Pot. Per. = Permit for potash exploration

Pot. Les. = Potash lease

Reference: Abstract No. 29990 and 29989



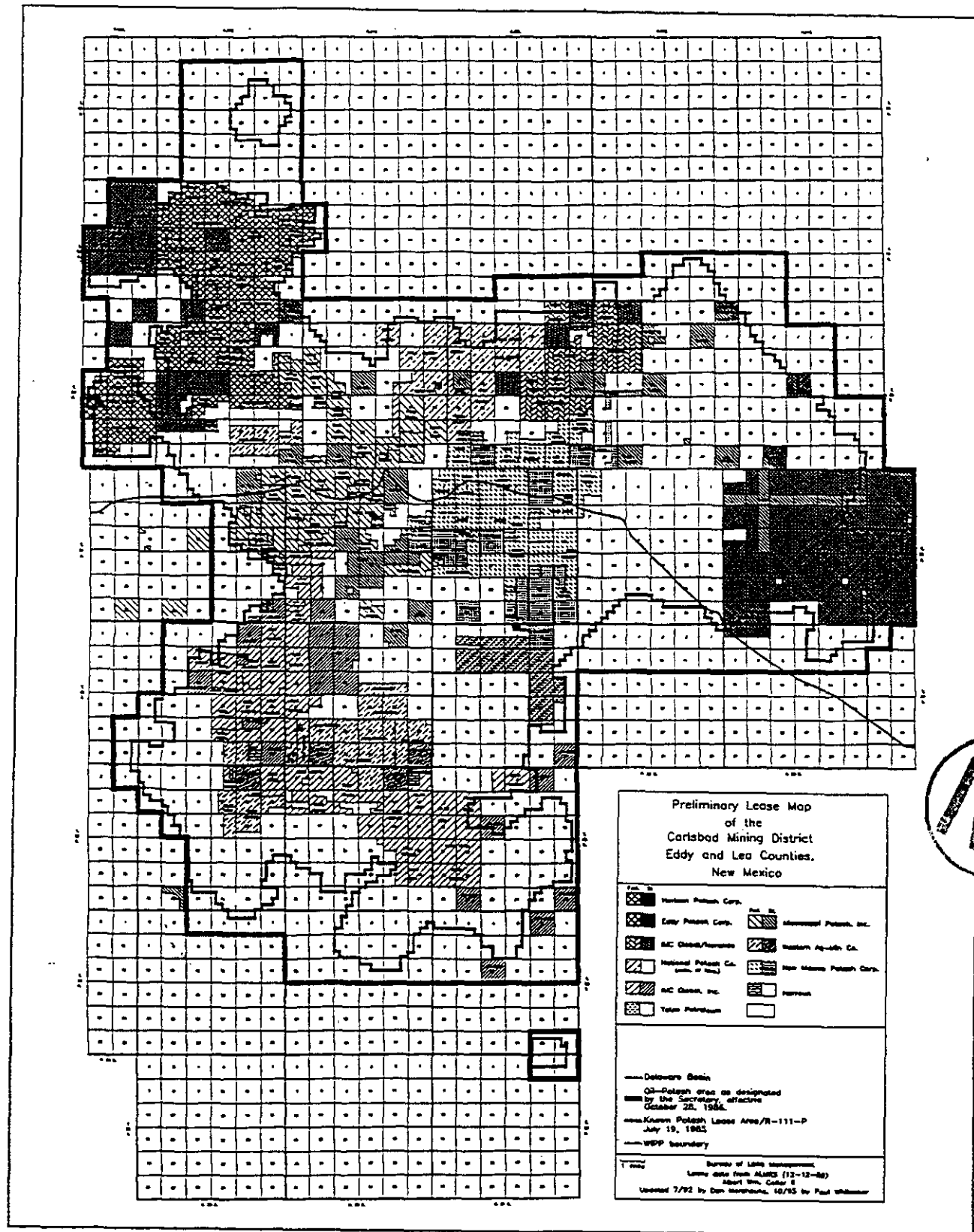


Figure 1  
1995 Potash Lease Map

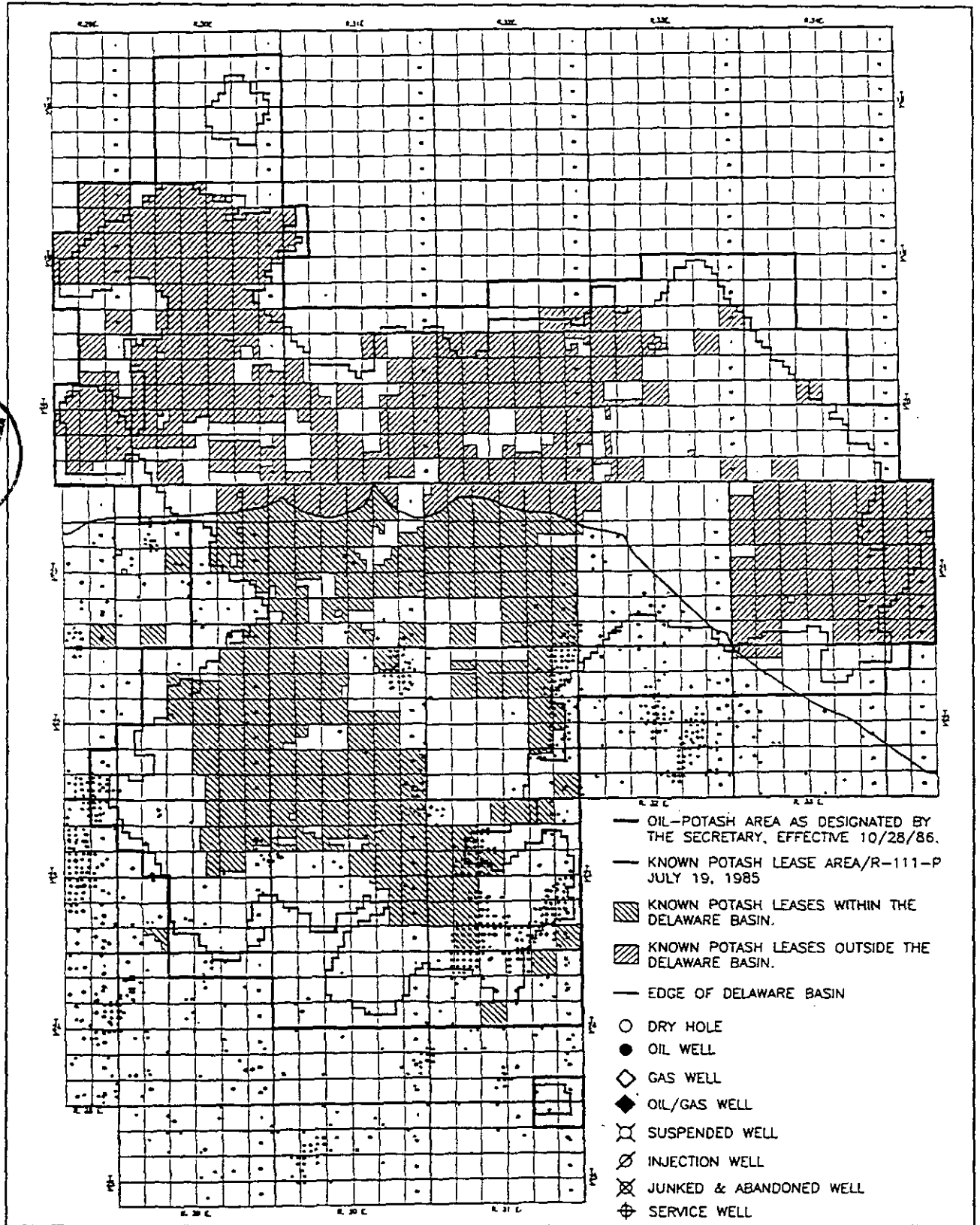


Figure 2  
Oil and Gas Wells Within the Carlsbad Potash Enclave

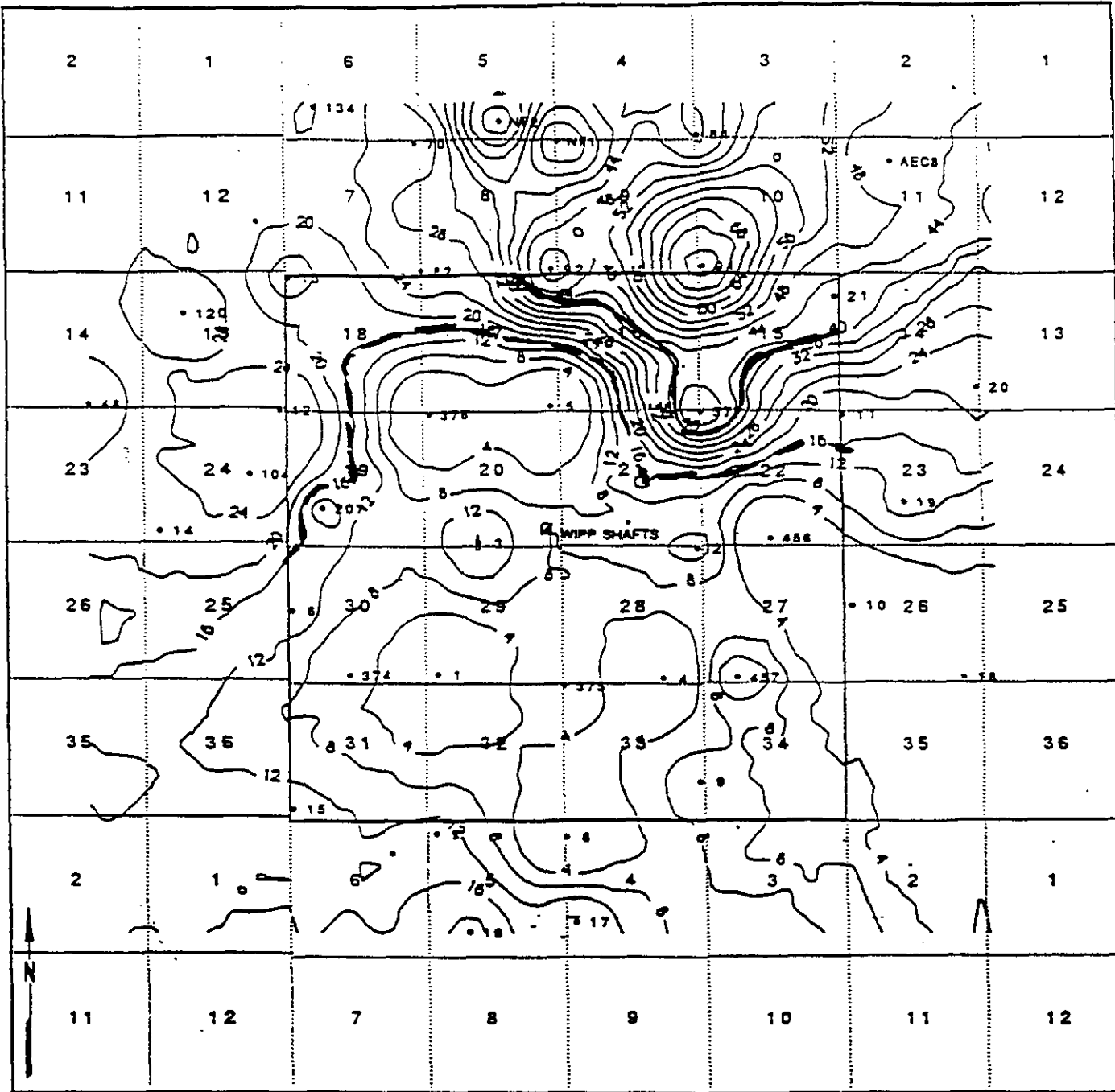


Figure 3  
Langbeinite Reserves Based on NMBMMR.



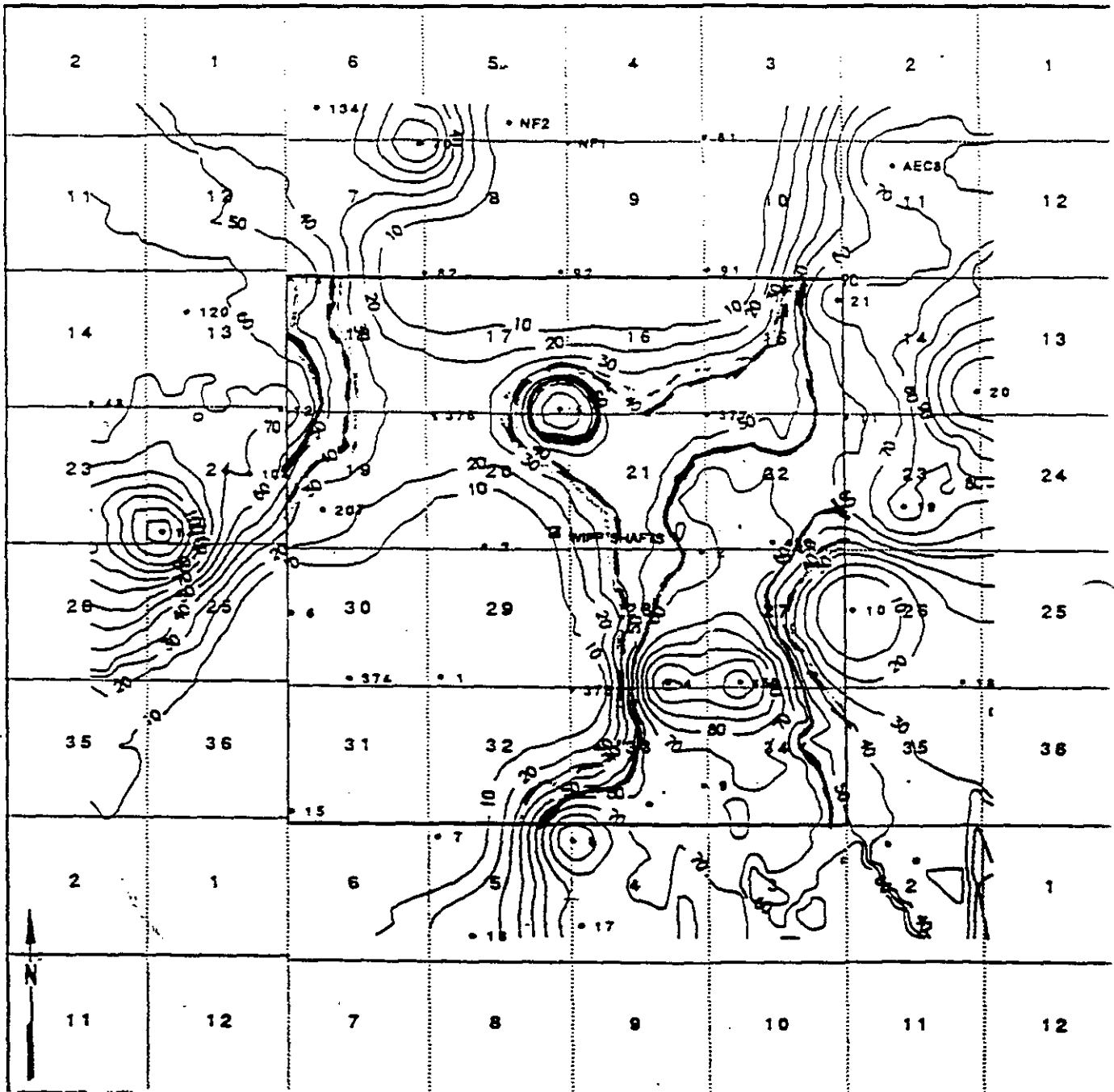


Figure 4  
Sylvite Reserves Based on NMBMMR.

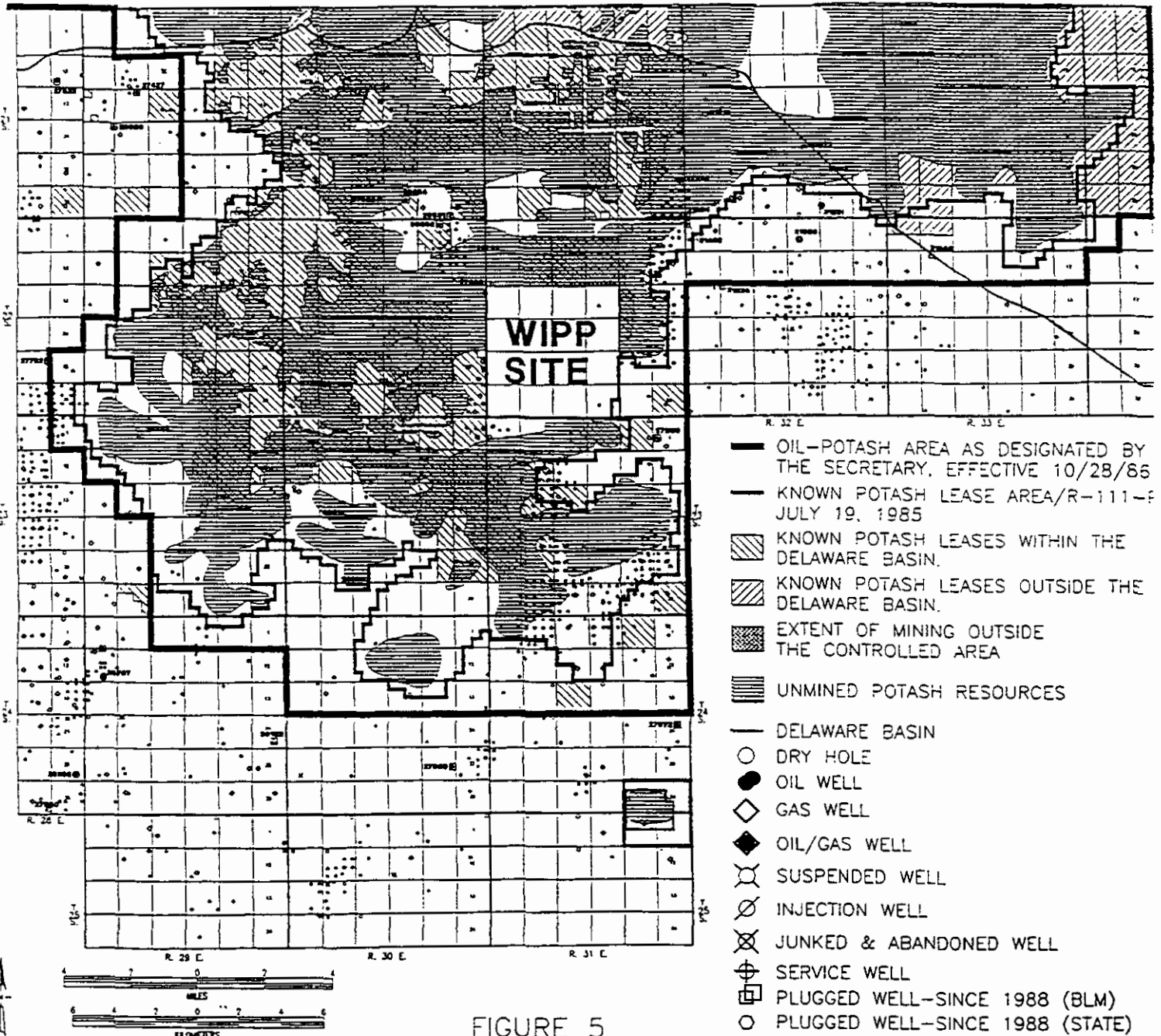


FIGURE 5  
Extent of Mining Outside the Controlled Area



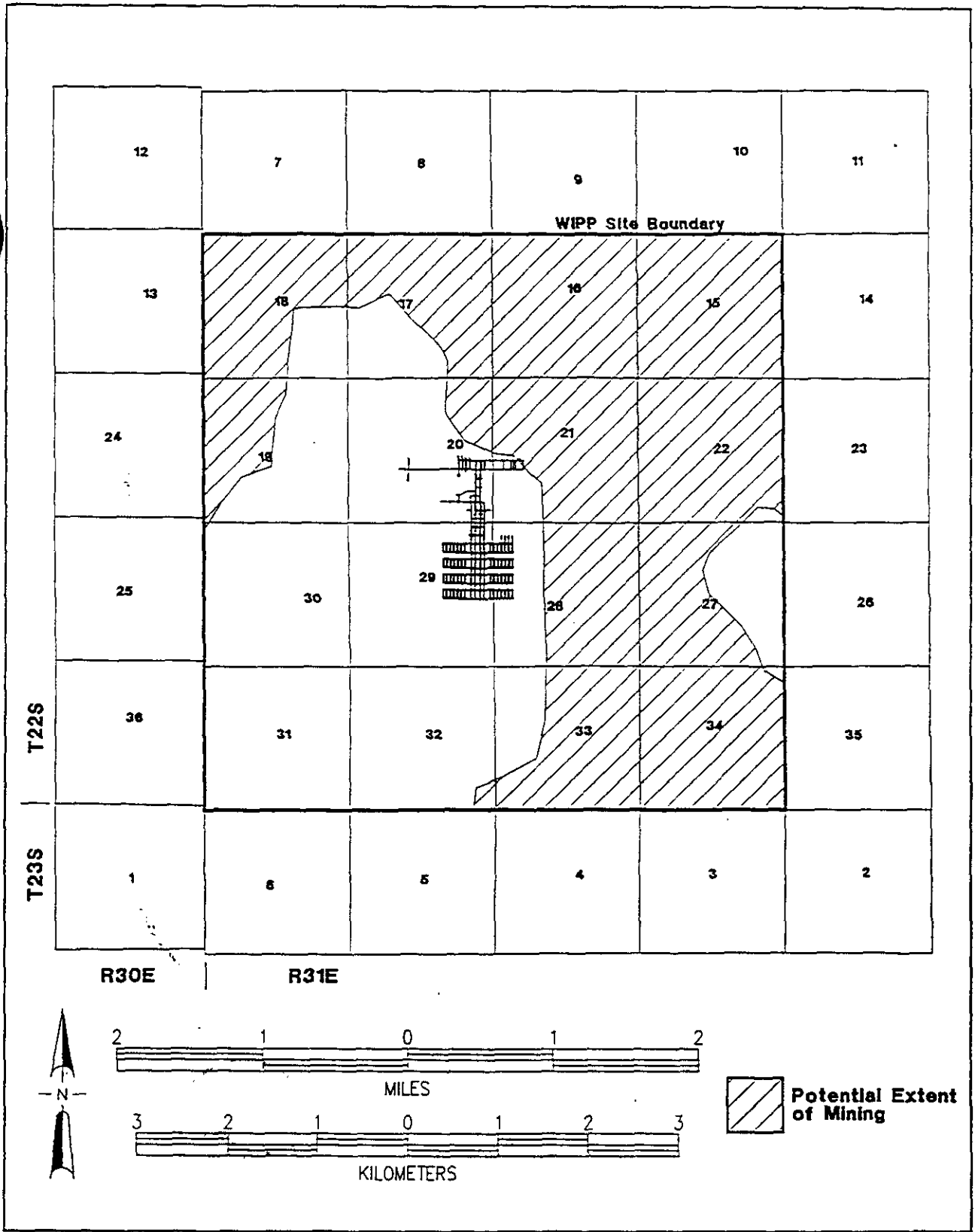


Figure 6  
Potential Extent of Mining Based on Lease Grade Ore (1993 BLM Lease Map)

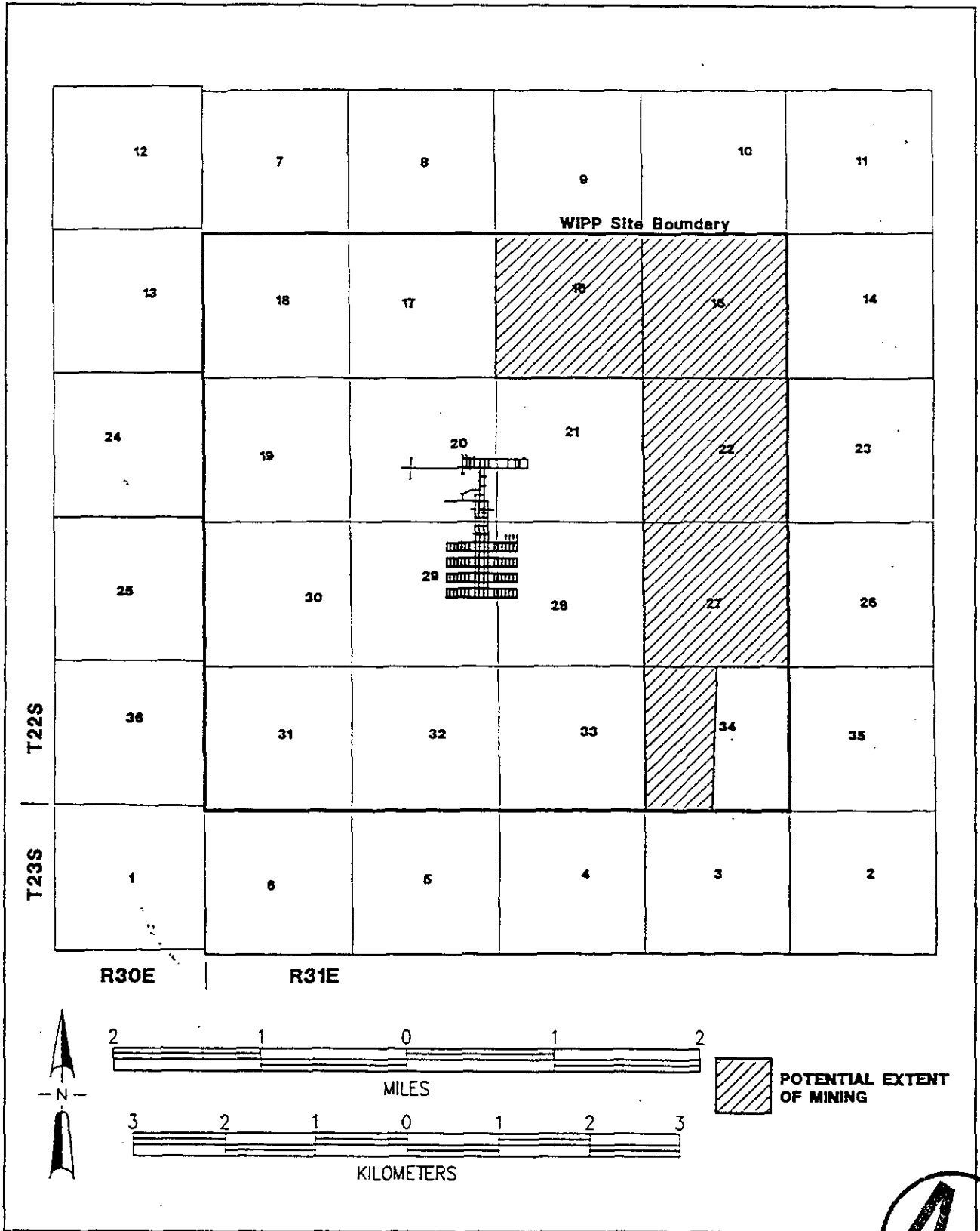


Figure 7  
 Potential Extent of Mining Based on Historically Leased Areas  
 Within the LWA Containing Economic Ore Grade

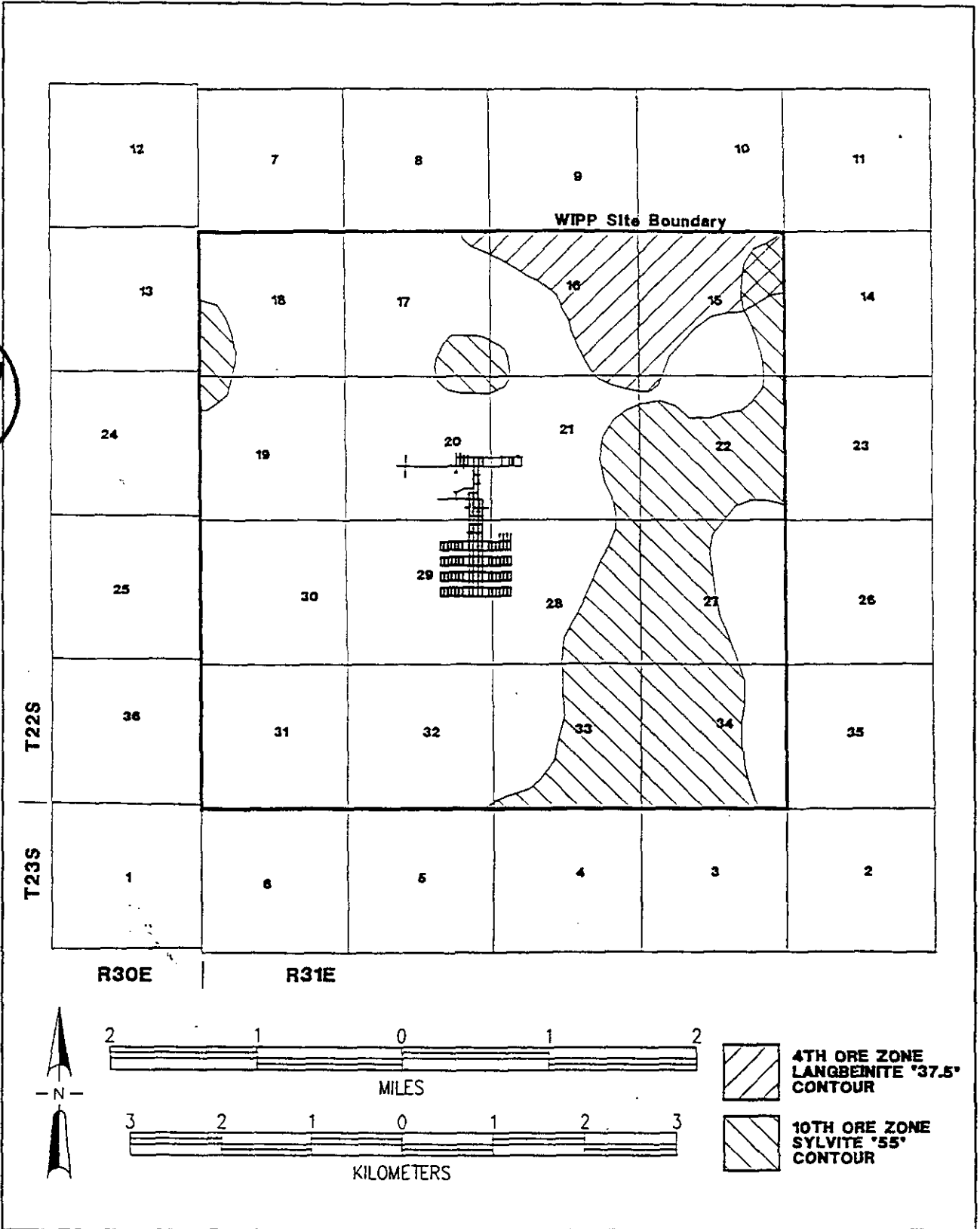
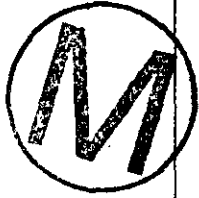


Figure 8  
Extent of Mining of Economic Grade Ore Based on NMBMMR Report

---

**Title 40 CFR Part 191  
Compliance Certification  
Application  
for the  
Waste Isolation Pilot Plant**

**MASS Attachment 15-6**



**THIS PAGE INTENTIONALLY LEFT BLANK**



WPO 39167

INFORMATION ONLY Sandia National Laboratories

Albuquerque, New Mexico 87185-1324

date: July 11, 1996

to: file (SWCF-A Records Center, SWCF-A:WBS1.1.5.2.3:TD:QA: Non-Salado  
Tracer Test Interpretations, Interim Simulations, WPO#37450)

*Lucy Meigs* *Jim McCord*  
from: Lucy Meigs and Jim McCord, MS - 1324

subject: Physical Transport in the Culebra Dolomite

Attached is a letter report that briefly describes the recent work that has been done to characterize the physical transport processes in the Culebra dolomite. It also describes the rationale for the physical transport parameters used for the SECOTP2D calculations in the performance assessment calculations. Additional detailed information on the interpretations of the tracer test data and additional detail on discussion in this memo will be contained (or referenced) in the record package into which this memo is being placed (WPO#37450).



Copy to:  
Margaret Chu, MS 1335  
Peter Davies, MS 1324  
Al Lappin, MS 1324  
Rick Beauheim, MS 1324  
Tom Corbet, MS 1324  
Hans Papenguth, MS 1341  
Larry Brush, Ms1341  
Jim Nowack, MS1320  
George Perkins, MS1341  
Bob Holt, MS1324

# Physical Transport in the Culebra Dolomite

by Lucy C. Meigs and James T McCord

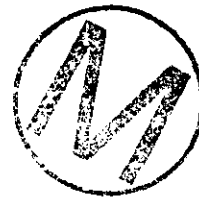
7/11/96



---

**Title 40 CFR Part 191  
Compliance Certification  
Application  
for the  
Waste Isolation Pilot Plant**

**MASS Attachment 15-7**



## Physical Transport in the Culebra Dolomite

The Culebra Dolomite Member of the Rustler Formation is being studied as a possible transport medium for radionuclides released from the WIPP repository by future inadvertent human intrusion. This letter report describes data collection and data analyses which led to our current conceptual model of physical transport in the Culebra. It also covers how the conceptual model is implemented in the performance assessment (PA) of the WIPP site, and parameterization of the PA numerical models of physical transport in the Culebra.

### Characterization of the Culebra for Development and Testing of Conceptual Models

In order to determine the important processes (advection, dispersion and diffusion) controlling contaminant transport and to evaluate the physical transport properties of the Culebra dolomite, a series of tracer tests has been conducted. Among the most important issues is whether the Culebra should be modeled as a single-porosity medium with transport only in the fractures or whether there may be significant interaction with the "matrix" (double-porosity medium). Convergent-flow tracer tests were conducted within the Culebra at three locations (H-3, H-6, and H-11 hydropads) between 1981 and 1988. These tests showed rates and amounts of solute transport to be strongly dependent on flow direction, and suggested that a physical retardation mechanism was affecting transport. The tracer-breakthrough curves from these tests were simulated using a homogeneous double-porosity continuum model (SWIFT II). These simulations showed that the observed transport behavior could be explained by a combination of anisotropy in horizontal hydraulic conductivity and matrix diffusion. These tests ruled out conceptualizing the Culebra as a homogeneous single-porosity medium (Jones et al., 1992). However, significant questions remained as to whether other processes such as heterogeneity in hydraulic conductivity could have caused the tailing in the breakthrough curves that was attributed to matrix diffusion.



Additional tracer tests have recently been conducted at the H-11 and H-19 hydropads. These tests included single-well injection-withdrawal tests and multiwell convergent-flow tests at both locations. The results of a preliminary tracer test conducted May-July 1995 at the H-19 hydropad revealed that at this site, transport was slower than at previous sites tested. The relatively high advective porosity (greater than 0.05, larger than typical fracture porosities) that appears to be required to model these data caused us to question our previous conceptualization of the Culebra. Through careful reexamination of the geology and stratigraphy of the Culebra, we have developed a clearer picture of the important processes that control transport.

The Culebra has non-uniform properties both horizontally and vertically. This has been demonstrated with both hydraulic and tracer tests. The upper portion of the Culebra has a much lower permeability and does not appear to provide pathways for rapid transport (see effective thickness discussion below). Examination of core and shaft exposures has

revealed that there are multiple scales of porosity within the Culebra including: fractures ranging from microscale to potentially large, vuggy zones, and interparticle and intercrystalline porosity (Figure 1). Flow occurs within fractures, within vugs where they are connected by fractures, and probably to some extent within interparticle porosity where the porosity is high, such as "chalky" lenses. At any given location, flow will occur in response to hydraulic gradients in all places that are permeable. The variation in peak arrival time in tracer breakthrough curves between the H-11 and the H-19 hydropads suggests that the types of porosity contributing to rapid advective transport vary spatially. In addition to advective transport of solutes, diffusive transport will occur into all connected porosity. Thus, diffusion can be an important process for effectively retarding solutes by transferring mass from the porosity where advection (flow) is the dominant process into other portions of the rock. Diffusion into stagnant portions of the rock also provides access to additional surface area for sorption. When the permeability contrast between different scales of connected porosity is large, transport can effectively be modeled by dividing the system into advective porosity (often referred to as fracture porosity) and diffusive porosity (often referred to as matrix porosity).



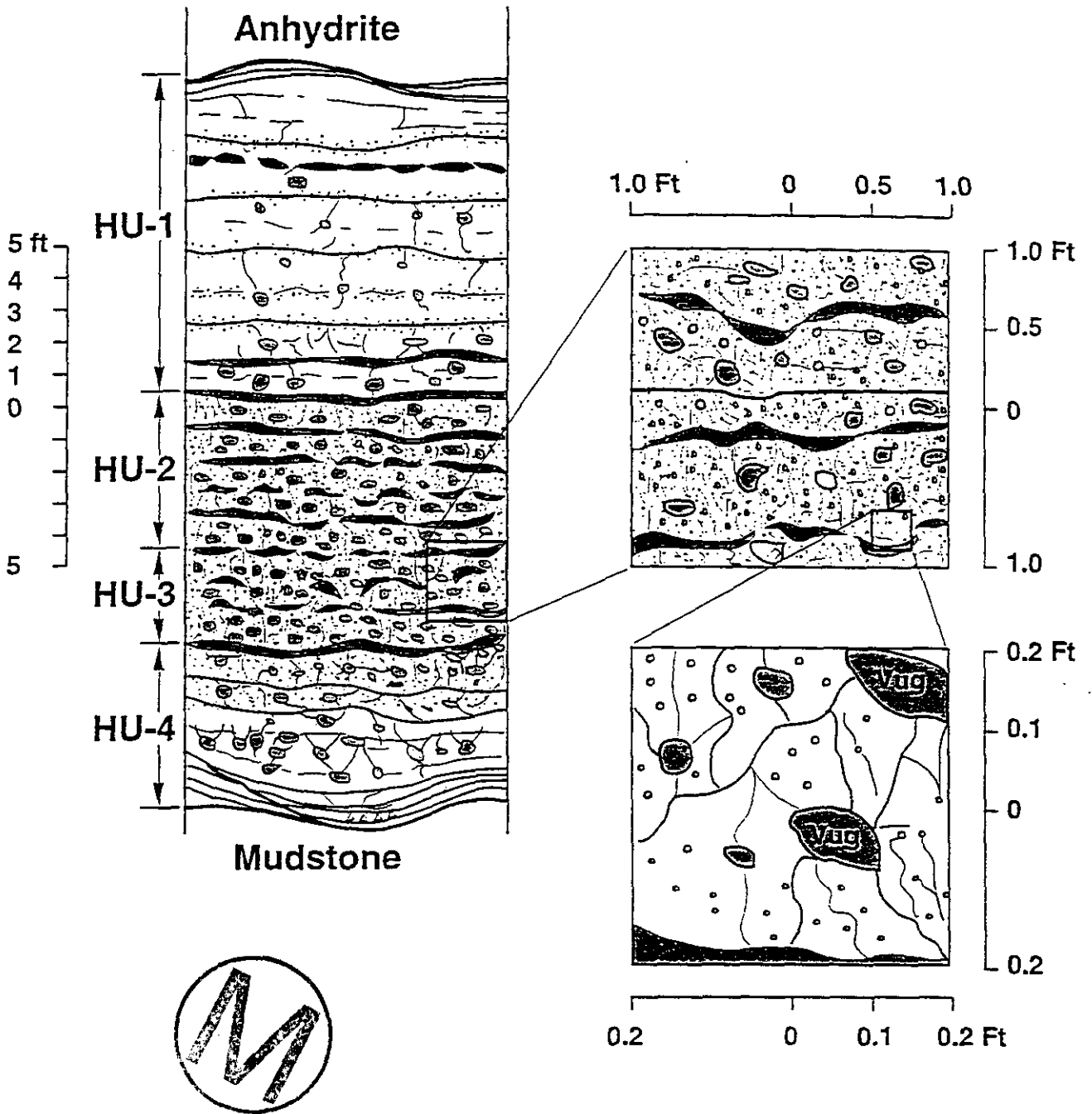
The interpretations of tracer test data to date have relied on both homogeneous and heterogeneous single- and double-porosity continuum models (SWIFT II and THEMME). Spatial variations in advective transport are represented in numerical simulations of the tracer tests with random fields of hydraulic conductivity. Interpretations completed thus far have shown that the single-well injection-withdrawal test data from both the H-11 and H-19 hydropads cannot be explained by heterogeneity alone. Simulations of cumulative mass recovery during the withdrawal phase of the single-well tests with both homogeneous and heterogeneous models suggest that mass recovery should be very rapid for single-porosity media. The Culebra tracer test data, however, show a much slower cumulative mass recovery, as would be anticipated if some sort of diffusional process was controlling mass recovery (i.e. if matrix diffusion is playing a significant role).

In summary, the major physical transport processes that affect actinide transport through the Culebra dolomite include advection (through fractures and other permeable porosity), dispersive spreading during advection due to heterogeneity, and matrix diffusion (between fractures and matrix or more generally, diffusion between adjacent regions with large permeability contrasts). Sorption also exerts an important control on transport, however this memorandum focuses on physical transport rather than chemical transport.

#### PA Modeling of Physical Transport in the Culebra

At the Performance Assessment (PA) scale, spatial variability in advective transport is represented by heterogeneous transmissivity fields that have been conditioned on available point transmissivity data and transient pressure data. In the PA calculations, the lower permeability of the upper portion of the Culebra has been approximated by eliminating this portion of the Culebra from the transport model. The possible spatial variability in transport properties (diffusion and sorption rates) has not been taken into

Figure 1. Multiple scales of Culebra porosity based on examination of core, shaft mapping and Raax logging (Holt, 1996).





account in the PA model. Attempts have been made to take into account the variability by limiting the parameter ranges to the expected effective spatial averages across the site and, when unquantified uncertainties exist, by providing conservative estimates of transport parameters (i.e. parameters that could lead to greater releases than expected). For instance, with respect to effective Culebra thickness (see next section), field data indicate that only the lower  $4 \pm$  m actively participates in flow at most locations sampled. Despite the fact that our rather sparse sampling network prevents us from ruling out the existence of regions where the entire 7 m of Culebra is active in the physical transport process, we have conservatively specified that PA calculations should consider the Culebra to be only 4m thick everywhere.

The PA for WIPP models transport in the Culebra with SECOTP2D which is a double-porosity model. The physical transport parameters required by SECOTP2D are: (1) effective thickness (See parameter records package in the Sandia WIPP Central Files (SWCF-A), WPO#37223), (2) advective porosity (often referred to as fracture porosity) (WPO#37227), (3) diffusional porosity (often referred to as matrix porosity) (WPO#37228), (4) half matrix block length (defined as one-half the thickness of a matrix slab between two parallel plate fractures) which represents specific surface area to volume ratio for matrix diffusion (WPO#37225), (5) diffusive (or matrix) tortuosity (WPO#37226), and (6) dispersivity (WPO#s 37230 and 37231). Effective thickness, diffusive porosity, and diffusive tortuosity were all specified based on field or laboratory measurements. Half matrix block length and advective porosity were specified based on the interpretation of tracer test data from the H-3, H-11 and H-19 hydropads (Hydro Geo Chem, Inc., 1985; Stensrud et al., 1990, Beauheim et al., 1995). Dispersivity values were developed based on comparison of values inferred from tracers tests to large-scale values expected due to heterogeneity at the PA scale. A description of the rationale for the distribution of each of these parameters is provided below.

#### *Effective Thickness*

The effective thickness used for the SECOTP2D calculations is 4.0 m. This effective thickness represents the median Culebra total thickness within the land withdrawal boundary (LWB) (7 m) minus the median (and mean) thickness of Unit 1 (upper Culebra) within the LWB (3 m) as defined by Holt (1996). There is considerable information that indicates that there are significant vertical stratigraphic variations in the Culebra (Holt and Powers, 1984, 1986, 1988, 1990). Based on the descriptions of numerous cores it can be concluded that the basic stratigraphy of the Culebra dolomite is continuous across the land withdrawal boundary area (Holt, 1996; Holt and Powers 1988). Recent hydraulic tests at the H-19 hydropad (Kloska et al., 1995) have indicated that the permeability of the upper portion of the Culebra is significantly lower than the permeability of the lower Culebra at this hydropad. Hydrophysical (fluid) logging also suggest that most of the flow is coming from the lower portion of the Culebra at H-19 (Results of COLOG work, WPO# 38402). Tracer tests have confirmed that at the H-19 hydropad the upper portion of the Culebra does not play a significant role in solute transport. Tracers injected into

the upper Culebra at H-19b3, H-19b5, H-19b7 only showed up at the pumping well (H-19b0) at barely detectable levels, whereas tracers injected into the lower Culebra or the full Culebra at these wells showed up at the pumping well in significant concentrations (Beauheim et al., 1995; and H-19 tracer test data (WPO# 37452)). In descriptions of the Culebra dolomite in the Air Intake Shaft, Holt and Powers (1990) noted that most of the fluid observed to come out of the Culebra came from the lower portion of the Culebra. Mercer and Orr (1979) report the results of a tracer ( $^{131}\text{I}$ ) and temperature survey run at the H-3 hydropad which indicated that, within the resolution of the test, 100 percent of the flow out was in the lower approximately 10 ft of the Culebra. This test thus suggests that at H-3 the upper 14 ft of Culebra has a very low permeability. Hydraulic testing at well H-14 found that at this location the permeability of both the upper and the lower Culebra was quite low. At H-14 the permeability of the upper Culebra is slightly higher than the permeability of the lower Culebra (Beauheim, 1987). In summary, the bulk of the data points to the fact that in many locations the majority of the flow and transport appears to be taking place in the lower portion of the Culebra, i.e. excluding hydrostratigraphic unit 1. There may be locations where the entire Culebra participates in transport, but for lack of evidence along the off-site pathway, a thinner thickness has been selected. If additional evidence were to be collected that indicated that the entire Culebra thickness should be used in the PA model, the use of this larger thickness would result in slower transport and a decrease in releases.

#### *Diffusive Porosity*

The diffusive porosity distribution used for the SECOTP2D calculations is:

Minimum	0.10
10th Percentile	0.11
25th percentile	0.12
50th percentile	0.16
75th percentile	0.18
90th percentile	0.19
Maximum	0.25



This porosity distribution is derived from laboratory measurements. Boyle's Law helium porosity measurements have been made on 103 Culebra core plugs from 17 locations as reported in Kelley and Saulnier (1990), as well as additional porosity measurements recently completed by Terra Tek (WPO#38234). Water resaturation porosity measurements were also made for a subset of the cores. All measurements were very similar; the average difference between the water resaturation porosity and the Boyle's Law helium porosity was less than 0.005. The methodology used for these porosity measurements and the comparisons made are described in Kelley and Saulnier (1990). A spreadsheet in the diffusive porosity parameter records package (WPO#37228) summarizes all the Boyle's Law helium porosity data that have been collected. This spreadsheet summarizes the maximum, minimum, median and average for all data, data averaged by well, and well averages averaged by hydropad, and all data averaged by

hydropad. The hydropad averages of the data were used to develop the distribution presented above since the wells at an individual hydropad are very close together as compared to the spacing of all wells. As expected, averages from the hydropads give a narrower distribution than the distribution of all data. In the PA simulations (SECOTP2D), a single value of diffusive porosity is used across the entire model domain for a given realization. The value used for diffusive porosity clearly should be the effective average diffusive porosity encountered along the expected off-site pathway. Thus it does not make sense to include the extreme individual data values in the distribution for use by PA.

#### *Diffusive Tortuosity*

The diffusive tortuosity used for the SECOTP2D calculations is 0.11. This tortuosity value is the median tortuosity calculated from 36 core measurements at 13 locations as reported in Kelley and Saulnier (1990) together with additional measurements recently completed by Terra Tek (WPO#38234). (The measurements reported by Kelley and Saulnier (1990) were also made by Terra Tek.) Terra Tek first determined the formation factor based on electrical-resistivity measurements of core plugs. The formation factor results subsequently were used to calculate tortuosity. Tortuosity is a measurement of the tortuous nature of the pore structure within the rock. The smaller the value, the more tortuous the pathway and the slower the diffusion rate. The methodology used for the determination of formation factor and the calculation of tortuosities is described in Kelley and Saulnier (1990). A spreadsheet in the diffusive tortuosity parameter records package (WPO#37226) summarizes all the tortuosity data. Diffusive tortuosity is fixed parameter in PA calculations because there is a relatively small range to the data with few outliers.

#### *Half Matrix Block Length*

The matrix half-block length distribution used for the SECOTP2D calculation is a uniform distribution ranging from 0.05 to 0.5 m (i.e., full matrix block length values from 0.1 to 1.0 m), with a single value drawn from this distribution for each realization (implying that a single sampled value should represent an average of spatially variable block lengths along the expected "off-site pathway"). This distribution is derived from results of simulating the tracer tests conducted at the H-3, H-11, and H-19 hydropads. Numerical simulations were performed with double-porosity continuum models with both homogeneous and heterogeneous hydraulic conductivity fields. The homogeneous approach utilized the SWIFT-II transport code, and the heterogeneous approach used the THEMM code; both are being qualified per WIPP QAP 19-1. (See WPO#37450 for additional information on simulations.)

Both modeling approaches yielded consistent results for each well-to-well path with regard to matrix block length. It should be pointed out that for some paths the best fit block length is somewhat smaller than the minimum value of the range (e.g., H-11b2), and for some paths the best fit is larger than the recommended range (e.g., H-3b1) for the PA distribution. However, as mentioned above, the PA distribution is really a

distribution of expected spatial averages, since each realization utilizes a single value for block length for the entire simulation domain. It is also important to remember that the tracer test results reflect transport behavior over paths of lengths represented by the well spacing, or lengths ranging from 10 to 30 meters. Considering these two facts, the entire range of matrix block length values inferred from the tracer tests has been truncated to yield the PA distribution which ranges uniformly from 0.1 to 1.0 m. Any single value drawn from the distribution should represent an aerial average for the exit pathway of 2.5 km length, roughly the distance from the center of the waste panels to the land withdrawal boundary. We strongly feel that the extreme value of matrix block greater than 1.0 m will not occur over regions as large as the exit pathway. It should be noted that simulations with a large matrix block length (small surface area for diffusion) will lead to more releases (compared to simulations with small matrix block lengths) because there will be less diffusion and in turn less accessible surface area for sorption.

In general, the matrix block length and advective porosity were the two primary fitting parameters inferred from comparing simulation results to field data. This is because essentially all of the other physical transport parameters could be measured independently with semi-quantifiable and rather small uncertainties; these other parameters were thus considered "fixed values" in the simulations (See WPO#37439). In an effort to obtain extreme values for matrix block length (as well as advective porosity), some of the interpretive simulations stressed the fixed parameters towards the endpoints of their uncertainty range. The "stressing" of fixed parameters was performed in a deliberate fashion such that all changes to the fixed values would "push" the fitted parameter value in the same direction. For instance, to obtain the minimum matrix block length one would decrease the well spacing, the free-water diffusion coefficient and the diffusive porosity, and increase the pumping rate. Simulations with stressed parameters were only conducted for those pathways that had either very large or very small block lengths for the best fit simulations with the fixed parameters at our best estimate. The best-fit matrix block lengths for the stressed simulations lie at or beyond the endpoints of the best-fit distribution (and well beyond the endpoints of the recommended PA distribution). Again, as alluded to in the preceding paragraph, while such extreme values of matrix block length may be valid for simulating transport in the Culebra at some locations within the WIPP simulation domain, it is considered highly unlikely that they occur over regions approaching the length scale of the entire exit pathway. Thus the recommended PA distribution for aerially-averaged matrix block length has endpoints less extreme than the hydropad-scale fitted values. A uniform distribution is recommended because it gives equal probability to all values within the distribution. Even though tracer test interpretations to date suggest that there may be a somewhat higher probability that the block length should be at the lower end of the distribution, given the facts that we have only a limited number of tests sites and that smaller block lengths will yield slower travel paths to the PA compliance boundary (e.g., more physical retardation), we have chosen to recommend a uniform distribution.



One final note which must be addressed relates to the fact that the PA model (SECOTP2D) utilizes a parallel plate model for simulating double-porosity (fracture and matrix) transport, whereas our tracer test interpretive tools (SWIFT II and THEMME) utilize spherical models for simulating the matrix block geometry. (The matrix block length is conceptualized as the thickness of a matrix block between two fractures and represents the surface area to volume ratio for diffusion between the advective porosity and the diffusive porosity.) One important consideration results from this difference in conceptualization of physical retardation via matrix diffusion. This consideration is important with respect to matrix diffusion parameters, particularly when the time scale of a solute pulse duration is small with respect to the diffusion time scale for solute to move from the fracture-block interface to the center of the block. When the pulse duration time scale is small compared to the diffusion-to-block-centroid time scale (e.g., relatively large blocks), the diffusing solute never "feels" solute diffusing in from the other side of the block and it behaves as if it is diffusing into an infinite length block. In these cases, the surface area for diffusion determines the diffusion rate and one can directly convert from the spherical model to the parallel plate model by dividing the block length determined using the spherical blocks by three. On the other hand, when the diffusion-to-block-centroid time scale is equal to or less than the pulse duration time scale (e.g., for relatively small blocks, or long solute pulse durations), solutes invading matrix blocks from opposite sides "meet" at the centroid, resulting in decreased concentration gradients and concurrent decreases in physical retardation due to decreased matrix diffusion. When the blocks become saturated, the spherical and parallel plate block model block lengths can be considered equivalent. At this limit, the double-porosity transport model converges on a single porosity model with all of the pore space (advective + diffusive porosity) immediately accessible by solutes (thus no fast fracture flow paths with rapid transport to the compliance boundary). Between the extremes of large blocks with essentially infinite diffusion and small blocks which allow immediate complete solute saturation of all porosity (equivalent to single-porosity with high porosity), the block length obtained by a spherical model would be between 1-3 times larger than that that would be obtained with a parallel plate model. Given that the conversion between spherical and parallel plate models depends on the parameters of the simulation, that we expect the smaller block sizes in the distribution given to PA to have small diffusion time scales compared to expected pulse duration's time scales, and that the larger blocks will yield faster travel paths to the PA compliance boundary with less physical retardation, we have chosen not to divide our block lengths by three for the recommended PA distribution.



### *Advective Porosity*

The advective porosity distribution used for the SECOTP2D calculation is log-uniform over a range from  $1 \times 10^{-4}$  to  $1 \times 10^{-2}$ . This distribution was derived from numerical simulation of the tracer tests conducted at the H-3, H-11, and H-19 hydropads, and comparing simulated to observed tracer breakthrough data at the pumping well. As mentioned above for matrix block length, two different double-porosity conceptual

models were applied, a homogeneous media approach and a heterogeneous media approach. The homogeneous approach utilized the SWIFT-II transport code, and the heterogeneous approach used the THEMM code. (See WPO#37450 for additional information on simulations.)

Both modeling approaches yielded consistent results for each well-to-well path with regard to advective porosity. As was the case for matrix block length, for some paths the best-fit advective porosity is somewhat smaller than the minimum value of the range (e.g., H-11b3) and for some paths the best fit is larger than the recommended range (e.g., H-19b2, b3, b4, b5, b6, b7). It is important to remember that the tracer test results reflect transport behavior over paths of lengths represented by the well spacing, or lengths ranging from 10 to 30 meter. The entire range of best fit values from the tracer tests has been truncated for the PA distribution based on the fact that the PA transport model utilizes a single value for advective porosity for the entire simulation domain. Recall that single value should represent an aerial average for the exit pathway. We strongly feel that the extreme values of advective porosity less than  $1 \times 10^{-4}$  will not occur over regions as large as the exit pathway, and thus aerial averages lie between these two endpoints. It should be noted that simulations with a small advective porosity will lead to more releases (compared to simulations with large advective porosity) because there will be faster transport resulting in less time for diffusion and in turn less accessible surface area for sorption.

As mentioned above, the advective porosity and matrix block length were the two primary fitting parameters inferred from comparing simulation results to field data. Again, in an effort to obtain extreme values for matrix block length and advective porosity, some of the interpretive simulations stressed the fixed parameters towards the endpoints of their uncertainty range. The "stressing" of fixed parameters was performed in a deliberate fashion such that all changes to the fixed values would "push" the fitted parameter value in the same direction. Simulations with stressed parameters were only conducted for those pathways that had either very large or very small block lengths for the best fit simulations with the fixed parameters at our best estimate. The best-fit advective porosity for the stressed simulations lie at or beyond the endpoints of the best-fit distribution (and well beyond the endpoints of the recommended PA distribution). Again, as alluded to previously, while such extreme values of advective porosity may be valid for simulating transport in the Culebra at some locations within the WIPP simulation domain, it is considered highly unlikely that they occur over regions approaching the length scale of the entire exit pathway. Thus the recommended PA distribution for aerially-averaged advective porosity has endpoints less extreme than the hydropad-scale fitted values. A log uniform distribution is recommended because it gives equal probability to all values in log space. There is not sufficient data from the three hydropad test sites to create a meaningful probability distribution other than log uniform. Two of the tracer test sites have a relatively low advective porosity and one site has a high advective porosity.



### Dispersivity

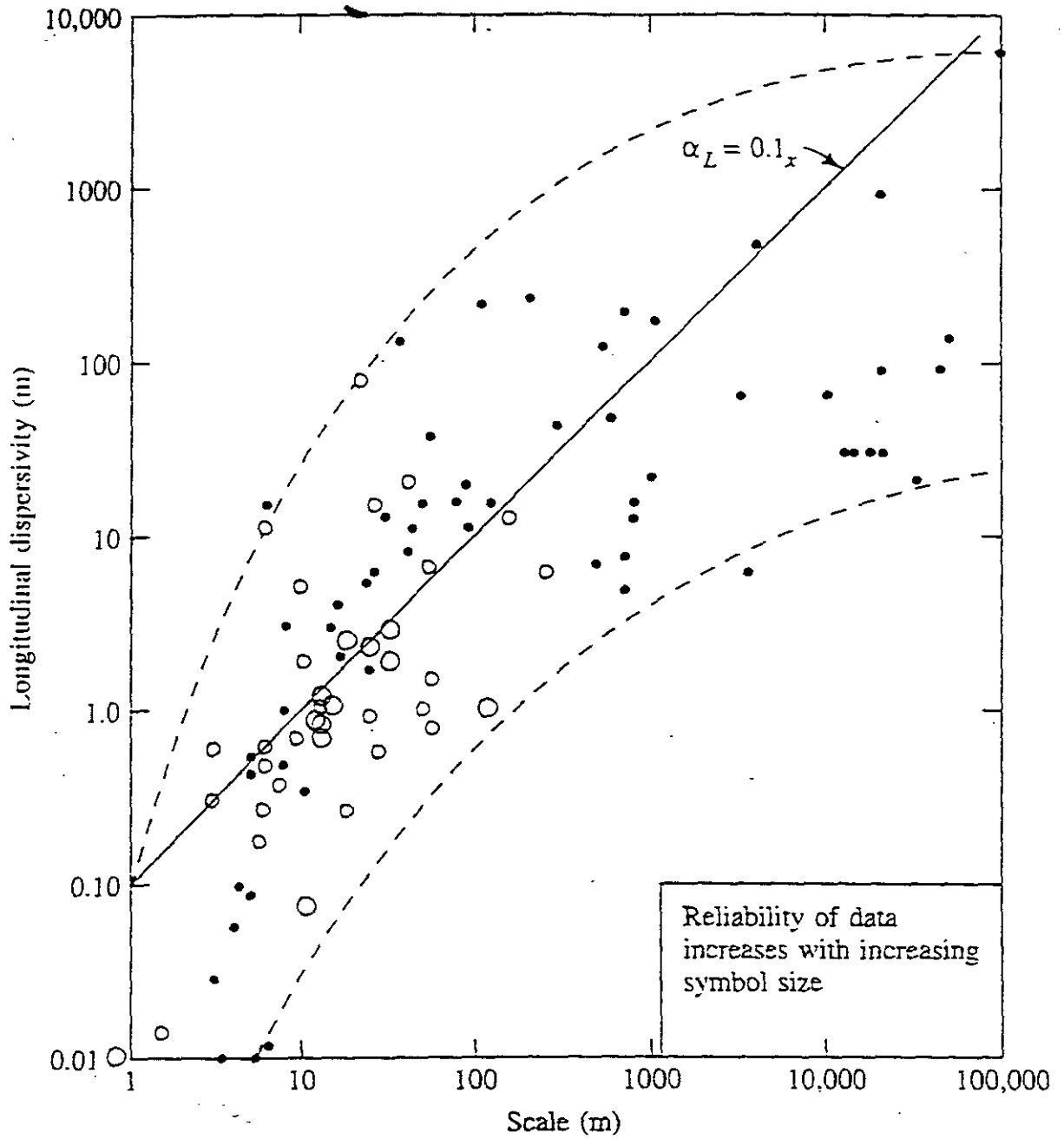
For the PA transport simulations using SECOTP2D, we recommend using a longitudinal and transverse dispersivity equal to zero. If, for numerical stability and/or convergence reasons, a non-zero value is desired, we recommend a constant value of 2 m or smaller. For simulations using a non-zero longitudinal dispersivity, we recommend a longitudinal to transverse dispersivity ratio of 10:1. The rationale for this recommendation lies in the fact that dispersive spreading due to permeability heterogeneity at the PA scale appears to overwhelm dispersive mixing observed at smaller (e.g., hydropad) scales (see detailed discussion below). Given that PA models for flow and transport in the Culebra explicitly account for heterogeneity in the permeability fields, there is no need to specify a discrete dispersivity value to account for mixing at the PA and smaller scales.



Research into solute dispersion in groundwater over the past couple of decades has identified a characteristic trend in dispersivities over a wide range of length scales of interest. The trend clearly shows that dispersivity tends to increase as one moves from a laboratory column scale (cm) to the field scale (m), with larger field problems exhibiting generally higher dispersivity than smaller field problems. This trend perhaps is best summarized by the well-known Gelhar figure (e.g., Gelhar, 1986; Gelhar et al., 1992) in which lab and field data from a large number of experiments are presented on a single plot; this plot is reproduced here as Figure 2. This figure clearly shows the longitudinal dispersivity,  $\alpha_L$ , increasing with the scale of the problem. Also shown in the plot are dashed curves which approximate the min-max envelope of the data and the straight line  $\alpha_L = 0.1L$  where  $L$  is the length scale of the experiment domain. The  $\alpha_L = 0.1L$  line represents the "rule of thumb" often employed when one simulates field-scale problems without the luxury of having site-specific field-scale dispersivities. Notable for the purpose of the WIPP PA simulations is the fact that at scales greater than 1 km, all data values fall below the  $0.1L$  line (most of them substantially below the line with values ranging from  $0.01L$  to  $0.001L$ ).

For the WIPP PA, we are interested in transport from the waste panel area to the land withdrawal boundary (LWB). For the most likely curvilinear exit trajectories, this distance is on the order of 2.5 to 3 km. Unfortunately, our largest scale site-specific data for the dispersivity of the Culebra is from the hydropad tracer tests, with well spacings ranging between 10 and 43 m. When interpreting the results of hydropad tracer tests conducted in the Culebra, best fits with homogeneous media models generally used dispersivities less than or equal to  $0.1L$ . Furthermore, hydraulic testing at the hydropad sites yielded estimates of the lnK variance ( $\sigma_{\ln K}^2$ ) and lnK correlation scale ( $\lambda$ ) product of less than 1.5 m. Stochastic analyses of flow and transport in heterogeneous aquifers (e.g., Gelhar, 1986) derive this product as an estimator of asymptotic macrodispersivity,  $\sigma_{\ln K}^2 \cdot \lambda = \alpha_L$ . In summary, hydraulic and tracer testing of the Culebra dolomite at the WIPP site indicate that at the hydropad scale the dispersivity is generally less than 2 m. Based on Figure 2, at a length scale of an exit trajectory from the waste panels to the LWB (~3

Figure 2. Laboratory and field measured values of longitudinal dispersivity as a function of scale of measurement. The largest circles represent the most reliable data (Adapted by Fetter, 1993, from Gelhar, 1986).



km) we would expect dispersivities to range somewhere between 10 and 1000 m (or a normalized dispersivity  $A=\alpha/L$  to vary between .0033 and 0.33).

This gross estimate of large scale dispersivity derived from Figure 2 can be compared to site-specific spreading estimates using the PA flow model. The PA groundwater flow and transport simulations explicitly acknowledge heterogeneity in the Culebra permeability fields by providing a gridblock by gridblock variation in permeability, with that variation conditioned on permeability measurements/observations from hydropad scale hydraulic testing (i.e., T-fields generated by GRASP-INV, see Appendix TFIELD). One can estimate the effective dispersivity associated with the heterogeneous permeability fields by tracking particles from the source (waste panel) area to the exit (LWB) location, and computing the temporal statistics of the particle travel time from source to exit. Equation 10.7 in Domenico and Schwartz (1990) show that one can use the temporal statistics to compute the dispersivity from such a particle tracking exercise:

$$\alpha_t = \frac{v\sigma_t^2}{2t} \quad (1)$$

where  $v$  is the average pore water velocity (computed as the distance divided by the mean travel time),  $\sigma_t^2$  is the variance of particle travel time, and  $t$  is the mean travel time. We implemented this approach by tracking particles released along a line in the middle of the waste panel area (with the line parallel to the LWB) to the Land Withdrawal Boundary, and the particle tracking results yielded the input parameters required for equation 1 ( $\sigma_t^2$  and  $t$ ). This particle tracking was performed on all 100 heterogeneous permeability field realizations generated by GRASP-INV for the 1996 PA (undisturbed by mining). Results of this particle tracking approach show heterogeneity-induced spreading to yield PA-scale dispersivities ranging from approximately 10 m to approximately 1000 m (normalized values between .003 and 0.3). This result is entirely consistent with published results from other experiments conducted around the world published before 1992 (e.g., Figure 2), and these dispersivities are significantly larger than those inferred from the hydropad tracer test results. We therefore feel that, given no site-specific large-scale data on dispersivities, we can trust that the transmissivity heterogeneity explicitly accounted for in the Culebra flow (SECOFL2D) simulations will impart a reasonable amount of dispersive solute spreading on simulated actinide releases with no need to specify additional spreading through the dispersivity parameter in SECOTP2D.

Gelhar et al. (1992) also summarize experimental results related to transverse dispersivity, and they show that the ratio of longitudinal to (horizontal) transverse dispersivity generally ranges between 2:1 and 50:1 and exhibits no clear trend with problem scale. For the WIPP site, no definitive / highly reliable data set exists to provide an estimate of transverse dispersivity. Again, we feel that the heterogeneity in the flow simulations will cause a reasonable amount of spreading, and we should not take credit

for additional spreading by specifying a dispersivity for SECOTP2D which exceeds that caused by the transmissivity heterogeneity.

Based on the above data, analysis, and discussion, any specified value of longitudinal dispersivity less than roughly 2 m will yield similar results for solute transport in the Culebra dolomite from the WIPP waste panel area to the LWB. Assuming that the numerical codes used correctly solve the governing partial differential equations, simulations using local dispersivities less than or equal to 2 m will yield results consistent with field-scale dispersive spreading observations as reported by Gelhar et al. (1992). Given the lack of WIPP site-specific information related to transverse dispersivity, we rely entirely on previous studies (e.g., see Gelhar et al., 1992) to recommend a ratio of longitudinal to transverse dispersivity equal to 10:1.

#### *Parameter Cross Correlations*

One might suspect the possibility of some cross correlation between sampled parameters. To test this suspicion, we have prepared scatter plots of interpreted results from the hydropad test sites which yielded the physical transport parameters used to develop the PA parameter distributions (H-3, H-11, and H-19). Scatter plots of well-to-well transmissivity versus well-to-well advective porosity and matrix block length showed no observable trends, nor did a scatter plot of advective porosity versus matrix block length. These results strongly suggest a lack of correlation between these parameters, and therefore the recommended PA distributions include no cross correlations.



#### *References*

- Beauheim, R. L. 1987. *Interpretations of Single-Well Hydraulic Tests Conducted at and Near the Waste Isolation Pilot Plant (WIPP) Site, 1983-1987*. SAND87-0039.
- Beauheim, R. L., L.C. Meigs, G.J.Saulnier, and W.A. Stensrud, 1995. Culebra Transport Program Test Plan: Tracer Testing of the Culebra Dolomite Member of the Rustler Formation at the H-19 and H-11 Hydropads on the WIPP Site. (Tracer test data will be in WPO#s 37452, 37467, and 37468.)
- Cauffman, T.L., A.M. and J.P. McCord. 1990, *Ground-Water Flow Modeling of the Culebra Dolomite*, Volume II: Data Base. SAND89-7068/2
- Domenico, P., and F.W. Schwartz, 1990. *Physical and Chemical Hydrogeology*, John Wiley Publishing.
- Fetter, C.W., 1993. *Contaminant Hydrogeology*, Macmillan Publishing Co., 458 pp.
- Gelhar, L.W., 1986. Stochastic subsurface hydrology from theory to applications, *Water Resources Research*, v.22(9): 135s-145s.
- Gelhar, L.W., C. Welty, and K. Rehfeldt, 1992. A critical review of data on field-scale dispersion in aquifers, *Water Resources Research*, v.28(7): 1955-1974.
- Hydro Geo Chem, 1985. *WIPP Hydrology Program, Waste Isolation Pilot Plant, SENM, Hydrologic Data Report #1*, SAND85-7206, 710pp.

- Holt, R.M. 1996. unpublished letter report entitled *Hydrostratigraphy of the Culebra Dolomite Member of the Rustler Formation in the WIPP Region* (WPO#38225).
- Holt, R. M. and D.W. Powers, 1984, *Geotechnical Activities in the Waste Handling Shaft*. WTSD-TME-038; U.S. Department of Energy by TSC and International Technology Corporation
- Holt, R. M. and D.W. Powers, 1986, *Geotechnical activities in the Exhaust Shaft*, DOE-WIPP 86-008, U.S. Department of Energy, WIPP Project Office, Carlsbad, NM
- Holt, R. M. and D.W. Powers. 1988. *Facies Variability and Post-Depositional Alteration Within the Rustler Formation in the Vicinity of the Waste Isolation Pilot Plant, Southeastern, New Mexico*. DOE-WIPP 88-004, U.S. DOE, WIPP Project Office, Carlsbad, NM.
- Holt, R. M. and D.W. Powers. 1990. *Geologic mapping of the Air Intake Shaft at the Waste Isolation Pilot Plant, Southeastern New Mexico*. DOE-WIPP 90-051, U.S. Department of Energy, WIPP Project Office, Carlsbad, NM
- Jones, T.L., V.A. Kelley, J.F. Pickens, D.T. Upton, R.L. Beauheim, and P.B. Davies. 1992. Integration of Interpretation Results of Tracer Tests Performed in the Culebra Dolomite at the Waste Isolation Pilot Plant Site, SAND92-1579.
- Kelley, V.A. and G.J. Saulnier. 1990. *Core Analyses for Selected Samples from the Culebra Dolomite at the Waste Isolation Pilot Plant Site*. SAND90-7011.
- Kloska, M.B., G.J. Saulnier, Jr., and R.L. Beauheim. 1995. *Culebra Transport Program Test Plan: Hydraulic Characterization of the Culebra Dolomite Member of the Rustler Formation at the H-19 Hydropad on the WIPP site*. (Results to be contained in WPO#s 38400 and 38401.)
- Mercer, J.W. and B.R. Ott. 1979. *Interim data report on the geohydrology of the proposed Waste Isolation Pilot Plant Site in southeastern New Mexico*, U.S. Geological Survey Water Resources Investigations Report 79-89.
- Stensrud, W.A., M.A. Bame, K.D. Lantz, J.B. Palmer, and G.J. Saulnier, 1990. *WIPP Hydrology Program, Waste Isolation Pilot Plant, Southeastern New Mexico, Hydrologic Data Report #8*, SAND89-7056.



**THIS PAGE INTENTIONALLY LEFT BLANK**



WPO# 30802

FEP NS-9, Two-dimensional assumption for Culebra Calculations

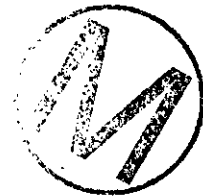
Summary Memo of Record

T. Corbet

*T. Corbet*

21 September 1995

INFORMATION ONLY



- Statement of recommended screening decision

The Culebra is part of a three-dimensional hydrologic system in which slow vertical flow across confining layers plays an important role. Regional modeling performed for this analysis indicates that treating the Culebra as a two-dimensional perfectly-confined hydrostratigraphic unit is a valid simplification for the purposes of PA modeling. In order for the two-dimensional calculations to be defensible, however, their relationship to a fully three-dimensional conceptual model must be documented.

- Statement of screening issue

A two-dimensional model is implemented in the present PA modeling system to calculate flow and transport in the Culebra. The basis for the assumption that a two-dimensional model, and its associated boundary conditions, adequately represents flow in this unit for the purposes of PA has not been systematically investigated or documented. The principles of regional groundwater flow in layered sediments leads us to believe that slow vertical leakage occurs through the overlying Tamarisk member, but available field observations provide limited information about the rate and direction of this leakage. Vertical leakage might impact flow and transport calculations in the Culebra in several ways. Some error will be introduced into calibrated transmissivity fields if leakage is significant but not included in inverse calculations. Even if transmissivity fields are without systematic error, flow fields might not represent actual conditions if zero leakage is assumed for two-dimensional flow calculations.

There is a second issue concerning the two-dimensional assumption. That is whether or not vertical components of flow and/or vertical heterogeneity within the Culebra should be modeled. It is not included in this analysis.

- Approach

I performed calculations using a three-dimensional regional model to examine how the Culebra in the vicinity of the WIPP interacts with other hydrostratigraphic units. These calculations are the same as those used in FEP NS-8 to evaluate the impact of climate change. The model boundary and initial conditions, parameters, and results are presented in the SMOR for that FEP. Table 1 summarizes the parameters used in the calculations. The analysis for this FEP differs from the climate FEP in that more emphasis is placed here on the vertical leakage across the upper and lower surfaces of the Culebra.

The regional calculations suggest that a large portion of the total flow through the Culebra in the controlled area might be by vertical leakage. Additional calculations with the GRASP-INV code to see how much the calibrated transmissivity fields and release paths and travel times would be altered if vertical leakage was accounted for in the inverse solution of the T fields and the two-dimensional flow calculations are planned but not completed at this time (memo attached).

*Not Attached in this copy. It is available in SWCF.*

*Kurt Larson 7/11/96*

- Results and discussion

These calculations suggest that vertical leakage downward from the Magenta makes a significant contribution to the total inflow to the Culebra at the scale of the controlled area. The percent of the total flow into this portion of the Culebra that is due to leakage is uncertain mainly because the vertical hydraulic conductivity of the Tamarisk at the scale of the nodal blocks used is not well known. The percent contribution of vertical leakage ranges from 3 to 50 percent for the steady-state calculations (Table 2) and from 6 to 66 percent for the transient simulations (Tables 3 and 4). The combined range, rounded to the nearest 5 percent, is 5 to 65 percent.

The undisturbed hydraulic conductivity of the anhydrites that make up most of the Tamarisk Member was assumed to be either  $10^{-12}$  or  $10^{-13}$  m/s. As expected, the percent contribution of vertical leakages is larger for those calculations ( 14/41, 23/50, 24/51, bc, c1, c4, c5, c8) using the larger conductivity value. The best fit with observed heads is transient simulation c5 which results in a 66 percent contribution of vertical leakage. However, transient simulations with a anhydrite conductivity of less than  $1 \times 10^{-12}$  m/s were not performed. It is possible that such simulations would also result in heads similar to those observed and would have a smaller contribution from vertical leakage.

In each of these calculations, all of the vertical leakage between the Magenta and Culebra in the controlled area is directed downward. This condition is indicated by the fact that, in all calculations, zero percent of the flow out of the Culebra is by vertical leakage across its upper surface. These results are supported by field observations of fresh-water heads in the Magenta and Culebra. In areas in which the Tamarisk is intact, observed fresh-water heads are higher in the Magenta than in the Culebra. However, even these observations are not conclusive in that fluid pressures and densities in the strata between the Magenta and Culebra are not known.

These calculations strongly suggest that all flow out of the Culebra in the controlled area is by lateral flow. This conclusion is important in that it shows that a two-dimensional model is able to represent realistic release paths. Also, calculated vertical leakage in or out of the Culebra across its lower surface is negligible. Little vertical leakage will occur across the lower surface of the Culebra if, as assumed in these calculations, that no laterally continuous unit with high conductivity exists in the Rustler Fm. below the Culebra.

- Basis for recommended screening decision

As discussed above, the simulations performed for this analysis suggest that an uncertain but probably significant amount of the total flow into the portion of the Culebra within the controlled area is by vertical leakage across the top of the Culebra. All of the flow out of this portion of the Culebra is by lateral flow along the Culebra. That all of the outward flow is lateral indicates that all of the reasonably expected release paths can be included in a two-dimensional simplification of the Culebra. This is perhaps the most important point to be considered in evaluating the



applicability of the two-dimensional model and the strongest argument in its favor.

The two-dimensional simplification, however, does not properly account for the vertical leakage into the Culebra. Assuming that vertical leakage into the Culebra is negligible potentially impacts calculated specific discharge fields in two ways. First, ignoring vertical leakage in the inverse calculations of the T fields introduces some error into the T fields themselves. Second, using only fixed heads along lateral boundaries to generate specific discharge fields is only an approximate method of representing the actual flow field.

It is thought that both types of approximation introduced by assuming that leakage is negligible are acceptable for the purposes of PA calculations. The impact on the T fields is thought to be acceptably small because they are partially calibrated to transient data from pumping tests. We know that leakage does not impact the pumping tests because a definite leakage signature does not show up in the drawdown data. The impact of assuming negligible leakage when generating specific discharge fields is more difficult to address by reasoned argument. The plan to compare travel times from two-dimensional calculations that include leakage to those that do not should be completed to complement the discussion here. However, it is reasonable to assume that there is sufficient data control on transmissivities and heads that the two-dimensional calculations provide representative flow fields. It must be remembered that the intent of these calculations is not to determine a single "correct" flow field but rather to generate multiple realizations of the flow field that, if sampled, provide a representation of uncertainty.

Although the two-dimensional model is well suited for detailed analysis of flow and transport of radionuclides given certain boundary conditions, it does not provide a method for determining these boundary conditions or for estimating how they might change with time. This information must come from reasoned arguments based on conceptual models, field observations, or from results of models that are designed to simulate natural flow conditions at a basin scale. The conceptual models must be fully three-dimensional in order to provide a defensible basis for the two-dimensional calculations.



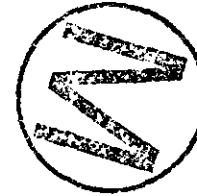


Table 1. Model parameter values which vary form calculation to calculation.

Calculation	Potential Recharge (mm/yr)	Dewey Lake Conductivity (m/s)	Intact Anhydrite Conductivity (m/s)	Disrupted Zone Conductivity (m/s)	Intact Culebra Conductivity (m/s)	Intact Magenta Conductivity (m/s)	Specific Yield
11	0.1	$2 \times 10^{-7}$	$10^{-13}$	$3.2 \times 10^{-6}$	$3.2 \times 10^{-8}$	$3.2 \times 10^{-9}$	
38	1.0	$2 \times 10^{-7}$	$10^{-13}$	$3.2 \times 10^{-6}$	$3.2 \times 10^{-8}$	$3.2 \times 10^{-9}$	
14	0.1	$2 \times 10^{-7}$	$10^{-12}$	$3.2 \times 10^{-6}$	$3.2 \times 10^{-8}$	$3.2 \times 10^{-9}$	
41	1.0	$2 \times 10^{-7}$	$10^{-12}$	$3.2 \times 10^{-6}$	$3.2 \times 10^{-8}$	$3.2 \times 10^{-9}$	
12	0.1	$2 \times 10^{-8}$	$10^{-13}$	$3.2 \times 10^{-6}$	$3.2 \times 10^{-8}$	$3.2 \times 10^{-9}$	
39	1.0	$2 \times 10^{-8}$	$10^{-13}$	$3.2 \times 10^{-6}$	$3.2 \times 10^{-8}$	$3.2 \times 10^{-9}$	
20	0.1	$2 \times 10^{-7}$	$10^{-13}$	$3.2 \times 10^{-7}$	$3.2 \times 10^{-8}$	$3.2 \times 10^{-9}$	
47	1.0	$2 \times 10^{-7}$	$10^{-13}$	$3.2 \times 10^{-7}$	$3.2 \times 10^{-8}$	$3.2 \times 10^{-9}$	
23	0.1	$2 \times 10^{-7}$	$10^{-12}$	$3.2 \times 10^{-7}$	$3.2 \times 10^{-8}$	$3.2 \times 10^{-9}$	
50	1.0	$2 \times 10^{-7}$	$10^{-12}$	$3.2 \times 10^{-7}$	$3.2 \times 10^{-8}$	$3.2 \times 10^{-9}$	
21	0.1	$2 \times 10^{-8}$	$10^{-13}$	$3.2 \times 10^{-7}$	$3.2 \times 10^{-8}$	$3.2 \times 10^{-9}$	
48	1.0	$2 \times 10^{-8}$	$10^{-13}$	$3.2 \times 10^{-7}$	$3.2 \times 10^{-8}$	$3.2 \times 10^{-9}$	
24	0.1	$2 \times 10^{-8}$	$10^{-12}$	$3.2 \times 10^{-7}$	$3.2 \times 10^{-8}$	$3.2 \times 10^{-9}$	

Calculation	Potential Recharge (mm/yr)	Dewey Lake Conductivity (m/s)	Intact Anhydrite Conductivity (m/s)	Disrupted Zone Conductivity (m/s)	Intact Culebra Conductivity (m/s)	Intact Magenta Conductivity (m/s)	Specific Yield
51	1.0	$2 \times 10^{-8}$	$10^{-12}$	$3.2 \times 10^{-7}$	$3.2 \times 10^{-8}$	$3.2 \times 10^{-9}$	
bc	0.1-5.0	$2 \times 10^{-7}$	$10^{-12}$	$3.2 \times 10^{-6}$	$3.2 \times 10^{-8}$	$3.2 \times 10^{-9}$	0.01
c1	0.1-0.5	$2 \times 10^{-7}$	$10^{-12}$	$3.2 \times 10^{-6}$	$3.2 \times 10^{-8}$	$3.2 \times 10^{-9}$	0.01
c4	0.1-5.0	$2 \times 10^{-7}$	$10^{-12}$	$3.2 \times 10^{-6}$	$3.2 \times 10^{-8}$	$3.2 \times 10^{-8}$	0.01
c5	0.1-5.0	$2 \times 10^{-7}$	$10^{-12}$	$3.2 \times 10^{-5}$	$3.2 \times 10^{-8}$	$3.2 \times 10^{-9}$	0.01
c7	0.1-5.0	$2 \times 10^{-7}$	$10^{-12}$	$3.2 \times 10^{-6}$	$3.2 \times 10^{-7}$	$3.2 \times 10^{-9}$	0.01
c8	0.1-5.0	$2 \times 10^{-7}$	$10^{-12}$	$3.2 \times 10^{-6}$	$3.2 \times 10^{-8}$	$3.2 \times 10^{-9}$	0.05

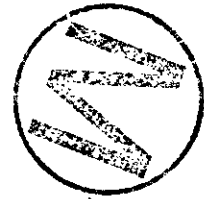


Table 2. Mass balance of flow in the Culebra over the controlled area.

Calculation	Flow In (% Total)			Total Flow (m <sup>3</sup> /yr)	Flow Out (% Total)		
	Top	Base	Lateral		Top	Base	Lateral
11	3	1	95	4723	0	1	99
38	4	1	95	10481	0	1	99
12	8	2	90	6801	0	1	99
39	5	2	94	9813	0	1	99
14	29	1	70	5955	0	1	99
41	33	1	66	13758	0	1	99
20	3	1	96	6254	0	1	99
47	4	2	94	6280	0	1	99
21	6	2	92	7615	0	1	99
48	5	2	93	6462	0	1	99
23	23	1	77	7079	0	1	99
50	31	2	68	8778	0	1	99
24	41	2	58	10700	0	1	99
51	31	2	68	9799	0	1	99



Table 3. Mass balance of flow in the Culebra over the controlled area at the present time.

Calculation	Flow In (% Total)			Total In (m <sup>3</sup> /yr)	Flow Out (% Total)			Total Out (m <sup>3</sup> /yr)
	Top	Base	Lateral		Top	Base	Lateral	
bc	28	1	71	7146	0	1	99	7150
c1	28	1	71	6612	0	1	99	6614
c4	18	1	81	6430	0	1	99	6434
c5	66	2	31	4523	0	1	99	4528
c7	6	0	94	49080	0	0	100	49083
c8	31	1	68	11003	0	1	99	11007

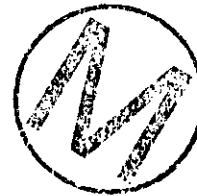
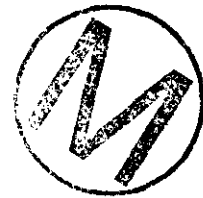


Table 4. Mass balance of flow in the Culebra over the controlled area at 10,000 years in the future.

Calculation	Flow In (% Total)			Total In (m <sup>3</sup> /yr)	Flow Out (% Total)			Total Out (m <sup>3</sup> /yr)
	Top	Base	Lateral		Top	Base	Lateral	
bc	30	1	69	13426	0	1	99	13426
c1	34	1	65	12753	0	1	99	12753
c4	22	1	77	12207	0	1	99	12207
c5	34	1	65	16016	0	1	99	16016
c7	7	0	92	67970	0	0	100	67970
c8	30	1	69	13426	0	1	99	13426



## CORRESPONDENCE

None

## REFERENCES

Freeze, R.A., and J.A. Cherry. 1979. *Groundwater*. Englewood Cliffs, NJ: Prentice-Hall.

Freeze, R.A., and P.A. Witherspoon. 1967. "Theoretical Analysis of Regional Groundwater Flow: 2. Effect of Water-Table Configuration and Subsurface Permeability Variation," *Water Resources Research*. Vol. 3, no. 2, 623-634.

Hubbert, M.K. 1940. "The Theory of Ground-Water Motion," *The Journal of Geology*. Vol. 48, no. 8, pt. 1, 785-944.

Powers, D.W., and R.M. Holt. 1990. "Sedimentology of the Rustler Formation Near the Waste Isolation Pilot Plant (WIPP) Site," *Geological and Hydrological Studies of Evaporites in the Northern Delaware Basin for the Waste Isolation Pilot Plant (WIPP), New Mexico, Field Trip #14 Guidebook, Geological Society of America 1990 Annual Meeting, Dallas, TX, October 29-November 1, 1990*. Leaders: D.W. Powers, R.M. Holt, R.L. Beauheim, and N. Rempe. Dallas, TX: Dallas Geological Society. 79-106.

Toth, J. 1963. "A Theoretical Analysis of Groundwater Flow in Small Drainage Basins," *Journal of Geophysical Research*. Vol. 68, no. 16, 4795-4812.

Swift, P.N. 1993. "Long-Term Climate Variability at the Waste Isolation Pilot Plant, Southeastern New Mexico, USA," *Environmental Management*. SAND91-7055. Vol. 17, no. 1, 83-97.

WIPP PA (Performance Assessment) Department. 1992-1993. *Preliminary Performance Assessment for the Waste Isolation Pilot Plant, December 1992*. SAND92-0700, Vols. 1-5. Albuquerque, NM: Sandia National Laboratories.

Records Package for FEP NS-8b. October 1995. Albuquerque, NM: Sandia National Laboratories.

## VERIFICATIONS AND ASSESSMENTS

No formal independent assessments were conducted.

No Corrective Action Reports were generated.

The attached signature pages at the front of this document indicate the technical and lead staff signatures and dates of review for completeness and accuracy.

See included comment sheet (page 29).

Management, technical, editorial, and QA reviews of this records package were performed and comments were addressed to complete the records package as indicated by the signatures on the attached pages at the front of this document.



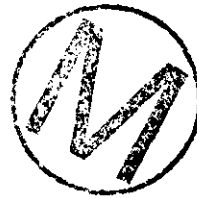
---

**Title 40 CFR Part 191  
Compliance Certification  
Application  
for the  
Waste Isolation Pilot Plant**

**MASS Attachment 15-8**



**THIS PAGE INTENTIONALLY LEFT BLANK**



WPO38797



Sandia National Laboratories

Operated for the U.S. Department of Energy by Sandia Corporation

Albuquerque, New Mexico 87185



date: 6/19/96

to: Jon C. Helton

*Christine T. Stockman*

from: Christine T. Stockman

INFORMATION ONLY

subject: Treatment of colloids in Culebra transport

On 6/6/96, we (D. R. Anderson, H. W. Papenguth, W. G. Perkins, J. L. Ramsey, C. T. Stockman, A. Treadway, and P. Vaughn) had a meeting to discuss the transport of colloids within the Cuelbra. Here is a summary of our decisions for each colloid type:

Mineral Fragments and Microbe Colloids

Hans Papenguth reported that mineral fragment and microbe colloids were filtered within a short distance in Culebra rocks. In his 6/11/96 memo he quotes filtration coefficients of 0.1/cm and 0.5/cm for mineral fragment and microbe colloids respectively. Because any mineral fragment or microbe colloid that is transported up the borehole will be filtered out of the flow stream within a short distance of the borehole, further modeling of this transport is unnecessary. This was also documented in a 6/4/96 memo from W. G. Perkins.

Actinide Intrinsic Colloids

I proposed that the inventory carried by intrinsic colloids was so small that it could safely be ignored. Plutonium is the only actinide of interest that forms significant intrinsic colloids (Papanguth 4/22/96). Using the latest inventory estimates (Watkins, 1996) and estimates of the EPA units associated with this inventory (Sanchez, 1996), I have calculated the maximum EPA units that could be released in 40,000 m<sup>3</sup> of brine containing 1e-9M Pu intrinsic colloids (Papanguth 4/22/96) to be about .006.

	table 4 *	table 6 *			
	EPA units	total moles	moles/unit	fraction of Pu	EPA units released
Pu238	6416	6.41E+02	9.99E-02	.012	.005
Pu239	<u>1954</u>	<u>5.35E+04</u>	<u>2.74E+01</u>	<u>.988</u>	<u>.001</u>
total Pu		5.41E+04			.006

\* Sanchez, 1996

For each isotope, the EPA units released = 4e+7 l \* 1e-9 M \* isotope fraction/(moles/unit). .006 EPA units could only be released to the Culebra for the one vector that releases 40,000 m<sup>3</sup> of brine and only if all this brine is all released at time zero. In real vectors, the Pu238 decays away during early years, and Pu239 is the only significant isotope in latter years. If all the release occurred in latter years, then the maximum EPA units that could be released would be .001. Even if transport of intrinsic colloids were instantaneous from the borehole to the boundary, that release could never be more that .006 EPA units and thus can be safely ignored.

---

**Title 40 CFR Part 191  
Compliance Certification  
Application  
for the  
Waste Isolation Pilot Plant**

**MASS Attachment 15-9**



**THIS PAGE INTENTIONALLY LEFT BLANK**



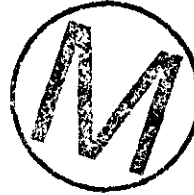


INFORMATION ONLY

date: June 4, 1996

to: James L. Ramsey, MS-1328 (6849)

from: W. George Perkins, MS-1320 (6832)



subject: Calculations of Filtration for Microbial and Mineral Fragment Colloids

In our meeting on June 3, 1996, we agreed that I would provide you with calculations that demonstrate the effects of filtration on the subject colloid types.

In his presentation at the DOE Consultation with the State of New Mexico on May 21, 1996, Hans W. Papenguth presented experimental evidence to the effect that microbial and mineral-fragment colloids are removed from suspension by filtration on being passed through crushed-dolomite columns. The effect of the filtration can be expressed by the formula

$$C/C_0 = \exp(-\gamma x), \quad (1)$$

where  $C_0$  is the concentration of colloid at the column inlet,  $C$  is the concentration at distance  $x$  from the inlet, and  $\gamma$  is a "decay constant" that describes the exponential decrease in colloid concentration. If  $x$  is expressed in cm (centimeters),  $\gamma$  is expressed in  $\text{cm}^{-1}$ . The values of  $\gamma$  that were presented to the DOE Consultation with the State of New Mexico were:

$$\gamma = 0.3 \text{ cm}^{-1} \text{ for mineral fragments,}$$

$$\gamma = 0.5 \text{ cm}^{-1} \text{ for microbes.}$$

Values of  $C/C_0$  for several values of  $x$  for the two colloid types are given in Table 1 and plotted in Figure 1. Clearly, within a very short distance for either type of colloid, the remaining colloid population has been reduced by filtration to an extremely small fraction of the inlet value. The "half-distance" for mineral fragments is slightly over 2 cm, and the "half-distance" for microbes is even smaller.

Based on these calculations, we propose that Performance Assessment should ignore these colloid species, as they will effectively disappear within distances well below 50 cm (which is less than typical calculation mesh sizes).

**Table 1. Calculations of  $C/C_0$  as a function of distance traveled in Culebra Dolomite rock for microbial and mineral-fragment colloids.**

x (cm)	$C/C_0$ (Mineral Fragments)	$C/C_0$ (Microbes)
0.0	1.00E+00	1.00E+00
1.0	7.41E-01	6.07E-01
2.0	5.49E-01	3.68E-01
3.0	4.07E-01	2.23E-01
4.0	3.01E-01	1.35E-01
5.0	2.23E-01	8.21E-02
6.0	1.65E-01	4.98E-02
7.0	1.22E-01	3.02E-02
8.0	9.07E-02	1.83E-02
9.0	6.72E-02	1.11E-02
10.0	4.98E-02	6.74E-03
15.0	1.11E-02	5.53E-04
20.0	2.48E-03	4.54E-05
25.0	5.53E-04	3.73E-06
30.0	1.23E-04	3.06E-07
40.0	6.14E-06	2.06E-09
50.0	3.06E-07	1.39E-11
60.0	1.52E-08	9.36E-14
70.0	7.58E-10	6.31E-16
80.0	3.78E-11	4.25E-18
90.0	1.88E-12	2.86E-20
100.0	9.36E-14	1.93E-22



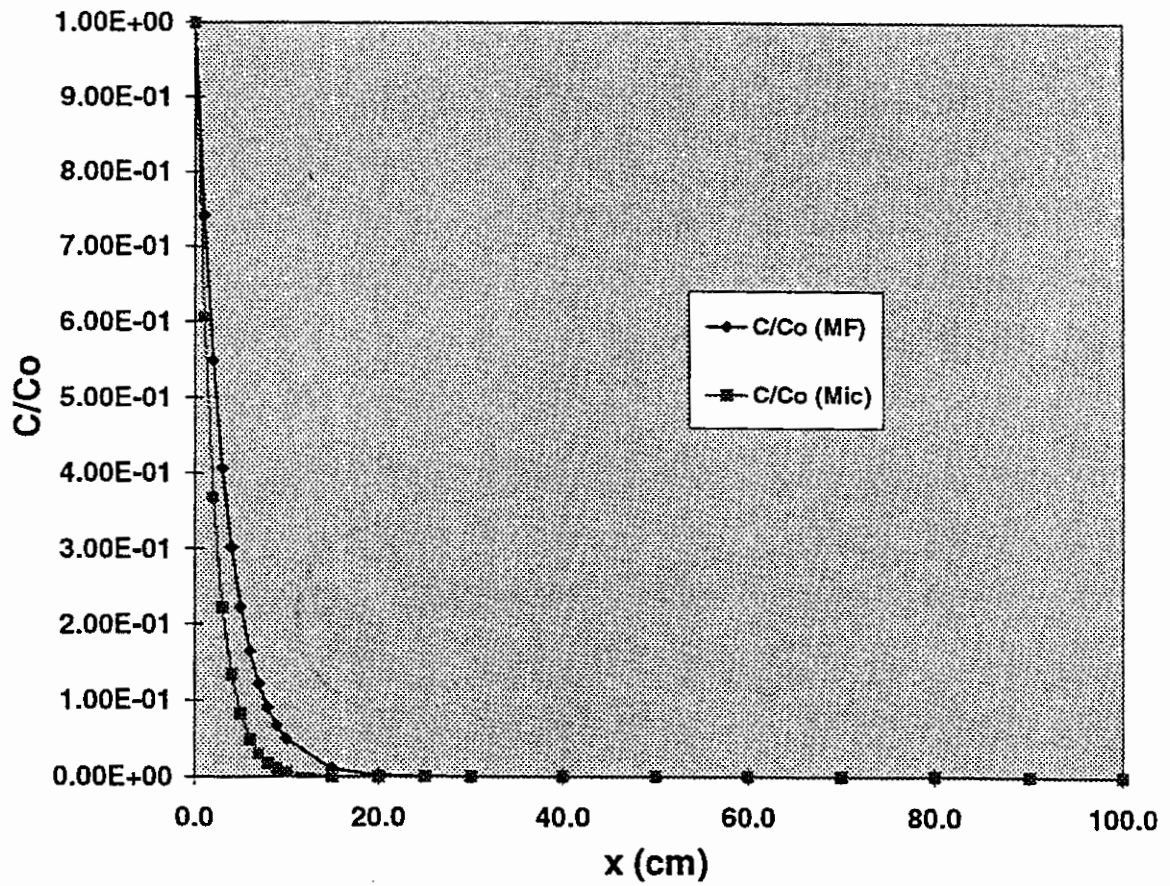


Figure 1. Plot of  $C/C_0$  as a function of distance traveled in dolomite for microbial and mineral-fragment colloids.



Copy to:

MS 1320 E. James Nowak, 6831

MS 1320 Hans W. Papenguth, 6832

MS 1320 W. George Perkins, 6832

MS 1328 Hong-Nian Jow, 6841

MS 1328 D. Richard Anderson, 6849

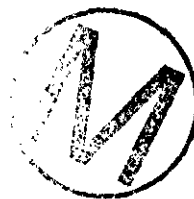
MS 1335 Margaret S. Y. Chu, 6801

MS 1341 John T. Holmes, 6832

MS 1395 Les E. Shephard, 6800

MS 1395 Melvin G. Marietta, 6821

SWCF-A:1.1.10.2.1:Colloid Characterization and Transport:QA



---

**Title 40 CFR Part 191  
Compliance Certification  
Application  
for the  
Waste Isolation Pilot Plant  
  
MASS Attachment 15-10**



**THIS PAGE INTENTIONALLY LEFT BLANK**



WPO 40484

## Sandia National Laboratories

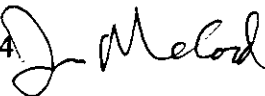
Albuquerque, New Mexico 87185-1324

date: 2 September 1996

SWCF-A: WBS 1.1.5.2.3. TD: QA

to: Kurt Larson, 6747/MS 1341

from: Jim McCord, 6115 / MS 1324



subject: Cross-Correlations for WIPP PA: Culebra Physical Transport Parameters

In section 3.4 of the *Analysis Plan for Determination of Physical Transport Parameters for the Culebra Dolomite* (hereafter referred to as the Analysis Plan), McCord and Meigs (1996) discuss the need for integrating the results from interpretive analysis of the Culebra tracer tests to yield a set of physical transport parameter distributions to be used in the performance assessment (PA) model for the WIPP. Based on the results of the interpretive analyses of the tracer tests integrated with other hydraulic and geologic data / information, we have recommended conceptualizing the Culebra dolomite as an equivalent homogeneous fractured media with no parameter cross-correlations. With this memo, I outline the reasons for including no cross-correlations between parameters.

To help explain our rationale, it is helpful to look at data and results collected to date. Culebra physical transport parameters for which we provided values to PA consisted of Culebra thickness, matrix tortuosity, diffusive porosity, advective porosity, matrix block length, and dispersivity. Section 3.4 of the Analysis Plan suggested a possible cross-correlation between transmissivity and the degree of double-porosity transport behavior at a hydropad location. This initial inference was based on the results from the H-11 and H-19 hydropads. Perhaps the most direct way to test such a correlation is to construct scatter plots between transmissivity and dual porosity parameters (e.g., matrix block length and advective porosity). Figure 1 shows such plots, constructed using transmissivity and physical transport parameters inferred from hydraulic and tracer test results at the H-3, H-11, and H-19 hydropads. A brief inspection of the plots presented in Figure 1 reveal no obvious correlations between transmissivity and the physical transport parameters. It has been noted that in some cases plotting scattergrams of the serial ranks of parameters can reveal correlations which are unapparent from scattergrams of parameter values (Helton et al., 1992). We therefore also plotted the serial rank of both the advective porosity and the matrix block length against the serial rank of transmissivity and against each other. These scatter plots are presented in Figure 2, and again no correlations are suggested. Furthermore, no trends or zoning patterns are apparent in the distribution of physical transport parameters across the WIPP site. Based on these results, we opted against recommending that the WIPP PA consider crosscorrelations between the transmissivity and the physical transport parameters. In summary, the data collected to date indicate that no correlations exist between transmissivity and physical transport parameters for the Culebra dolomite.

copies:  
6115 Lucy Meigs

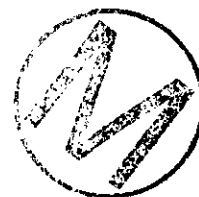




Fig. 2. Scatter plots of ranks for T and physical transport parameters.

